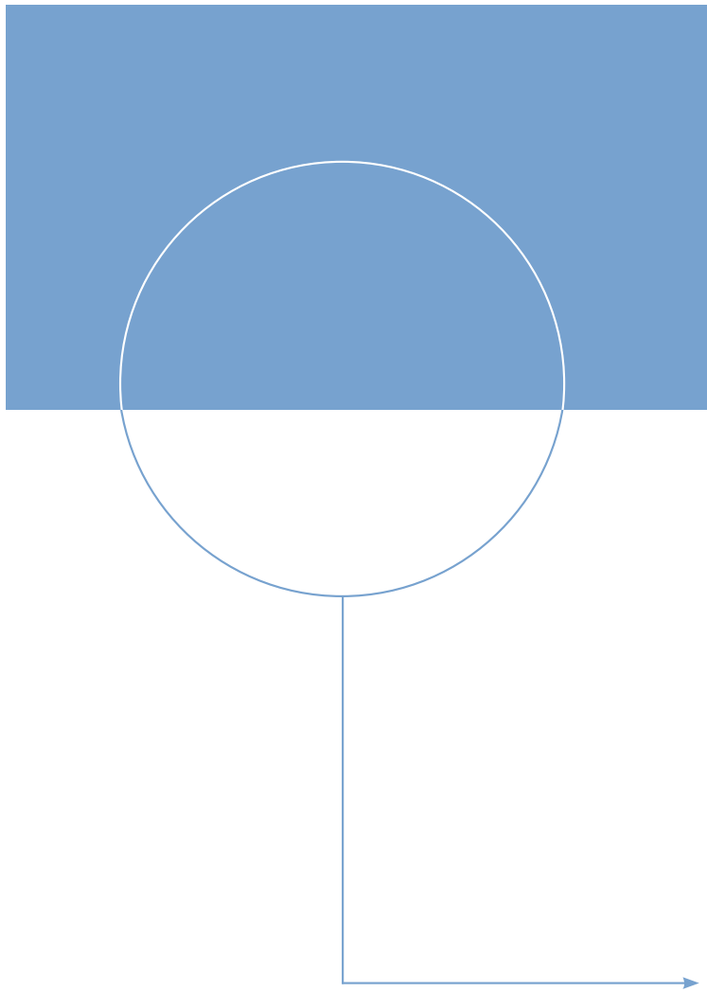

Master's thesis

2022

Shizhe Zhang

**NTNU**
Norwegian University of
Science and Technology
Faculty of Natural Sciences
Department of Biotechnology and Food Science

Shizhe Zhang

# Extraction and characterization of bioactive natural products from brown seaweed *Alaria esculenta*

July 2022

NTNU
Norwegian University of
Science and Technology

NTNU
Norwegian University of
Science and Technology

NTNU
Norwegian University of
Science and Technology

# Extraction and characterization of bioactive natural products from brown seaweed *Alaria esculenta*

Shizhe Zhang

Master's thesis in Biotechnology
Submission date: July 2022
Supervisor: Finn Lillelund Aachmann
Co-supervisor: Leesa Jane Klau

Norwegian University of Science and Technology
Department of Biotechnology and Food Science

# Preface

The work described in this thesis was conducted at the Norwegian Biopolymer Laboratory, Department of Biotechnology and Food Science at Norwegian University of Science and Technology in Trondheim, Norway, in cooperation with the Department of Chemistry and Bioscience at Aalborg University in Aalborg, Denmark.

I would like to thank my supervisor Professor Finn Lillelund Aachmann and co-supervisor Dr. Leesa Jane Klau for providing the opportunity to this project in Trondheim and in Aalborg, as well as for their invaluable advice and infinite patience throughout the project. Many thanks to Professor Reinhard Wimmer at Aalborg University for the warm help both in and outside of the lab during my stay in Denmark. I would also like to express my gratitude to the staff engineers in the lab for their guidance on many practical details. Special thanks to Leesa, every meeting with you was enlightening from every aspect.

I am also very thankful to my friends for being cheerful around. And lastly, my mother has always been showing her greatest support and love. Love you mom.

July 1, 2022

NTNU, Trondheim

Shizhe Zhang

# Abstract

Natural products are chemical compounds found in natural sources including terrestrial and marine organisms. In addition to their nutritional values, natural products can also exhibit health benefits such as antipathogenic, antioxidant and antidiabetic, which are known as bioactivities. Compared to plants, seaweeds have similar chemical composition, yet are a more sustainable source for food and bioactive natural products, and therefore have been drawing an increasing attention in recent years. For instance, countries in Europe have expanded the seaweed production and harvest, with Norway contributing more than half of the volume. The two primary seaweed species harvested in Norway are the brown seaweeds *Alaria esculenta* and *Saccharina latissima*. In this study, the focus has been on the extraction, fractionation and characterization of bioactive natural products from these two species. During fractionation bioassays were employed to measure the bioactivities: the total phlorotannin contents (TPhCs) of the seaweed extracts were quantified by 2,4-dimethoxybenzaldehyde (DMBA) assay, and enzyme inhibition assays including collagenase and amylase were used. The separation techniques included liquid-liquid partitioning, macroporous adsorptive resins XAD-16, Sephadex® LH-20 column chromatography, and preparative reversed-phase HPLC-MS. High resolution QToF LC-MS was used to pinpoint m/z ratios that may represent the bioactive compounds in the active fractions. New fractions were generated based on the identified m/z ratios and were tested for $\alpha$-amylase inhibition.

Out of the four crude extracts of the enzyme-treated *A. esculenta* and *S. latissima* by absolute methanol and 70% (v/v) ethanol, the methanol extract of *A. esculenta* showed the highest TPhCs of 0.63 mg phloroglucinol equivalents/g dry residue, and $\alpha$-amylase and collagenase inhibition of 46% and 15%, respectively. A large-scale methanol

extract of *A. esculenta* was thus prepared and fractionated following the bioactivity of $\alpha$-amylase inhibition. Fractions were characterized by $^{1}$H 1D and 2D NMR spectroscopic techniques. The carotenoid metabolites loliolide and its isomer, (+)-epiloliolide, were for the first time identified from the species *Alaria esculenta*. The other fractions were complex mixtures that contained sugar, glycerol and lipid moieties. NMR spectroscopy was used to assign partial structures of these moieties that were identified as glycerolipids. Additional signals were also observed and were hypothesized to represent degraded phlorotannins or phenyl-terminated lipid, hydroxylated lipids and conjugated lipids. The results suggest that the natural products in *A. esculenta* are highly likely to inhibit $\alpha$-amylase.

# Symbols and Abbreviations

***A. esculenta*** *Alaria esculenta.*

***S. latissima*** *Saccharina latissima.*

**ALA** $\alpha$-linolenic acid.

**COSY** Correlation Spectroscopy.

**DGDG** Diglycosyldiacylglycerol.

**DGMG** Diglycosylmonoacylglycerol.

**DHA** Docosahexaenoic acid.

**DMBA** 2,4-dimethoxybenzaldehyde.

**DPPH** 2,2-diphenyl-1-picrylhydrazyl.

**EPA** Eicosapentaenoic acid.

**GL** Glycerolipid.

**H2BC** Heteronuclear 2-Bond Correlation.

**HMBC** Heteronuclear Multiple-Bond Correlation Spectroscopy.

**HPLC** High Performance Liquid Chromatography.

**HSQC** Heteronuclear Single-Quantum Correlation Spectroscopy.

**LC** Liquid Chromatography.

**m/z ratio** mass-to-charge ratio.

**MGDG** Monoglycosyldiacylglycerol.

**MGMG** Monoglycosylmonoacylglycerol.

**MS** Mass Spectroscopy.

**NMR** Nuclear Magnetic Resonance.

**NOE** Nuclear Overhauser Effect.

**NOESY** Nuclear Overhauser Effect Spectroscopy.

**ppm** Parts per million.

**PUFA** Polyunsaturated fatty acid.

**QToF** Quadruple Time-of-Flight.

**SQDG** Sulphaquinovosyldiacylglycerol.

**TPhC** Total phlorotannin content.

**UV-vis** Ultraviolet-visible.

# Table of Contents

# 1 Introduction

## 1.1 Background

Natural products have long been obtained by humans from microbes, animals and plants of terrestrial and marine origins. The definition of natural products varies: some restrict them within the category of secondary metabolites that are not essential in the growth and development (Shepard, 2007; Springob and Kutchan, 2009), while others include all substances found in nature (Hanson, 2003). For the purpose in this work, the latter definition is adopted: natural products are diverse compounds including carbohydrates, lipids, carotenoids and polyphenols that can be extracted from natural sources (Springob and Kutchan, 2009). The inclusion allows the exploration of a wider range of compounds on their bioactivites, which are the physiological effects beyond nutritional values (Cazarin et al., 2022). These effects often refer to antipathogenic, antiinflammatory, antioxidant and antidiabetic abilities that promote health benefits (Hamzam1olu and Gökmen, 2016).

Development of novel drugs and nutraceuticals rely on the discovery of the bioactive natural products through screening for a specific bioactivity. The process includes: extraction from the organism; purification of the extracts; *in vitro* or *in vivo* assays to screen the bioactive components; isolation of the compound from the bioactive fractions; and finally identification through analytical means such as ultraviolet-visible (UV-vis) spectroscopy, mass spectroscopy (MS), nuclear magnetic resonance spectroscopy (NMR) (Stuart et al., 2020). The method, called bioassay-guided fractionation, has been widely utilized, especially on plant extracts as plants have shown many bioactivities (Springob and Kutchan, 2009).

With the development of the society, however, a sustainable obtainment of the functional food and natural products without impairing the environment has become one of the major topics. Seaweeds have been drawing an increasing attention as an alternative to plants: they allow massive cultivation in the seas and oceans without the use of lands and fertilizers, and contain rich bioactive natural products (Tiwari and Troy, 2015). The potential substitution to plants is attributed to the similar chemical composition of seaweeds, where polysaccharides, minerals, lipids, pigments and polyphenols are present in both plants and these multicellular organisms. Approximately 70% of the cultivated seaweed biomass is used for human consumption, and the remaining is mainly utilized for the phycocolloid (alginate, agar and carrageenan) production (Schiener et al., 2015). Moreover, the exploration on how to fully exploit the seaweed biomass is ongoing, in addition to its uses as animal feed, fertilizers and biofuels (Tiwari and Troy, 2015).

Global seaweed production is dominant in Asian countries including China, Indonesia, South Korea and Japan with more than 97% share in 2019, while Europe produced approximately 0.3 million tonnes, representing 0.8% of the total volume (FAO, 2022). Although this is an emerging industry, Europe has been expanding the seaweed biomass production and harvest, with Norway leading the process, contributing more than half of the volume in Europe (Araújo et al., 2021; FAO, 2022). The harvest amounts of cultivated seaweed and the corresponding values in Norway from 2015 to 2020 have increased from 51 tonnes to 336 tonnes, and from 178,000 NOK to 8,618 NOK, respectively, indicating a intensively increasing trend of seaweed harvest for aquacultural use (Fiskeridirektoratet, 2022).

## 1.2 Brown seaweeds

Mainly differentiated by the pigments, seaweeds are classified into three groups: Green seaweeds (Chlorophyta), red seaweeds (Rhodophyta), and brown seaweeds (Phaeophyta) (Chapman, 2013), among which the brown seaweeds are the most abundant group. The brown color comes from fucoxanthin, a xanthophyll pigment. In Norway, brown seaweed species *Saccharina latissima* (*S. latissima*) and *Alaria esculenta* (*A. esculenta*) are the most harvested (Figure 1.1) (Fiskeridirektoratet, 2022; P. Stévant and Chapman, 2017).


**Figure 1.1:** Brown seaweeds *Alaria esculenta* and *Saccharina latissima* (Roleda et al., 2018)

There is a growing interest on the bioactive potentials of the species. For instance, antioxidant and antiinflammatory activities of the two species were investigated (Afonso et al., 2021); Einarsdóttir et al. (2022) tested the antioxidant activity of *A. esculenta*'s extract using Pulsed Electric Field-assisted extraction; Bioactive contents including fucoxanthin and polyphenols were quantified in *A. esculenta* and *S. latissima* (Castejón et al., 2021a; Marinho et al., 2019; Mohammed

et al., 2021a; Stefaniak et al., 2019; Stévant et al., 2018). Overall in brown seaweeds, the activities were often attributed to carotenoids and polyphenolic compounds, yet other natural products including carbohydrates and lipids are also gaining attention on their bioactive potentials (Holdt and Kraan, 2011).

### 1.2.1 Carbohydrates

In brown seaweeds, carbohydrates are mainly present in the forms of alginates, laminarins, mannitol and fucoidans. Alginates are a group of linear polymers consisting of polyuronic acids, and are one of the major structural polysaccharides that organize the cell wall of brown seaweeds. Containing up to 40% dry weight, the brown seaweed is the most important source of alginates in phycocolloid production. Due to its gelling property, alginates have wide applications as hydrogel-based wound dressings in therapeutics and thickening agent in food industry and cosmetics (Zaharudin et al., 2017).

Sulfated polysaccharide fucoidans are another important group of structural polysaccharide, and they have been indicated with antimicrobial and antiviral effects (Holdt and Kraan, 2011). Antimicrobial activity has also been observed in laminarin from the brown seaweed *Cystoseira barbata* that it inhibits the growth of gram negative bacteria (Sellimi et al., 2018). However, these effects are highly dependent on the various compositions and molecular weights from different brown seaweed species (Holdt and Kraan, 2011). It is thus difficult to conclude on the bioactivities. Moreover, the structural polysaccharides can interact with proteins, metal ions and others, forming a rather rigid cell wall and providing strong barriers to the extraction of inner bioactive contents (Billakanti et al., 2013; Joana Gil-Chávez et al., 2013).

### 1.2.2 Lipids

Compared to carbohydrates, the lipids are not as abundant, forming up to 4.5% dry weight (Holdt and Kraan, 2011). Nevertheless, the bioactivity of brown seaweeds was largely contributed to the lipid contents, due to the production and accumulation of $\omega$-3 and $\omega$-6 polyunsaturated fatty acids (PUFA). Eicosapentaenoic acid (EPA, 20:5n3) and docosahexaenoic acid (DHA, 22:6n3) are the two major marine $\omega$-3 PUFAs derived from $\alpha$-linolenic acid (ALA, 18:3n3) (Figure 1.2), and are well-known for their health benefits including anti-hypertension and antiinflammatory effects (Holdt and Kraan, 2011; Lopes et al., 2021).

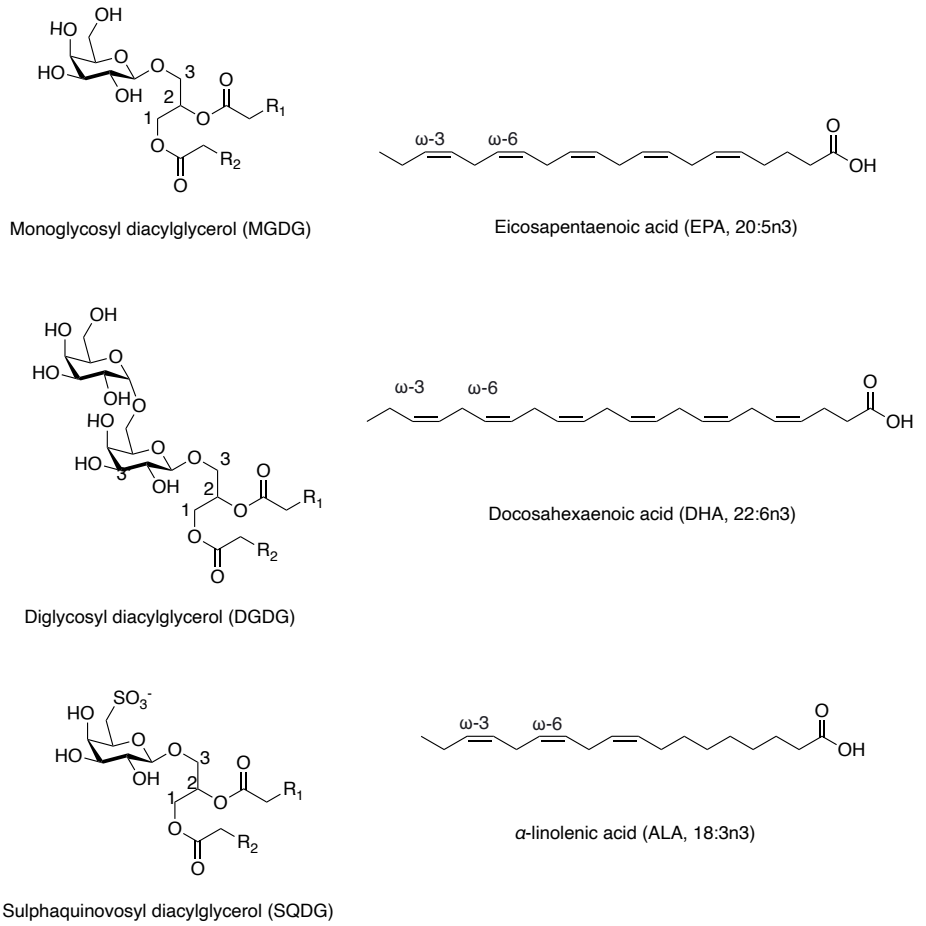


**Figure 1.2:** Common bioactive lipids in Brown seaweeds including MGDG, DGDG, SQDG, EPA, DHA and the precursor ALA. The sugar moieties in MGDG, DGDG and SQDG are shown with $\beta$-galactoses as they are the most common ones found in the lipids (Lopes et al., 2021).

In contrast to animals that the cell membrane is mainly formed by phospholipids, glycerolipids (GLs) are the most abundant membrane lipids of brown seaweeds. GLs are mainly present as monoglycosyl diacylglycerols (MGDG), diglycosyl diacylglycerols (DGDG), and sulphaquinovosyl diacylglycerols (SQDG), comprising sugar, glycerol and

two esterified fatty acid chains. Several monoglycosyl monoacylglycerols (MGMGs) and digalactosyl monoacylglycerols (DGMGs) with one lipid chain were also identified from brown seaweeds such as *Fucus vesiculosus* (da Costa et al., 2019). These GLs have shown multiple bioactivities including antimicrobial, antitumor and antidiabetic effects (Buedenbender et al., 2020; Lopes et al., 2021; Tanna and Mishra, 2018).

In the GLs from brown seaweeds, The most volatile esterified fatty acid chain is EPA, of which the esterification reduces the chance of oxidation and the subsequent loss of its bioactivities (Holdt and Kraan, 2011; Salehi et al., 2019). Nonetheless, the structures of the lipid chains can vary in terms of the degree of unsaturation, the configuration of the double bonds (*cis* or *trans*), branching, oxygenation, and hydroxylation, which result in different bioactivities of the GLs (Kenar et al., 2017; Lopes et al., 2021; Lu et al., 2019).

### 1.2.3 Carotenoids

Structurally similar to lipids with a polyene long chain, carotenoids, also known as tetraterpenoids, are a group of lipid-soluble pigments found in a wide range of organisms (Holdt and Kraan, 2011; Salehi et al., 2019). In brown seaweeds, fucoxanthin is the most abundant carotenoid and contributes to their brown color. Fucoxanthin has been reported with multiple bioactivities including antioxidant, anticancer, anti-obesity, antidiabetes and antiinflammatory (Holdt and Kraan, 2011; Lopes et al., 2021; Salehi et al., 2019). In particular, fucoxanthin is effective in preventing obesity and type II diabetes through different mechanisms: it can be upregulated by $w$-3 PUFAs through glucose transport and insulin release controls; *in vivo* study showed a decreased level of fat-producing precursor when fucoxanthin was present (Tanna and Mishra, 2018).

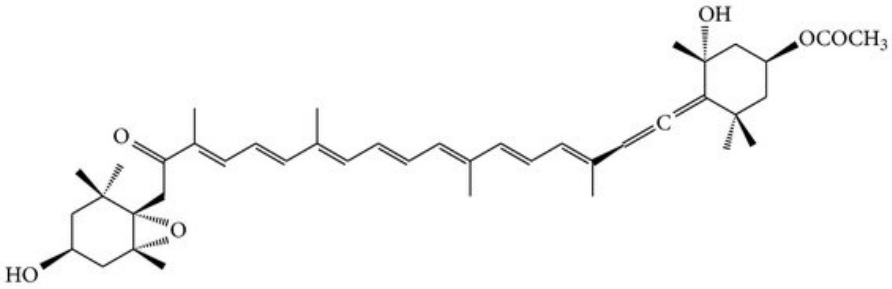


**Figure 1.3:** The structure of fucoxanthin. The figure is from (Zhang et al., 2015).

However, utilization of fucoxanthin is often difficult, as it is sensitive to oxygen, temperature, light and low pH that degradation often occurs in the process of extraction and isolation as well as during storage (Yusof et al., 2022). The mechanisms of fucoxanthin degradation are unclear, and the resulting products can be structurally diverse, including apo-fucoxanthinoids, aromatic norisoprenoids, monoterpenoids and terpenes (Repeta, 1989; Yusof et al., 2022).

### 1.2.4 Polyphenolic compounds

Polyphenolic compounds are important secondary metabolites, where in brown seaweeds they are mainly present in the forms of phlorotannins. Phlorotannins are a group of polymeric compounds composed of phloroglucinols (1,3,5-trihydroxybenzene), with their molecular weights ranging from 126 Da to larger than 10,000 Da. The drastic size range is attributed to the various degrees of polymerization and the different linkages, based on which phlorotannins are divided into four major groups: phlorethols with ether linkages; fucols with only aryl-aryl linkages; eckols with dibenzodioxin linkages; and lastly fucophloroethols with both ether and aryl-aryl linkages (Figure 1.4). The structural complexity is also due to the presence of isomers even at the same

molecular weight (Li et al., 2017). As a result, structural elucidation is diffcult and the reported bioactivities have often been attributed to the category instead of an identified phlorotannin.

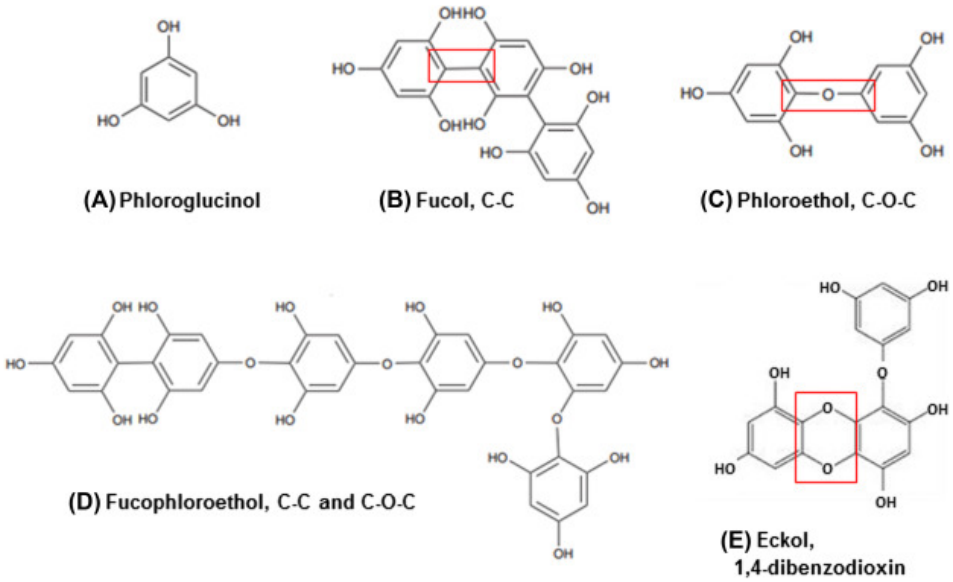


**Figure 1.4:** The structures of the phloroglucinol monomer (A) and the four categories of phlorotannins based on their different linkages (B–E). The figure is from (Hermund, 2018).

Nevertheless, phlorotannins from multiple brown seaweed species have been reported with antioxidant (Tanniou et al., 2013; Wang et al., 2012), antimicrobial (Buedenbender et al., 2020) and enzyme-inhibiting activities (Catarino et al., 2019). However, degradation of phlorotannins is prevalent which reduces their bioactivities (Okeke et al., 2021a).

## 1.3 Investigation into the bioactive natural products in brown seaweed

When an untargeted natural product is desired, a bioassay-guided approach is often applied to isolate the compound that exhibit the bioac-

tivity. The general procedure includes extraction and fractionation guided by one or more selected *in vitro* bioassays. The fractionation process is often repeated to ideally obtain a pure active fraction (Figure 1.5).

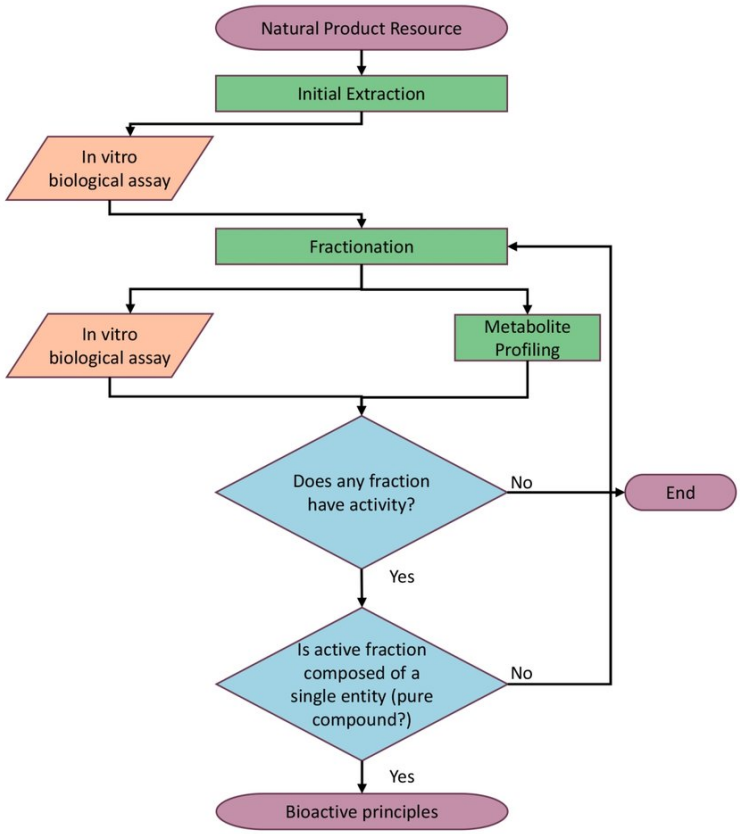


**Figure 1.5:** An illustration of the general scheme of bioassay-guided fractionation. The figure is from (Kellogg and Kang, 2020).

### 1.3.1 Extraction

Depending on the components of interest, different extraction methods can be used. As mentioned in Section 1.2.1, the cell wall polysaccharides are barriers to the extraction of bioactive compounds. Polysaccharide-

degrading enzymes such as cellulase, $\beta$-glucosidase and pectinase can be used to break down the polysaccharides and release the internal contents. It was reported that maximum polyphenol recovery was achieved with sole use of tannase (Joana Gil-Chávez et al., 2013).

Polarity of the extracting solvent is also critical in extraction. In general, polar solvents such as water, ethanol and methanol dissolve hydrophilic compounds, whereas bioactives with a lipid-like structure favor non-polar solvents such as hexane, toluene and chloroform. Miscible solvents can be mixed to create a solvent with a wide range of polarities, in particular when the chemical properties of the compounds are unknown. In fact, methanol, ethanol or acetone is often used in various ratios with water while extracting natural compounds from brown seaweeds (Catarino et al., 2019; Do et al., 2013; Tanniou et al., 2013).

### 1.3.2 Bioassay-guided fractionation

#### Bioassays

Diverse bioassays have been developed to screen different bioactive compounds. In brown seaweeds, several *in vitro* assays are commonly mentioned: 2,2-diphenyl-1-picrylhydrazyl (DPPH) method is applied to evaluate the antioxidant activity (Do et al., 2013; Tanniou et al., 2013); antimicrobial effects are tested by inhibition assays on different pathogenic microbes (Buedenbender et al., 2020; Holdt and Kraan, 2011); and Folin-Ciocalteu reaction can be used in both screening and quantifying the bioactive polyphenolic compounds (Do et al., 2013; Tanniou et al., 2013). However, this Folin-Ciocalteu method has a non-negligible drawback: any reducing compounds besides polyphenols can react with the reagent and give a high score (Amorati and Valgimigli, 2015). Hence, other more selective assays have been used, which not

only increase the specificity, but provide possibilities of screening compounds with other bioactivities.

2,4-dimethoxybenzaldehyde (DMBA) assay is a method specifically targeting phlolotannins, as DMBA reacts only with 1,3- or 1,3,5-substituted polyphenols and produce a color that can be detected at 510 nm. The total phlorotannin contents (TPhCs) can then be calculated from a calibration curve of a standard, typically the commercially available monomer, phloroglucinol. The reaction mechanism is not completely understood, but DMBA is believed to access to phlorotannins only through the unsubstituted 2,4 or 6 positions to induce the color change (Stern et al., 1996).

Another selective bioassay, the enzyme inhibition assay, is in particular valuable in discovering bioactive natural products for medicinal uses. This is because enzymes are involved in all kinds of disease development processes, and inhibition of enzymatic activity sees rapid and unambiguous effect. For instance, the polyphenolic substance quercertin was reported to inhibit kinases and combat inflammation (Ramsay and Tipton, 2017). In brown seaweeds, several metabolic enzymes have been used, including $\alpha$-amylase, $\alpha$-glucosidase and pancreatic lipase (Catarino et al., 2019; Zaharudin et al., 2017).

### Fractionation

Multiple methods have been developed to fractionate and purify a crude extract, with chromatographic techniques the most utilized. The principle of chromatography is that the mixture is dissolved in a solvent (gas or liquid) called the mobile phase, and separated on a material called the stationary phase. Molecules in the mixture have different affinities for the stationary phase, which allows each molecule to travel at a specific velocity, achieving the separation (E. O' Keeffe

and McLoughlin, 2019).

Chromatographic techniques can be classified into column chromatography and planar chromatography, based on the stationary bed shape. Thin Layer Chromatography (TLC) as a classic technique is a type of planar chromatography in which the stationary phase is on a plane. TLC has been more frequently utilized as a characterization method to screen certain compounds other than separation technique (E. O' Keeffe and McLoughlin, 2019; Jayabarath and Jeyaprakash, 2015). In contrast, column Chromatography is carried out in a tube packed with particles of a solid stationary phase, which are immersed in a liquid stationary phase. The sample mixture is added to the top of the column, and the mobile phase carries the sample through the system, where the compounds are separated and shown as different bands (Figure 1.6). The column chromatography has been utilized to obtain bioactive fractions from brown seaweeds: antibacterial fractions were obtained by column chromatography on silica gel (El-Shouny et al., 2017); fucoxanthin was purified from *Sargassum horneri* through octadecylsilyl (ODS) column chromatography (Ye et al., 2021), and identified from *(Sargassum filipendula* using silica gel stationary phase (Purnomo, 2017). In particular, many studies applied Sephadex® LH-20, a crosslinked dextran-based resin material (Mottaghipisheh and Iriti, 2020) as the stationary phase, and successfully separated and identified phlorotannins (Isaza Martínez and Torres Castañeda, 2013; Majik et al., 2015; Zhou et al., 2019) and galactolipids (Deal et al., 2003).

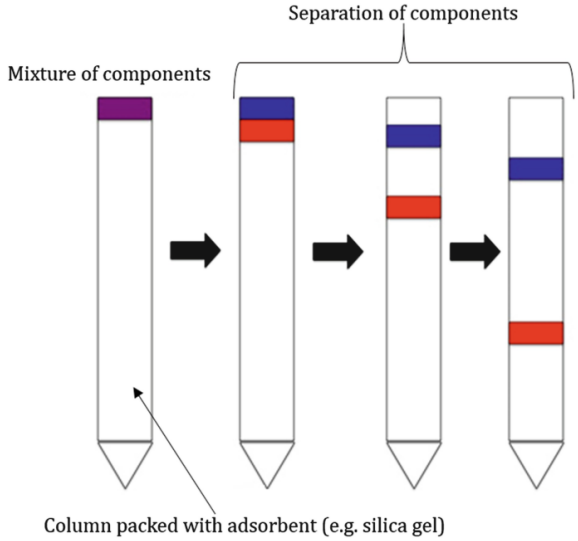


**Figure 1.6:** Graphic illustration of the column chromatography. The adsorbent packed inside the column is the material of the stationary phase, and the mixture of components is dissolved in a liquid mobile phase. Through time, each component is separated into different bands. The figure is from (Akash and Rehman, 2020).

A more common classification of chromatography is based on the state of the mobile phase, determining whether it is Liquid Chromatography (LC) or Gas Chromatography (GC). In the context of extracting and separating natural products from brown seaweeds, a reversed phase High Performance Liquid Chromatography (RP HPLC) is favored as the separation technique (Cavaliere et al., 2018). In contrast to the normal phase HPLC, the stationary phase of the RP HPLC is non-polar whereas the mobile phase is polar. Hence, sample molecules interact with the stationary phase through hydrophobic interactions. Based on that, RP HPLC has several advantages: the column such as C18, C8 and C6-phenyl columns are highly stable; different changes can be made on the polar mobile phase; and most importantly, it can be used on structurally diverse compounds with a high recovery (Batool and Menaa, 2020). Natural products including fucoxanthin,

phlorotannins and GLs have been successfully separated and identified from brown seaweeds using RP HPLC method (Buedenbender et al., 2020; Ye et al., 2021; Yotsu-Yamashita et al., 2013).

Other fractionation and purification methods are also utilized in combination with the chromatographic techniques. Liquid-liquid partitioning is often used as the first purification step of the crude extracts. Compounds in a mixture are partitioned by two immiscible solvents based on their solubilities in each solvent. In brown seaweeds, non-polar compounds including waxes and chlorophyll can be removed by n-hexane (E. O' Keeffe and McLoughlin, 2019; kawee ai et al., 2019).

Before directly applying chromatographic fractionation, the sample can also be purified through adsorptive macroporous resins. The technique of adsorption and desorption onto the non-ionic resins is proved to effectively recover non-polar or less polar natural compounds such as carotenoids and saponins (Li and Chase, 2010). For brown seaweeds, phlorotannins from *Macrocystis pyrifera* (Leyton et al., 2017) and from *Ecklonia cava* (Kim et al., 2014) were efficiently purified by adsorptive macroporous resins.

### 1.3.3 Analytical Methods

The step following fractionation is identify compounds from the bioactive fractions with the help of instruments. Spectroscopic methods including MS and NMR spectroscopy have been mostly applied in this process. In fact, combining a detection technique and the separation techniques allows rapid analysis of the fractions. For instance, HPLC fractionation is often coupled with UV-vis absorbance detection, LC separation is followed with MS identification, and so on (Patel et al., 2010).

### Ultraviolet-visible spectroscopy

Ultraviolet-visible spectroscopy (UV-vis) detects and quantifies compounds in a sample that absorbs light within the UV-vis region. In the context of seaweed extracts, bioactive compounds often contain double bonds, in which the $\pi$-electrons are in relatively high energy states that absorb light in the range of UV and visible light radiation. The electrons in the sample absorb light, resulting in a lower transmittance, and the light energy can be converted into electrical signals and displayed for analysis. The higher concentration of the compounds in the sample, the less light transmitted out. As a result, UV-vis spectrum indicates both the presence of a specific compound and the quantity. UV-vis spectroscopic technique is commonly coupled with LC and HPLC separation methods (Skoog and Holler, 2007).

### Mass Spectroscopy

Mass spectroscopy (MS) is an analytical tool for the identification of molecules. The principle of MS is generate ions through ionization of a molecule, separate the ions by their different mass-to-charge ratios (m/z ratios). The result is displayed in a mass spectrum of ion intensity versus m/z ratios to identify the molecule. While analyzing a mixture, MS is preferably combined with separation methods such as reversed-phase LC and HPLC, which is commonly used for handling polar nonvolatile compounds (Gross, 2017c).

The ionization possibly produces two types of ions: a molecular ion $M^+$ that often appears to be at the highest m/z ratio in the spectrum, and the fragment ions resulting from fragmentation of the molecular ion. For instance, ionization of a propane molecule produces 3 possible ions: the methyl cation with the m/z ratio of 15; the ethyl cation with the m/z ratio of 29; and the molecular ion of 44, which is approximately

the molecular mass of the propane (Figure 1.7). In LC or HPLC hyphenated MS while analyzing biological macromolecules, ionization is mostly achieved by the method of Electrospray Ionization (ESI) that ions are produced in a high voltage electrospray without much fragmentation, and the molecular ion peak is almost always present to imply the mass of the molecule directly (Gross, 2017a).

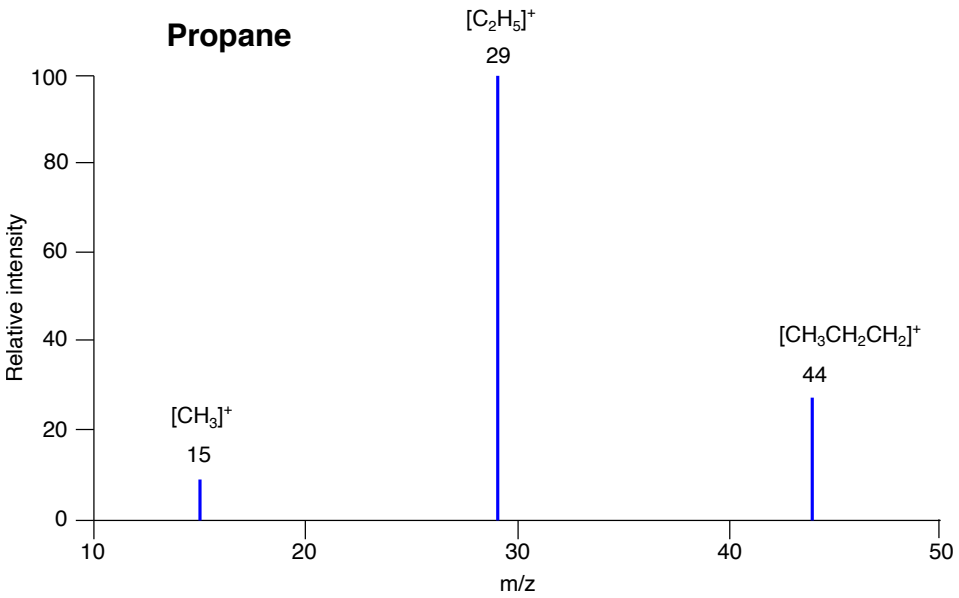


**Figure 1.7:** A simplified illustration of the MS spectrum of propane. Three major signals are demonstrated, with the most intense signal representing the fragmented ethyl cation; the signal with the highest m/z ratio 44 represents the molecular ion of propane. This figure is adapted from (Data, 2022).

In the process of ESI, however, adduct ions are often formed and their m/z ratios are displayed in the spectrum instead of the mass of the molecular ion. The prevalent adducts include $[M+H]^+$, $[M+Na]^+$ and $[M+K]^+$ with a mass difference to the molecular ion of 1, 23 and 39, respectively. These adduct ions can arise from multiple sources such as the eluting solvent additives, impurities and so on. When 0.1% formic acid is included in the mobile phase in LC-MS, for instance, $[M+H]^+$

are $[M+Na]^+$ are often observed in the spectrum (Kruve and Kaupmees, 2017). At the same time, the fragments can be lost as neutral molecules, for instance, a hydroxyl group under an acidic condition is lost in the form of $H_2O$, resulting in a $[M–H_2O+H]^+$ with a m/z ratio 18 subtracted from the $[M+H]^+$ adduct ion (Gross, 2017b). The adduct and the neutral loss facilitate the recognition of the m/z ratio of the molecular ion, and the identification of the molecule. Hence, the mass differences are worthwhile to know while interpreting a MS spectrum (Gross, 2017e).

LC and HPLC hyphenated mass spectroscopy also produces data in the form of a chromatogram, which is a plot of the signal intensity versus retention time. The chromatogram is composed of a series of mass spectra representing ions eluted at different retention times, providing an overview of the masses in a sample mixture (Gross, 2017c).

To present the m/z ratios either in a chromatogram or in a spectrum, a mass analyzer as part of the mass spectrometer separates the ions and a detector converts and displays the converted digital signals (Gross, 2017d). Different mass analyzers are combined: for example, a Quadruple Time-of-Flight (QToF) analyzer as a rising incorporates the benefits of the high resolution of the Time-of-Flight analyzer, and of the great accuracy of the Quadruple analyzer (Allen and McWhinney, 2019).

### Nuclear Magnetic Resonance Spectroscopy

Nuclear magnetic resonance (NMR) spectroscopy is a spectroscopic technique to solve the molecular structure. This is achieved by reflecting the unique chemical environment of each nucleus in a molecule utilizing the spin of the nuclei. An NMR-active nucleus can act as a magnet and spin around the axis of an external magnetic field in

a certain frequency. The frequency can be measured by applying an electromanetic pulse: a nucleus is excited and relaxes to its original equilibrium state, and generates a decaying signal as a function of time. The signal is then transformed to the function in the frequency domain of the spinning nucleus (Figure 1.8). Variance in the density of the surrounding electrons, through-bond coupling, and through-space coupling contribute to the different chemical environment of a nucleus, and the differences are visualized as distinct frequencies in an NMR spectrum.

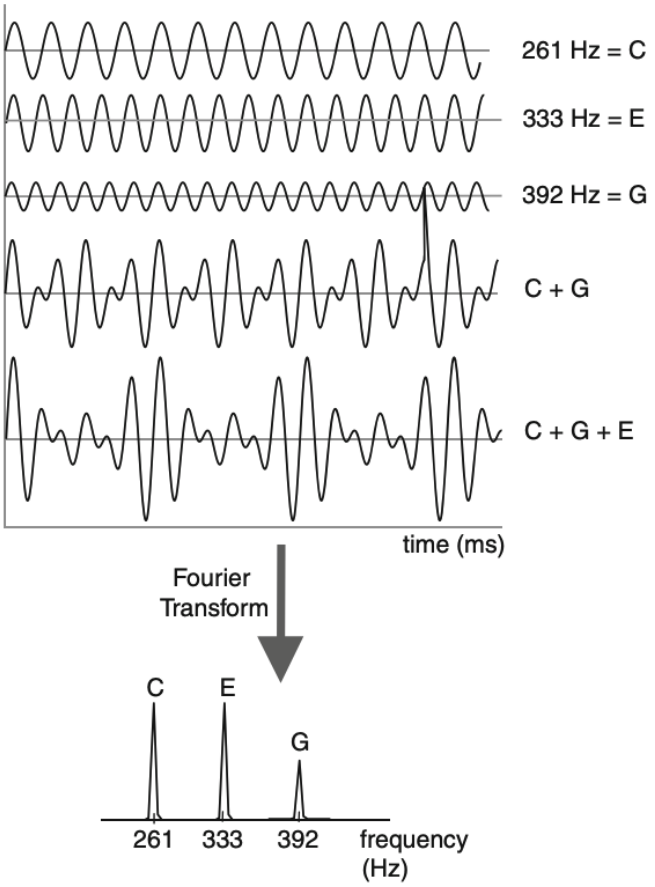


**Figure 1.8:** A graphical example of the transform from time domain to frequency domain. Three different frequencies were measured while the signals detected were displayed in the combined form: the curve of C+G+E is drawn as a function of time, which is transformed as a function of frequency with separate peaks. The figure is from (Doucleff et al., 2011).

### Chemical shift

Chemical shifts ($\delta$) are different frequencies at which nuclei spin, resulting from the shielding effect of the surrounding electrons. For a specific nucleus in a molecule, the greater the electron density and the strength of the external magnetic field, the greater the shielding on the

nucleus, and the lower its resonance frequency. In fact, the chemical shift is expressed in parts per million (ppm) that the resonance frequency and the frequency of the applied magnetic field are cancelled (Equation 1)

$$\delta = \frac{\nu_{\text{sample}} - \nu_{\text{standard}}}{\nu_{\text{spectrometer}}} \times 10^6 \tag{1}$$

Where $\nu_{\text{sample}}$ is the frequency (Hz) of the test sample, $\nu_{\text{standard}}$ is the resonance frequency (Hz) of metramethylsilane (TMS) as the standard, and $\nu_{\text{spectrometer}}$ is the specific operation frequency (MHz) of an NMR spectrometer. A million is multiplied to bring the value of the chemical shift to a reasonable number for simple expression. The chemical shift is therefore independent of the external magnetic field, and its value is standardized regardless of the spectrometer models operating at different frequencies (Simpson, 2012b).

By convention, a low chemical shift is on the right side of a spectrum, and the atom is described as more *shielded*. Whereas a higher value of ppm is displayed on the left, and the atom is more *deshielded*. Each nucleus in a molecule is imposed with different shielding environment, Hence, chemical shifts reflecting the unique environment are characteristic for molecular groups with certain atoms and structural patterns (Simpson, 2012a).

### Through-bond and through-space coupling

Besides the strength of the external magnetic field and the surrounding electrons, the spin of a nucleus is also affected by other nuclei through chemical bonds and through space. The phenomenon of through-bond coupling is called J-coupling. The frequency shift resulting from J-

coupling does not change the chemical shift of the nucleus, instead the peak is split into two or multiple peaks. The splitting patterns, as well as the amount of splitting known as J constant (in Hz), are useful in demonstrating the atomic orientations.

J-couplings are often denoted as $^{1}$J, $^{2}$J and $^{3}$J, with the superscript representing the number of bonds between the coupling spins. Sometimes couplings more than three bonds can arise when greater electron density is present, for instance, in an aromatic ring. $^{1}$J is the coupling between the geminal hydrogen and carbon, whereas $^{3}$J indicates a three-bond coupling. The magnitude of $^{3}$J implies the orientations of the vicinal spins, where the relation has been demonstrated by the Karplus relationship, a function of the $^{3}$J constant in relation to the dihedral angle between the spins. Ideally when the angle of the vicinal atoms is 90°, their orbitals are least likely to overlap, resulting in a low $^{3}$J constant; whereas 180°dihedral angle shows a high $^{3}$J constant. This relationship is in particular valuable in unravelling sugar compounds and identifying the anomers. For example, a D-Glucose have both H1 and H2 at axial positions of 180 degree ($\beta$-glucose) (Figure 1.9: A), the coupling constant is around 8 Hz, while $\alpha$-glucose with 60 degree has a smaller number of around 4 Hz (Figure 1.9: B) (Duus et al., 2001).

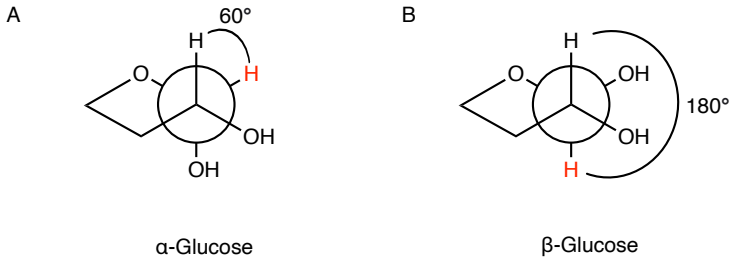


**Figure 1.9:** 60°and 180°dihedral angles between the vicinal hydrogens of H1 and H2 in $\alpha$-glucose (A) and $\beta$-glucose (B) in Newman projections, respectively. H1s attached to the anomeric carbons are marked red. The structures in A and B are only shown partially to demonstrate the angles.

The through-space coupling, or the nuclear Overhauser effect (NOE) arises when the nuclei are within a certain distance range and interact through space. The interactions are dependent on the relative orientations so that the precession of one nucleus affects the fields of the nearby nuclei. As a result, this NOE is in particular used in elucidating the molecular configurations (Simpson, 2012d).

### NMR experiments for natural product structure characterization

Bioactive natural products in brown seaweeds are organic compounds that are mainly consisted of hydrogen and carbon atoms. Hence, $^{1}$H one-dimensional (1D) as well as $^{1}$H-$^{13}$C two-dimensional (2D) NMR experiments are often used to characterize and elucidate the structures of the natural products. $^{1}$H 1D NMR experiment provides valuable information not only on the $^{1}$H chemical shifts, but also on the J-constants as discussed above. To deeply understand the structure of a rather complex natural product such as a glycerolipid, homonuclear 2D NMR experiments including $^{1}$H-$^{1}$H Correlation Spectroscopy (COSY) and $^{1}$H-$^{1}$H Nuclear Overhauser Effect Spectroscopy (NOESY), as well

as heteronuclear 2D NMR experiments including $^{1}$H-$^{13}$C Heteronuclear Single Quantum Correlation (HSQC), $^{1}$H-$^{13}$C Heteronuclear Multiple Bond Correlation (HMBC) and $^{1}$H-$^{13}$C Heteronuclear Two Bond Correlation (H2BC) are required. A 2D NMR spectrum generates cross peaks that correlate a chemical shift on one axis with a chemical shift on another axis. In a homonuclear 2D spectrum, a cross peak only refers to the signal off the diagonal; whereas in a heteronuclear 2D spectrum, any shown peaks are cross peaks (Simpson, 2012a).

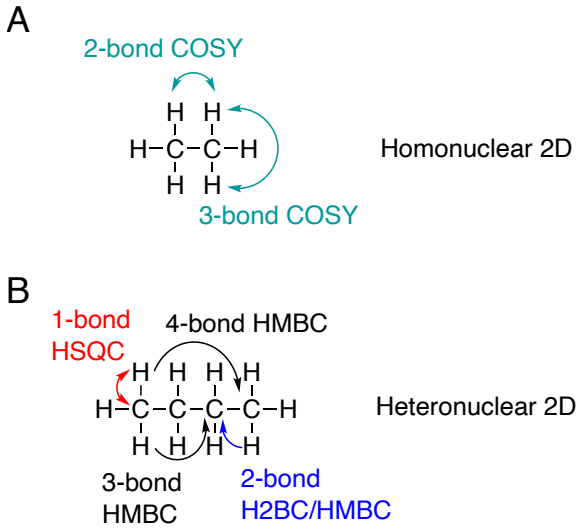


**Figure 1.10:** Homonuclear 2D NMR experiments including COSY of 2-bond and 3-bond correlation (A) and heteronuclear 2D NMR experiments including 1-bond HSQC, 2-bond H2BC, and 2-, 3- and 4-bond HMBC.

## COSY

The cross peaks in a $^{1}$H-$^{1}$H COSY spectrum indicate 2-bond or 3-bond correlations between hydrogens (Figure 1.10 A), which utilizes $^{2}$J- and $^{3}$J-coupling. As a result, the COSY experiment is often initiated to solve the molecular structure by providing unambiguous three-bond connection information (Simpson, 2012c).

### NOESY

The $^{1}$H-$^{1}$H NOESY experiment takes advantage of the NOE, providing insights on the orientations of the hydrogens. A cross peak in a NOESY spectrum means that the two hydrogens within 5 Å (Simpson, 2012d).

### HSQC

The HSQC spectrum shows cross peaks of the chemical shifts of the $^{13}$Cs and the chemical shifts of the directly attached $^{1}$Hs to the carbons (Figure 1.10 B). This one-bond correlation utilizes $^{1}$J of the J-coupling. The chemical shifts are characteristic for the specific functional groups, in this work even for the compound classes when the major components including carbohydrates, glycerolipids and polyphenols are known to be present in the brown seaweeds. The moieties of these components are annotated in Figure 1.11.

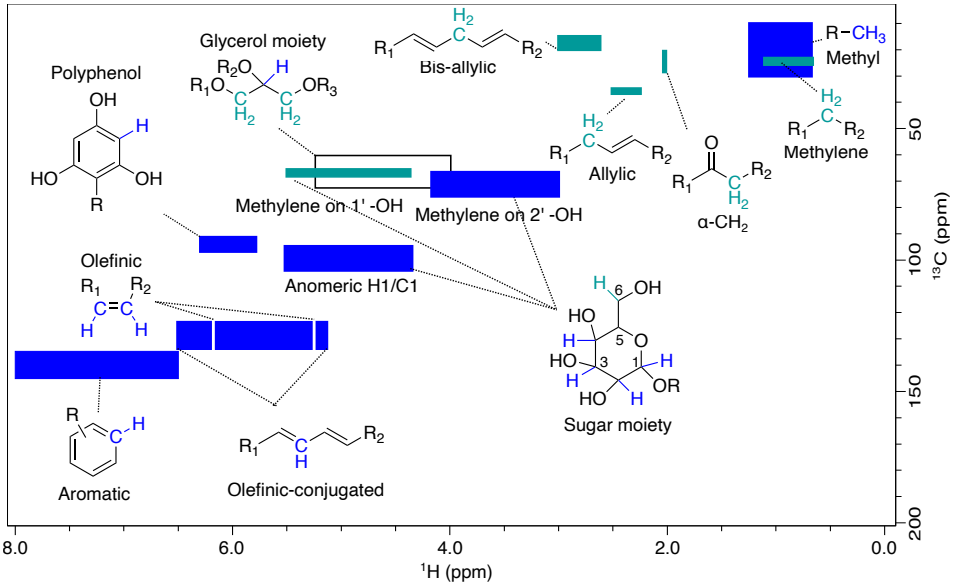


**Figure 1.11:** $^{1}$H and $^{13}$C chemical shifts of the representative moieties including unsaturated fatty acid chain, sugar, glycerol and polyphenolic moieties (Alexandri et al., 2017; Bubb, 2003; Duus et al., 2001; Simpson, 2012b; Society, 2022). CH and $CH_3$ groups are in blue whereas $CH_2$ groups are in green. The region in the open rectangle spans the chemical shifts of both CH and $CH_2$ groups in a glycerol moiety depending on the effects from radicals $R_1$, $R_2$ and $R_3$. The regions pointing to a sugar moiety are marked in accordance with the numbering convention of a pyranose, however, the sugar can also be a furanose.

### H2BC and HMBC

The HMBC and H2BC experiments are both 2D heteronuclear experiments which correlate hydrogens to the carbons that are not directly connected (Figure 1.10 B). The HMBC spectrum can show cross peaks between $^{1}$Hs and $^{13}$Cs that are up to 5 bonds away, and is in particular useful in correlating a hydrogen to a quaternary carbon that is not indicated in an HSQC spectrum. However, it does not distinguish the possibilities of $^{2}$J and longer-range couplings (Simpson, 2012c). COSY or H2BC technique is used prior to the HMBC experiment to connect neighboring atoms. The H2BC provides information only between $^{1}$Hs

and the $^{13}$Cs that are three bonds away, and is commonly applied to solve the linkages within a sugar moiety in an unambiguous manner, starting from the anomeric hydrogens (Petersen et al., 2006).

# 2 Aims of the Study

The principle objective of this study was to investigate the potential of biologically active natural products from the brown seaweed species *A. esculenta* and *S. latissima*. DMBA assay and enzyme inhibition assays including $\alpha$-amylase and collagenase were used to measure the total phlorotannin contents and the bioactivity, respectively. A bioassay-guided approach was applied to direct the fractionation process of the seaweed extract for the subsequent characterization. The specific aims were:

1. To compare crude extracts of *A. esculenta* and *S. latissima* in terms of their total phlorotannin contents and their enzyme ($\alpha$-amylase and collagenase) inhibiting effects;
2. To generate $\alpha$-amylase inhibiting fractions and to identify m/z ratios that may represent active compounds in these fractions using a bioassay-guided fractionation scheme combining QToF LC-MS;
3. To characterize the fractions containing the compounds of the identified m/z ratios by employing NMR spectroscopy and $\alpha$-amylase inhibition assay methods.

# 3 Materials and Methods

## 3.1 Materials

The two brown seaweed species, *A. esculenta* and *S. latissima*, were obtained from Seaweed Solutions (SES). The *A. esculenta* and *S. latissima* were cultivated at SES Seaweed's farm at Frøya (N63° 42.279' E8° 52.232') in the periods of January 6th, 2020–May 11th, 2020 and January 17th, 2020–May 19th, 2020. They were harvested and placed into 1000 L tanks with circulating seawater and vacuum-packed and frozen at the processing factory at Hitra (HitraMat). The frozen seaweeds were delivered to NTNU on June 9th, 2020. Approximately 500 g of each frozen seaweed sample were treated with enzyme NovoZymes' Cellic® CTec2 (gift from NovoZymes) and lyophilized (Martin Christ Beta 1-8 LD plus, Edwards vacuum pump type E2M18) (Jacobsen, 2021). A seaweed extract from the previous Mar3Bio project that had shown amylase inhibiting potential was obtained as a reference inhibitor for comparison.

The deionized $H_2O$ was Milli-Q ultra pure water. The methanol (≥99.8%), n-hexane (≥95%) ethanol (96%), glacial acetic acid and hydrochloric acid were of analytical grade and were purchased from VWR Chemicals. The deuterate methanol-*d4* (≥99.8 atom % D) was purchased from Merck Life Sciences (Sigma-Aldrich). The HPLC-graded solvents MeCN (≥99.8%) and $H_2O$ were purchased from VWR. The 2,4-dimethoxybenzaldehyde (DMBA) (≥99.8%) was purchased from Merck Life Sciences (Sigma-Aldrich). The Amberlite XAD-16 resin was purchased from Alfa Aesar™ (Thermo Fischer Scientific). The Sephadex® LH-20 resin was purchased from Merck Life Sciences (Cytiva). The EnzChek™ Gelatinase/Collagenase Assay Kit (# E12055, Invitrogen™) and the EnzChek™ Amylase Assay Kit (# E33651, Invitrogen™) were purchased from Thermo Fischer Scientific. The

$\alpha$-amylase from Bacillus sp. (Type II-A) was purchased from Merck Life Sciences (Sigma-Aldrich).

## 3.2 Extraction

### 3.2.1 Small-scale extraction

Approximately 1 g of dried *A. esculenta* and *S. latissima* materials were each covered with 10 mL of the extracting solvent of absolute methanol or 70% (v/v) ethanol, and placed into the ultrasonicator for 5 min. Each extraction was repeated 7 times and the extract was decanted through a filter paper (Whatman 113, 30 µm). Each clear extract was rotary evaporated under vacuum and stored at -20 °C for subsequent uses.

### 3.2.2 Large-scale extraction

Approximately 35 g of dried *A. esculenta* was extracted with a total of 2.45 L absolute MeOH using the same procedures as for the small-scale extraction. The clear extract was rotatory evaporated under vacuum and stored at -20 °C for subsequent uses.

### 3.2.3 Bulk-scale extraction for mass-targeting fractionation

Approximately 20 g of dried *A. esculenta* was added with 50 mL of absolute methanol and ultrasonicated for 5 min. The extract was decanted and the homogeneous extract was directly used for preparative HPLC fractionation described in Section 3.3.2.

## 3.3 Fractionation

The fractionation scheme is shown in Figure 3.1.

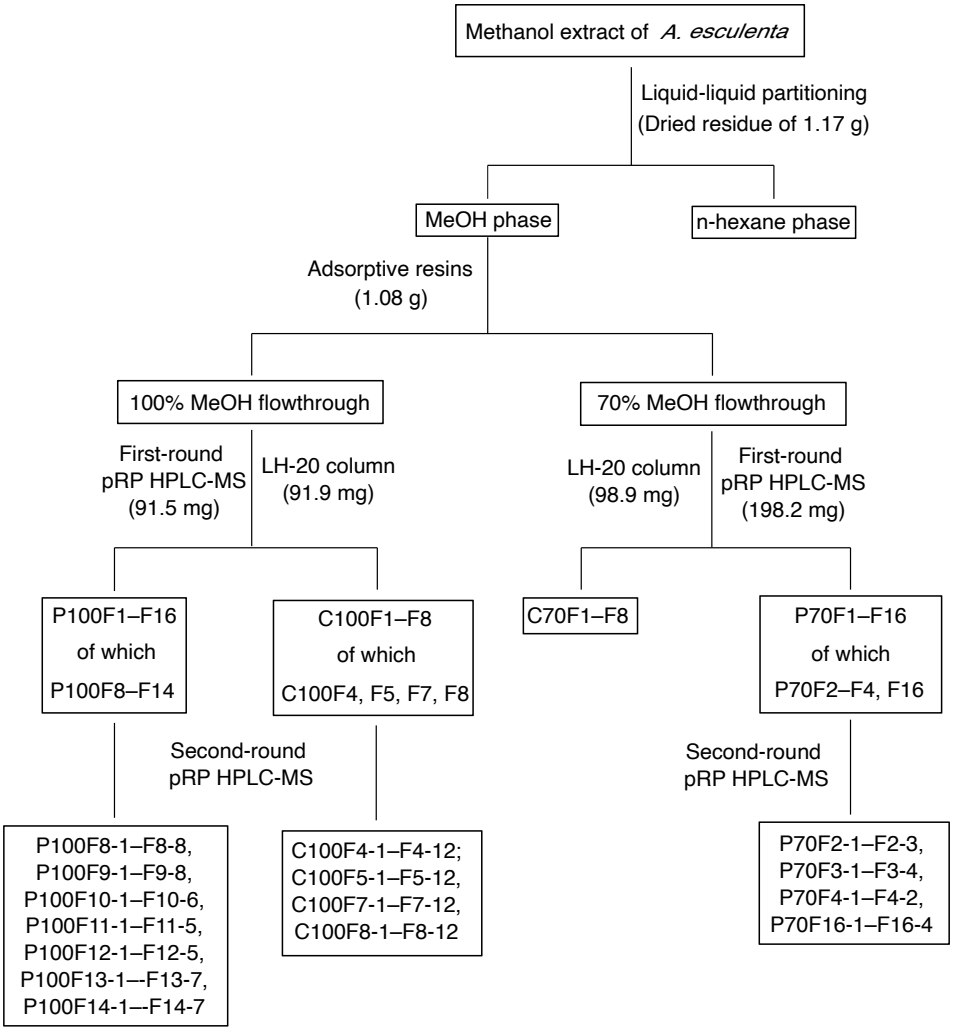


**Figure 3.1:** The fractionation scheme. The extract and fractions were indicated in the rectangles, whereas the separation techniques were next to the branches. pRP HPLC-MS = preparative reversed phase HPLC-MS.

### 3.3.1 Bioassay-guided fractionation

A series of bioassay-guided fractionation experiments including liquid-liquid partitioning, separation through adsorptive macroporous resins, and Sephadex® LH-20 column chromatography were conducted at

NTNU in Trondheim, Norway. Bioassays performed on the fractions were described later in Section 5.2.

**Liquid-Liquid partitioning** The dried residue (1.17 g) of the crude methanol extract of *A. esculenta* was dissolved in 250 mL absolute methanol and added with the same volume of n-hexane in a 1 L separation funnel. After shaking for multiple times, the n-hexane were separated from the methanol phase. The process of adding n-hexane to the methanol solution was repeated 5 times until the n-hexane phase showed no color. Both n-hexane and methanol solutions were rotary evaporated under vacuum and the dried residues were stored at -20 °C.

**Separation through adsorptive macroporous resins** Approximately 50 g of prewetted Amberlite XAD-16 macroporous resins were soaked in aqueous methanol and poured onto a Büchner funnel (Capacity of 500 mL) connected to a vacuum setup. Preconditioning of the resins was done by loading absolute, 70% (v/v) and finally 50% (v/v) methanol in order to wash the resins. The dried residue (1.08 g) of the methanol phase from liquid-liquid partitioning step was dissolved in 50 mL of 50% (v/v) methanol and loaded onto the resins. The resins were thoroughly flushed with 200 mL 70% followed by the same volume of absolute methanol for 4 times. The collected solutions were lyophilized and the residues were stored at -20 °C.

**Sephadex® LH-20 column chromatography** Portions of the dried residues of the 100% (v/v) flowthrough and 70% (v/v) flowthrough that weighed 91.9 mg and 98.9 mg, respectively, were dissolved in approximately 2 mL of absolute methanol and subject to column chromatography with a stationary phase of Sephadex® LH-20. The packed column was connected to a GE ÄKTA Start protein purification sys-

tem where the signals of each fraction were detected by a UV-detector (at wavelength of 280nm). The fractions from 70% flowthrough and 100% flowthrough were denoted as C70F1–8 and C100F1–8, respectively (Figure 3.1). Each fraction was lyophilized and the residues were stored at -20 °C.

### 3.3.2 Preparative RP HPLC-MS fractionation

Preparative reversed-phase (RP) HPLC-MS was performed on an Agilent 1260 infinity LC system (Agilent Technologies) with a diode array detector (190–900 nm), connected to a mass spectrometer with an electrospray source at Aalborg University in Aalborg, Denmark. The dissolved samples were separated on a Vydac 208TP510 5 $\mu$m C8 column or a Gemini 5 $\mu$m C6-Phenyl 110 Å column using a flow rate of 20 mL/min with a linear gradient of water ($H_2O$) and acetonitrile (MeCN), both added with 0.1% (v/v) formic acid. The gradient started at 10%, 25%, 40%, 50% or 70% MeCN, increasing to 100% over 7, 12 or 10 min and held for 5 min.

**First-round fractionation of the resin fractions** Portions of the lyophilized residues of the 100% and 70% flowthrough fractions from adsorptive macroporous resins that weighed 91.5 mg and 198.2 mg, respectively, were dissolved in approximately 2.5 mL MeCN and separated on a C8 column using a flow rate of 20 mL/min with a gradient starting at 25% MeCN and 75% $H_2O$ for the 100% flowthrough, and a gradient starting at 50% MeCN and 50% $H_2O$ for the 70% flowthrough. Fractions were collected every minute while the gradient increased to 100% MeCN in 12 min and held for 5 min, with a total of 16 fractions generated from each resin fraction. The fractions from 100% flowthrough were denoted as P100F1–16, and the fractions from 70% flowthrough as P70F1–16 (Figure 3.1).

**Second-round fractionation of the first-round fractions** The lyophilized residues of the first-round fractions, P100F8–F14, P70F2–4 and P70F16, were dissolved in MeCN and separated on a C8 column using a flow rate of 20 mL/min. For fractions P100F10, P70F2, P70F3 and P70F4, the gradient started at 25% MeCN and 75% $H_2O$, increased to 100% MeCN in 12 min and held for 5 min; for fractions P100F8, P100F9, P100F13, P100F14 and P70F16, the gradient started at 50% MeCN and 50% $H_2O$, increased to 100% MeCN in 12 min and held for 5 min; whereas for fractions P100F11 and P100F12, the gradient started at 70% MeCN and 30% $H_2O$, increased to 100% MeCN in 12 min and held for 5 min. The fractions were automatically collected according to the input masses (identified from QToF LC-MS described in Section 3.3.3), which were detected by the hyphenated MS apparatus. The second-round fractions were denoted as P100F8-1–F8-9, P100F9-1–F9-8, P100F10-1–F10-6, P100F11-1–F11-5, P100F12-1–F12-5, P100F13-1–F13-7, P100F14-1–F14-7, P70F2-1–F2-3, P70F3-1–F3-4, P70F4-1–F4-2, and P70F16-1–F16-4 (Figure 3.1).

**Second-round fractionation of column fractions** The lyophilized residues of the column fractions C100F4, C100F5, C100F7 and C100F8 that weighed 7.2 mg, 3.2 mg, 8.6 mg and 2.7 mg, respectively, were dissolved in approximately 500 $\mu$L MeCN and separated on a C8 column using a flow rate of 20 mL/min with a gradient starting at 40% MeCN and 60% $H_2O$. Fractions were collected every minute while the gradient increased to 100% MeCN in 7 min and held for 5 min, with a total of 12 fractions generated from each column fraction. The fractions were denoted as C100F4-1–F4-12, C100F5-1–F5-12, C100F7-1–C100F7-12, and C100F8-1–F8-12 (Figure 3.1).

**Mass-targeting fractionation** The homogeneous extract from bulk-scale extraction (Section 3.2.3) was separated on a C6-Phenyl column

using a flow rate of 20 mL/min with a gradient starting at 25% MeCN and 75% $H_2O$, increasing to 100% MeCN in 10 min and held for 5 min. The fractions were automatically collected according to the input masses (identified from QToF LC-MS described below), which were detected by the hyphenated MS apparatus. The MS data were processed with MZmine version 2.53 after conversion into .mzXML files.

### 3.3.3 QToF LC-MS

QToF LC-MS was performed on a Bruker compact ESI-qTOF mass spectrometer connected to a Hitachi LaChrome Elite HPLC at Aalborg University in Aalborg, Denmark. The dissolved sample was injected and separated on an Ascentis Xpress 2.7 $\mu$m C18 column using a flow rate of 1.2 mL/min with a linear gradient of $H_2O$ and MeCN, both added with 0.1% (v/v) formic acid. The gradient was initiated at 1% MeCN, increasing to 100% over 10 min and held for 5 min. The MS data were processed with MZmine version 2.53 after conversion into .mzXML files.

The samples include 100% and 70% flowthrough fractions from the adsorptive macroporous resins (Section 3.3.1), fractions from column chromatography and fractions from preparative RP HPLC, of which each dried residue was dissolved in approximately 100 $\mu$L methanol.

## 3.4 Bioassays

### 3.4.1 DMBA assay

DMBA assay was performed on a Tecan microplate reader (Infinite M200) following the general procedure described previously (Stern et al., 1996) with modifications. Equal volumes of DMBA (2%, m/v) and HCl (6%, v/v) both in glacial acetic acid were mixed to prepare

the work solution. 190µL of this solution was mixed with 10 $\mu$L of 50 mg/mL seaweed extract dissolved in glacial acetic acid in a 96-well transparent plate and the absorbance of the reaction was recorded at 510 nm at 12 time points with an interval of 10 minutes. The stable absorbance data at the 3599.9 s was used to determine the total phlorotannin content, based on a regression equation in the phloroglucinol calibration curve (concentrations of 0.013, 0.0063, 0.0031, 0.0016, 0.00078 and 0 mg/mL). The total phlorotannin content was thus expressed as mg phloroglucinol equaivalents/g dry residue.

The dried residues of the crude extracts, the fractions from liquid-liquid partitioning (Section 3.3.1), the fractions from macroporous resin fractionation (Section 3.3.1), and the fractions from column chromatography were subject to DMBA assay. For each seaweed sample except the ones from column chromatography, the absorbance was measured in triplicate. Microsoft Excel was used for calculations of average and standard deviation of the TPhCs.

### 3.4.2 Collagenase inhibition assay

Collagenase inhibition assay was performed on a Tecan microplate reader (Infinite M200) set for excitation at 485 ± 10 nm and emission detection at 530 ± 15 nm using EnzChek$^{TM}$ Gelatinase/Collagenase Assay Kit following the manufacturer's instructions. In short, 20 $\mu$L of 1 mg/mL substrate solution, 100 $\mu$L of 0.4 U/mL collagenase solution, and 80 $\mu$L of 15 mg/mL seaweed crude extract were mixed in a well of a 96-well black plate. A substrate control (20 $\mu$L substrate + 180 $\mu$L buffer), positive control (20 $\mu$L substrate + 100 $\mu$L enzyme + 80 $\mu$L buffer), and inhibitor control (20 $\mu$L substrate + 100 $\mu$L enzyme + 80 $\mu$L of 1mM 1,10-phenanthroline) were included. The fluorescence was recorded at room temperature at 12 time points with an interval of 10 minutes. The fluorescence intensity was expressed in arbitrary units,

and the fluorescence of the substrate control was subtracted from each value. The subtracted values at the time point of 3599.9 s were used for % inhibition calculation (Equation 2)

$$\% \text{ Inhibition} = \frac{\text{fluorescence of positive control} - \text{fluorescence of inhibitor}}{\text{fluorescence of positive control}} \times 100 \tag{2}$$

where the fluorescence of inhibitor were either from the reference inhibitor or the seaweed extracts.

### 3.4.3 $\alpha$-amylase inhibition assay

$\alpha$-amylase inhibition assay was performed on a Tecan microplate reader (Infinite M200) or a Tecan microplate reader (Spark 20M) set for excitation at 485 ± 12 nm and emission detection at 520 ± 12 nm using EnzChek$^{TM}$ amylase assay kit following the manufacturer's instructions. 20 $\mu$L of 0.5 mg/mL or 1 mg/mL substrate solution, 100 $\mu$L of 0.08 U/mL $\alpha$-amylase solution, and 80 $\mu$L of 1.2 mg/mL, 1.6 mg/mL, 6mg/mL, or of 1/10 of the dissolved seaweed samples were mixed in a well of a 96-well black plate. A substrate control (20 $\mu$L substrate + 180 $\mu$L buffer), positive control (20 $\mu$L substrate + 100 $\mu$L enzyme + 80 $\mu$L buffer), and negative control (20 $\mu$L substrate + 100 $\mu$L enzyme + 80 $\mu$L of 10 mg/mL reference inhibitor) were included. The fluorescence was recorded at room temperature at 12 time points with an interval of 10 minutes. The fluorescence intensity was expressed in arbitrary units, and the fluorescence of the substrate control was subtracted from each value. The subtracted values at the time point of 3599.9 s were used for % inhibition calculation (Equation 2).

**The crude extracts and resin fractions** Following the general procedure, the dried crude extracts, and the dried residues of the 100%

and 70% flowthrough from adsorptive macroporous resins of a final concentration of 6 mg/mL were subject to $\alpha$-amylase inhibition assay performed on a Tecan microplate reader (Infinite M200).

**The column fractions** Following the general procedure, the dried residues of the column fractions C100F1–F8 and C70F1–F8 of a final concentration of 1.2 mg/mL were subject to $\alpha$-amylase inhibition assay performed on a Tecan microplate reader (Infinite M200).

**The first- and second-round fractions** The lyophilized residue of each fraction generated from first-round fractionation of the resin fractions (Section 3.3.2), from second-round fractionation of the first-round fraction (Section 3.3.2) and from second-round fractionation of the column fractions (Section 3.3.2) were dissolved in 500 $\mu$L methanol, and 1/10 (100 $\mu$L) of the volume was taken out. 80 $\mu$L of the 100 $\mu$L was subject to the $\alpha$-amylase inhibition assay based on the general procedure. The assay experiments were performed on a Tecan microplate reader (Spark 20M).

**Mass-targeting fractions** Following the general procedure, the lyophilized residues of MF1–MF11 fractions (Section 3.3.2) of a final concentration of 1.6 mg/mL were subject to $\alpha$-amylase inhibition assay performed on a Tecan microplate reader (Infinite M200).

## 3.5 NMR experiments

NMR spectra were recorded at 25 °C on a Bruker Avance III 600 MHz spectrometer equipped with a 5 mm Z-gradient CP-TCI (H/C/N) TCI cryoprobe or a Bruker AV-IIIHD 800 MHz spectrometer equipped with a 5 mm CP-TCI z-gradient cryoprobe at NTNU in Trondheim, Norway. The NMR data were processed with Bruker TopSpin version

3.6.3. The following experiments were conducted: 1D proton (zg30), 1D proton with water suppression (noesygppr1d), 2D In-phase COSY (ipcosygppr-tr), 2D NOESY (noesyesgpph), 2D $^{13}$C HSQC with multiplicity editing (hsqcedetgpsisp2.3), 2D H2BC (h2bcetgpl3pr) and 2D HMBC with suppression of one-bond correlations (hmbcetgpl3nd). P1 was calibrated for each sample. $^{1}$H and $^{13}$C chemical shifts were internally referenced to the residual methanol signal.

**Crude extracts** Approximately 11 mg of the dried methanol extract of *A. esculenta*, 12 mg of the dried ethanol extract of *A. esculenta*, 14 mg of the dried methanol extract of *S. latissima*, and 14 mg of the dried ethanol extract of *S. latissima* were each dissolved in 500 $\mu$L of deuterate methanol-*d4* in a 5 mm NMR tube. NMR data of the four samples were recorded at 25 °C on a Bruker Avance III 600 MHz spectrometer. 1D proton (zg30) and 2D $^{13}$C HSQC with multiplicity editing (hsqcedetgpsisp2.3) experiments were conducted.

**Mass-targeting fractions** The mass-targeting fractions MF1–M11 with the approximate masses of 0.3 mg, 0.2 mg, 0.3 mg, 0.9 mg, 0.7 mg, 3.2 mg, 2.8 mg, 0.2 mg, 2.1 mg, 1.1 mg and 2.3 mg, respectively, were each dissolved in approximately 180 $\mu$L of deuterate methanol-*d4* in a 3 mm NMR tube. NMR data were recorded at 25 °C on a Bruker AVIIIHD 800 MHz spectrometer. The performed experiments include: 1D proton (zg30), 1D proton with water suppression (noesygppr1d), 2D In-phase COSY (ipcosygppr-tr), 2D NOESY (noesyesgpph), 2D $^{13}$C HSQC with multiplicity editing (hsqcedetgpsisp2.3), 2D H2BC (h2bcetgpl3pr) and 2D HMBC with suppression of one-bond correlations (hmbcetgpl3nd).

# 4 Results

## 4.1 Comparison of the crude extracts of the two species from two solvents on their bioactivities

The seaweed materials were treated with enzymes before they were subject to the extraction process. *A. esculenta* and *S. latissima* were each extracted with absolute methanol and 70% (v/v) ethanol. The four small-scale crude extracts were tested for $\alpha$-amylase and collagenase inhibition, and measured for their total phlorotannin contents (Table 4.1).

**Table 4.1:** Bioactivity data from the methanol and ethanol extracts of *A. esculenta* and *S. latissima*. Yields (%) of the dried extract residues relative to the dry weight of seaweed are displayed. $\alpha$-amylase and collagenase inhibition assays were carried out once for each crude extract. DMBA assays used to determine total phlorotannin content. *AE* = *A. esculenta*; *SL* = *S. latissima*; Me = Methanol; Et = Ethanol; TPhC = Total phlorotannin content (mg phloroglucinol equivalents/g dry residue).

| Species-Solvent | Yield | $\alpha$-amylase | Collagenase | DMBA |
|---|---|---|---|---|
| | % | % inhibition | | TPhC |
| *AE*-Me | 3.3 | 46 | 15 | 0.63 ± 0.083 |
| *AE*-Et | 8.9 | 36 | 12 | 0.54 ± 0.011 |
| *SL*-Me | 8.0 | 38 | <10 | 0.18 ± 0.061 |
| *SL*-Et | 14.0 | 23 | <10 | 0.10 ± 0.021 |
| Inhibitor control | - | 17 | 100 | - |

Higher yields of the dried residues (8.0% of the methanol extract and 14.0% of the ethanol extract) were obtained from *S. latissima* than from *A. esculenta* (3.3% of the methanol extract and 8.9% of the ethanol extract). In terms of the extracting solvents, 70% (v/v)

ethanol produced more extracts compared to methanol. All four extracts exhibited as active or higher $\alpha$-amylase inhibition ability than the reference inhibitor which was suspected active, with the methanol extract of *A. esculenta* showing the highest of 46% inhibition. This extract also had the greatest TPhCs. *A. esculenta* generally indicated a better performance on the DMBA assay, where the methanol and ethanol extracts showed 5-6 times of the TPhCs than the extracts of *S. latissima*. Collagenase inhibition was observed on *A. esculenta* extracts but not on *S. latissima* extracts, with the methanol extract of *A. esculenta* exhibiting slightly higher inhibition of 15% than the ethanol extract of 12%.

HSQC NMR data of the crude extracts were recorded and used to compared the functional group and compound types found within each extract (Figure 4.1).

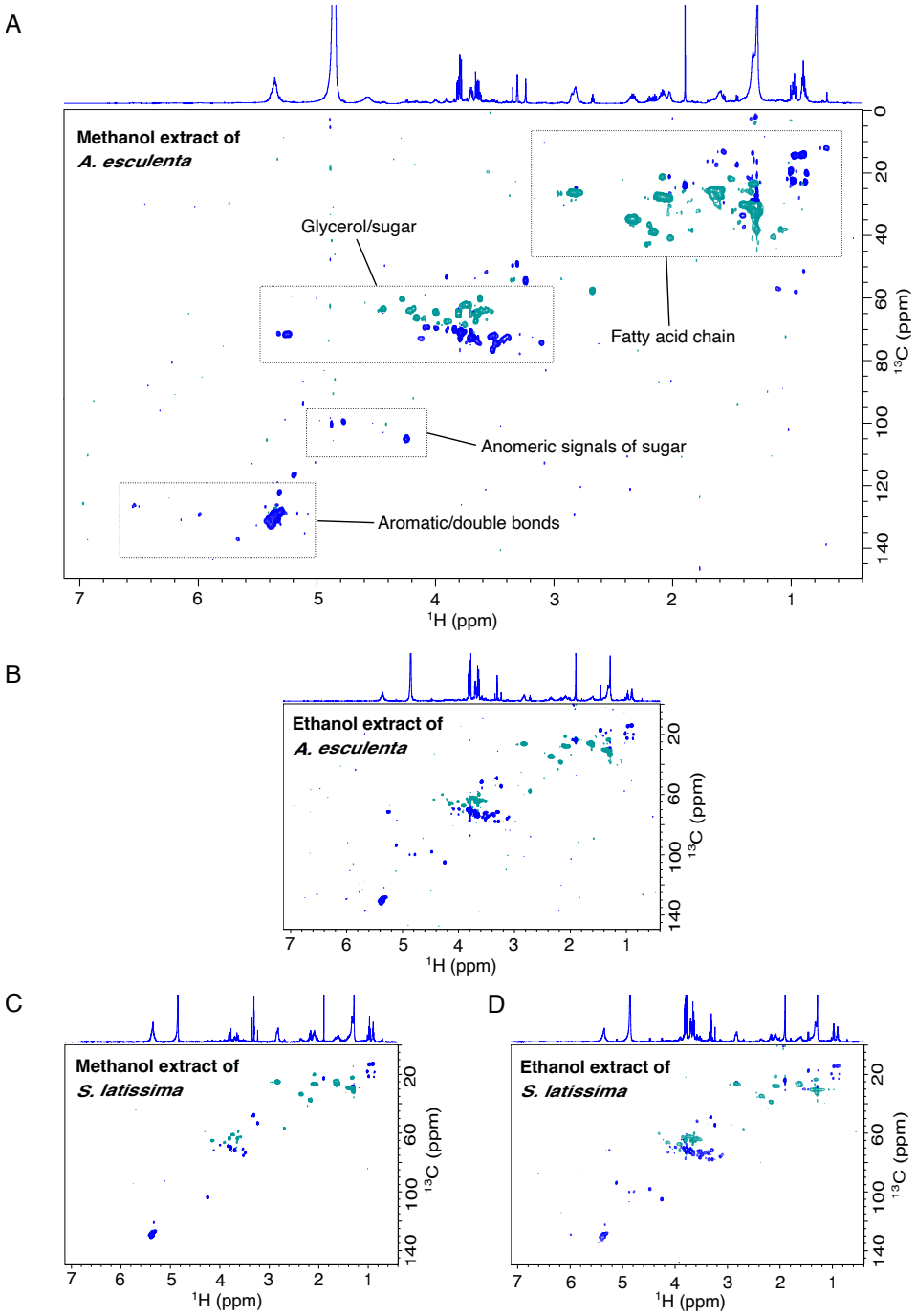


**Figure 4.1:** $^{1}$H/$^{13}$C HSQC spectra of the four crude extracts: methanol extract of *A. esculenta* (A) where general compound classes are annotated in the dotted rectangles; 70% ethanol extract of *A. esculenta* (B); methanol and 70% ethanol extract of *S. latissima* (C and D, respectively). $^{1}$H spectrum was displayed on top. CH or $CH_3$ groups are represented in blue, and $CH_2$ groups in green.

Although the crude extracts showed differences in enzyme inhibition and their TPhCs, the HSQC profiles were rather similar. Signals in the range of $\delta_H$ 0.8–3.0 and $\delta_C$ 10–40 were consistent with methyl and methylene groups in alkyl groups like those in fatty acid chains. $\delta_H$ 3.0–5.3 and $\delta_C$ 55–80 were indicative for the sugar or glycerol groups; the more shielded signals at around $\delta_H$ 4.0–5.0 and $\delta_C$ 100 pointed to the anomeric signals in a glycosidic linkage. The most shielded signals in the spectrum at $\delta_H$ 5.0–5.3 and $\delta_C$ 110–130 were due to the delocalization effect, and were consistent with double bonds or aromatic groups.

Based on its relatively better inhibition performances on both $\alpha$-amylase and collagenase assays, as well as its greatest amounts of phlorotannins, *A. esculenta* was selected as the species to be extracted by absolute methanol for the large-scale extraction and the further fractionation scheme.

## 4.2 Bioassay-guided fractionation scheme

The large-scale 100% methanol extract of *A. esculenta* was first purified using liquid-liquid partitioning to remove lipid components. The lipid-reduced methanol phase was subsequently separated through the adsorptive macroporous resins to generate two fractions differing in their polarities: a less polar 100% (v/v) methanol flowthrough, and a more polar 70% (v/v) methanol flowthrough. Both fractions were subject to column chromatographic fractionation (Figure 3.1). The bioactivity of the fractions from each step was monitored using the enzyme inhibition assays and the DMBA assay (Table 4.2; Figure 4.2).

**Table 4.2:** $\alpha$-amylase and collagenase inhibition and the total phlorotannin content of the fractions generated from the liquid-liquid partitioning and adsorptive macroporous resins. $\alpha$-amylase inhibition assays were tested once each time. MeOH = Methanol; TPhC = Total phlorotannin content (mg phloroglucinol equivalents/g dry residue).

| | Fractions | DMBA | $\alpha$-amylase |
|---|---|---|---|
| | | TPhC | % Inhibition |
| Solvent partitioning | 100% MeOH phase | 3.1 ± 0.04 | |
| | n-hexane phase | 1.5 ± 0.05 | |
| Macroporous resin | 100% MeOH flowthrough | 0.97 ± 0.006 | 58 |
| | 70% MeOH flowthrough | 0.039 ± 0.007 | 13 |

The TPhC in the methanol phase was higher than in the n-hexane phase. The two fractions through macroporous resins were tested for their bioactivities: the 100% methanol flowthrough indicated a much greater amount of TPhC and a better $\alpha$-amylase inhibiting ability than the 70% flowthrough. Both flowthrough fractions underwent the next fractionation step of column chromatography, and the TPhC and percent inhibition for $\alpha$-amylase were determined for each of the chromatographic fractions (Figure 4.2).

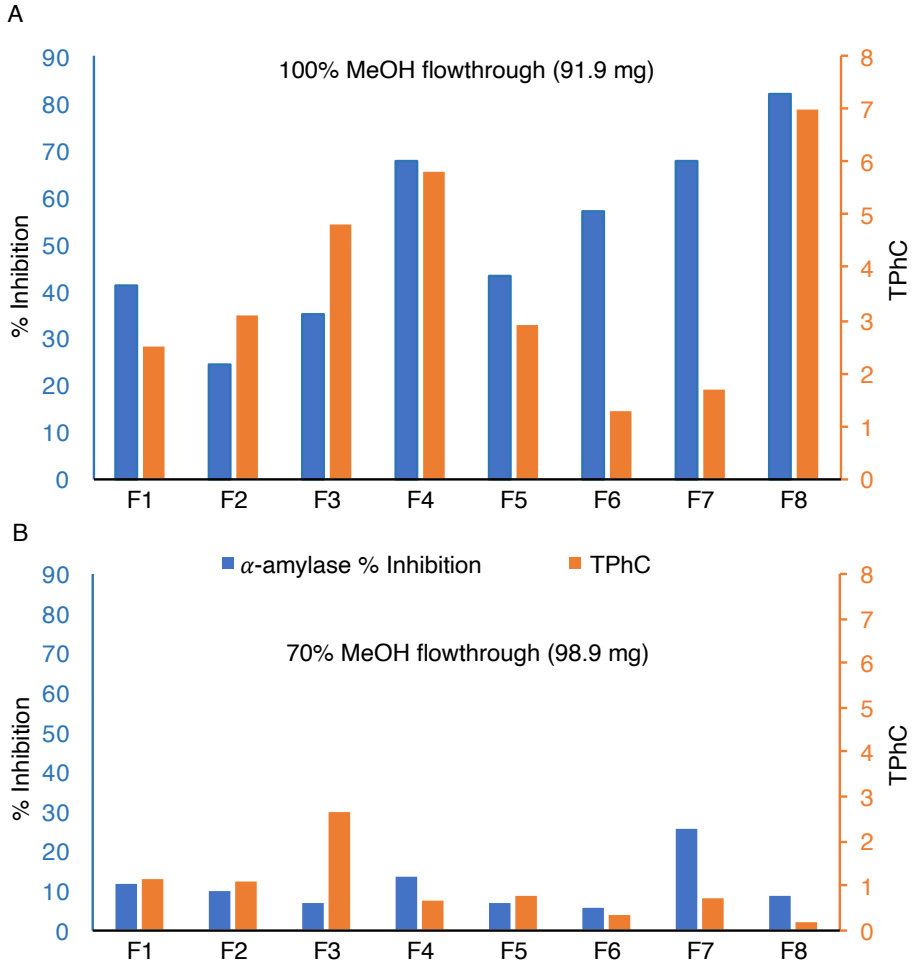


**Figure 4.2:** Comparison of TPhC and the $\alpha$-amylase % inhibition of the LH-20 column fractions for both the 100% methanol flowthrough (A) and the 70% methanol flowthrough (B). Both assays were only tested once for each fraction. MeOH = Methanol; TPhC = Total phlorotannin content (mg phloroglucinol equivalents/g dry residue).

The tested bioactivities of 100% fractions were generally higher than those of 70% fractions. From 100% methanol chromatographic fractions, the highest TPhC and percent inhibition were observed in F8, followed by fraction F4. F7 also showed high suppression on the en-

zyme, yet with relatively low content of phlorotannins; whereas F5, the next fraction eluted after F4, performed relatively good in both of the bioassay tests besides F8. F3 and F7 from the 70% flowthrough exhibited noticeably higher TPhC and better inhibition effect, respectively. Hence, these fractions were selected for the subsequent fractionation scheme.

## 4.3 Fractionation scheme in search for m/z ratios from $\alpha$-amylase inhibiting fractions

Because the 100% and 70% methanol flowthrough fractions exhibited $\alpha$-amylase inhibitions, they were both fractionated in two courses (Figure 3.1): the proportion that was subject to column chromatography was further separated by preparative HPLC, and several masses that potentially represent the active compounds in the enzyme-inhibiting fractions were marked using the QToF LC-MS tool; The rest of the proportions were directly subject to preparative HPLC followed by another round of preparative HPLC, and the fractions from both rounds were analyzed by QToF LC-MS to confirm the marked masses. m/z ratios were only identified and presented in Figure 4.3 when they appeared in the active fractions until the last round of separation.

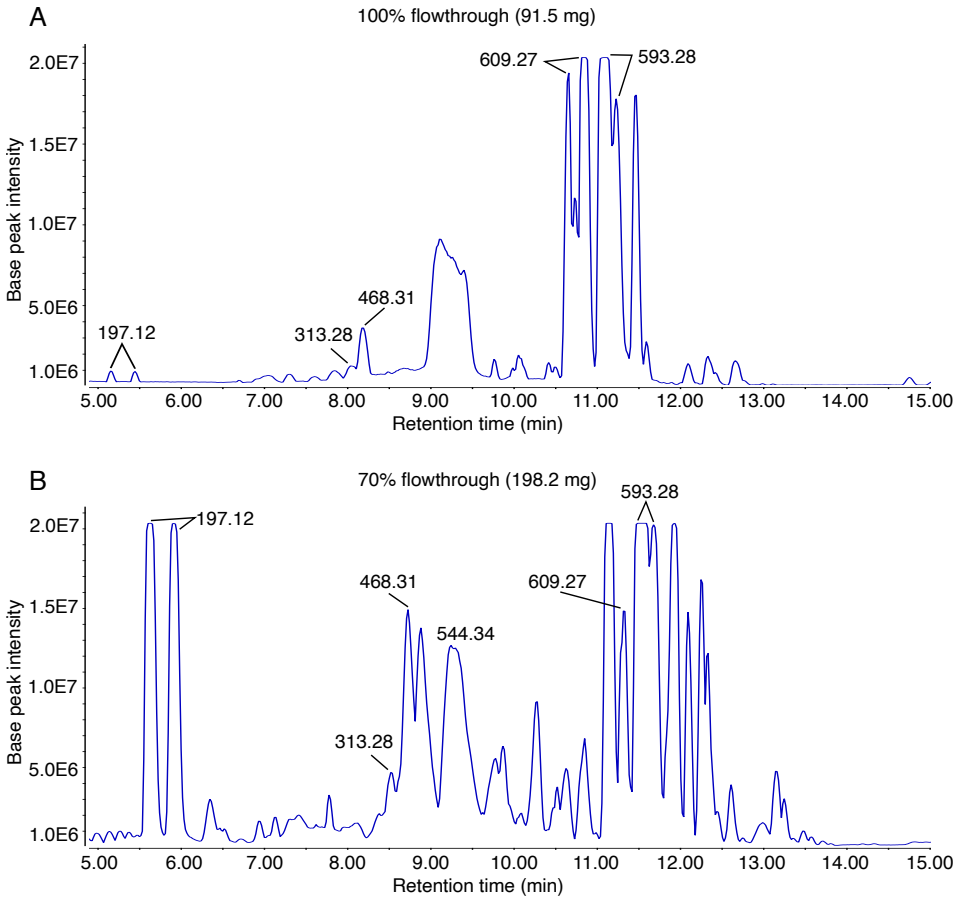


**Figure 4.3:** Common m/z ratios that were found in the amylase-inhibiting fractions from each step of mass-identifying fractionation process of the 100% methanol flowthrough (A) and 70% methanol flowthrough (B) fractions.

### 4.3.1 Active fractions containing an ion with m/z ratio of 197.12

The mass with an m/z ratio of 197.12 appeared in the active fractions after two-round separation of the 100% methanol flowthrough: C100F5 and P100F10 from the first-round separation; and C100F5-3, C100F5-4 and P100F10-1 fractions from the second-round fractionation (Figure 4.4 A).

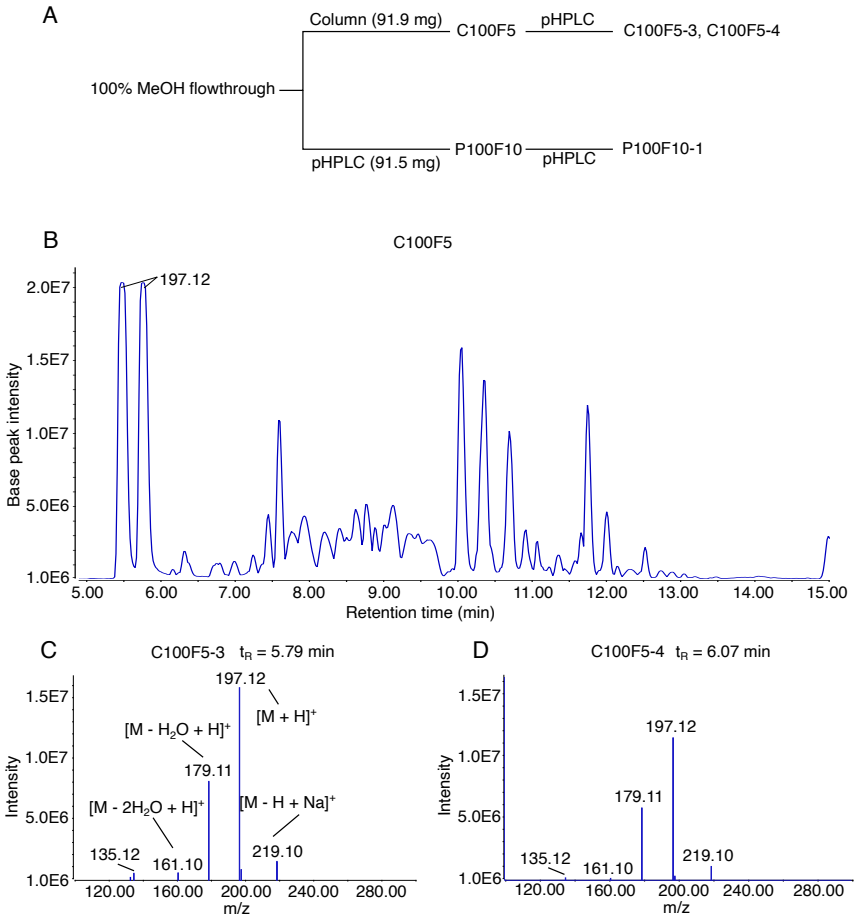


**Figure 4.4:** The chromatogram of the column fraction C100F5 (A) and the spectra of C100F5-3 (B) and C100F5-4 (C), the two fractions from C100F5. m/z ratio 197.12 were found in these fractions. Fragments of this compound were proposed as $[M–2H_2O+H]^+$, $[M–H_2O+H]^+$ and $[M + Na]^+$ (B). $t_R$ = Retention time; pHPLC = preparative HPLC.

### 4.3.2 Other m/z ratios identified in active fractions

Other compounds or fragments with the masses of 609.27, 593.28, 313.28, 468.31 and 544.34 (m/z ratios) were pinpointed in the same manner as 197.12 was. The MS spectra of the latest fractions which

had these masses were shown in Figure 4.5.

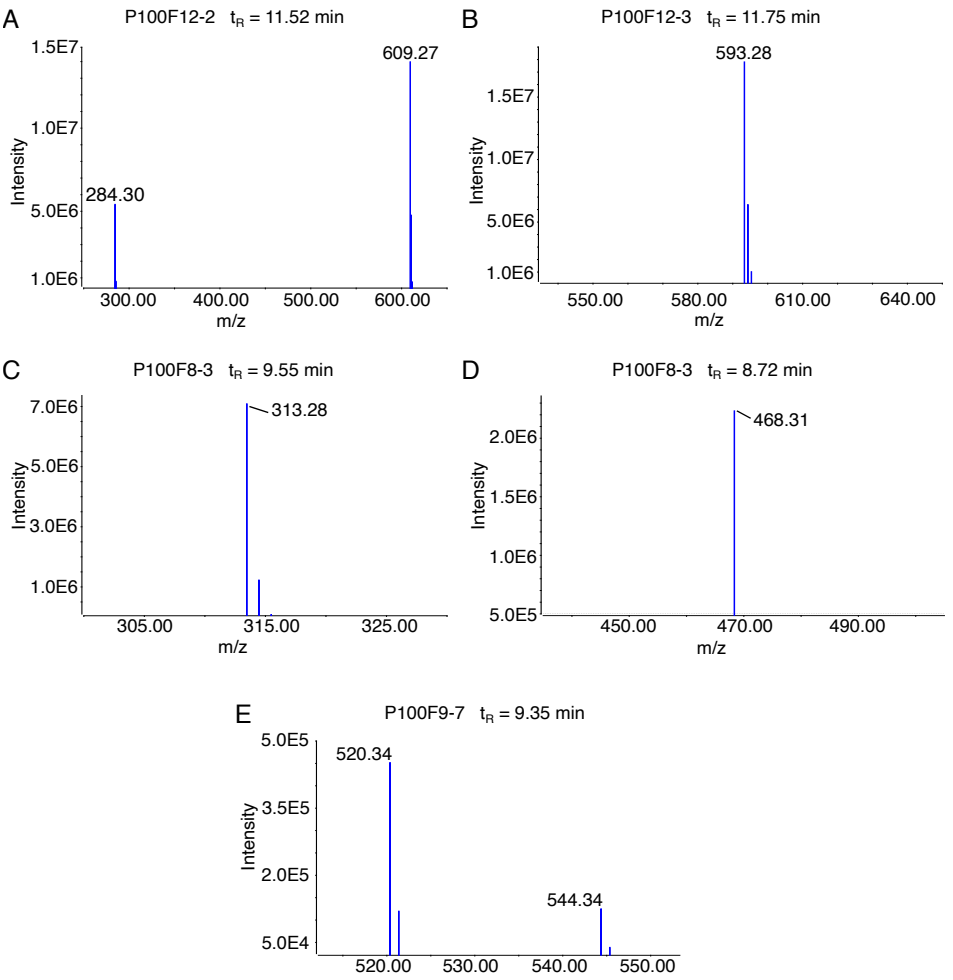


**Figure 4.5:** The MS spectra of the second-round fractions containing the compounds/ions with the masses of 609.27, 593.28, 313.28, 468.31 and 544.34 (m/z ratios). $t_R$ = Retention time.

The peak at 609.27 (m/z) was always accompanied with a less intense signal at 284.30 representing the adduct ion of the compound (Figure 4.5 A). Similarly, the spectra of the P100F8-3 fractions always showed

another peak at 520.34 next to the targeted signal of 544.34 (Figure 4.5 E). The compounds with masses of 593.28, 313.28 and 468.31 were only observed with the major peaks that were common in the fractions throughout the fractionation process (Figure 4.5 B, C and D).

## 4.4 Characterization and comparison of the enzyme inhibiting fractions with the targeted masses

The bulk methanol extract of *A. esculenta* was fractionated through preparative HPLC based on the identified masses. The simultaneous analytical HPLC-MS provided the basis for this mass-targeting fractionation, and thus each fraction was collected in a period of retention time that included the compound of the desired mass. The major m/z ratios in each fraction were obtained through analytical HPLC-MS, and the bioactivity in inhibiting $\alpha$-amylase of the fractions was compared (Table 4.3).

**Table 4.3:** Summary of the mass-targeting fractions MF1-MF11. The m/z ratios presented were the major ones observed from the corresponding chromatogram of each fraction. $t_R$ = Retention time; aHPLC-MS = analytical HPLC-MS.

| Compound/ Major moiety type | Fraction ID | $t_R$ (min) | aHPLC-MS | Amylase |
|---|---|---|---|---|
| | | | m/z | % Inhibition |
| (+)-epiloliolide | MF1 | 4.9 - 5.2 | 197; 279 | 16 |
| Loliolide | MF2 | 5.3 - 5.5 | 197; 279 | 24 |
| Glycerolipid | MF3 | 6.4 - 6.8 | 567; 279 | 39 |
| Glycerolipid | MF4 | 7.4 - 7.7 | 313; 279 | <10 |
| Glycerolipid | MF5 | 8.1 - 8.3 | 468 | <10 |
| Glycerolipid | MF6 | 8.3 - 8.6 | 542 | <10 |
| Glycerolipid | MF7 | 8.6 - 9.2 | 544 | <10 |
| Lipid | MF8 | 10.8 - 10.9 | 611 | <10 |
| Glycerolipid | MF9 | 11.1 - 11.4 | 609 | 17 |
| Glycerolipid | MF10 | 12.5 - 13.0 | 593 | 27 |
| Glycerolipid | MF11 | 13.8 - 14.5 | 564; 567; 279 | <10 |

The extracted 197, 313, 468, 609 and 593 from analytical HPLC-MS were believed to match with the 197.12, 313.28, 468.31, 609.27 and 593.28, respectively, obtained from QToF LC-MS analyses (Figure 4.3), as there were no numerically close numbers that could be mistaken in the corresponding retention time periods despite the fact that the analytical HPLC-MS was of lower resolution that the m/z ratios were determined as integers (Allen and McWhinney, 2019).

However, the MF6 containing the compound with a m/z ratio of 542 was separated due to the initial setting prior to the fractionation that the m/z ratio tolerance was set as ± 2. In addition, the $[M\text{-}H+Na]^+$ adduct giving a m/z ratio of 566 combining the ± 2 tolerance resulted in the separation of fractions MF3 and MF11 showing a 567. Similarly, MF8 containing major compound with a m/z ratio 611 was obtained, as the number was within the range of 609 + 2.

When the fractions were tested with their $\alpha$-amylase inhibition abilities, the fractions containing the compounds with the determined m/z ratios were active, except the fractions MF4 containing the compound with its mass of 313, and MF7 of 544. Whereas the fractions consisting of the compounds with their m/z ratios only selected because of the tolerance setup and the instrumental decision were all inactive, except the fraction MF3 showing 567.

Other major m/z ratios including 279 and 564 observed in MF1–MF4 and MF11 were indicative for the presence of impurities in the fractions.

### 4.4.1 Characterization of loliolide and (+)-epiloliolide

Compound 1: loliolide and compound 2: (+)-epiloliolide were identified from MF2 and MF1 fractions, respectively through 1D and 2D NMR experiments.

#### Loliolide

Compound 1 isolated from MF2 with a m/z ratio of 197 ($C_{11}H_{16}O_3$) was structurally elucidated as loliolide through HSQC, COSY and HMBC experiments (Figure 4.6, Table 4.4).

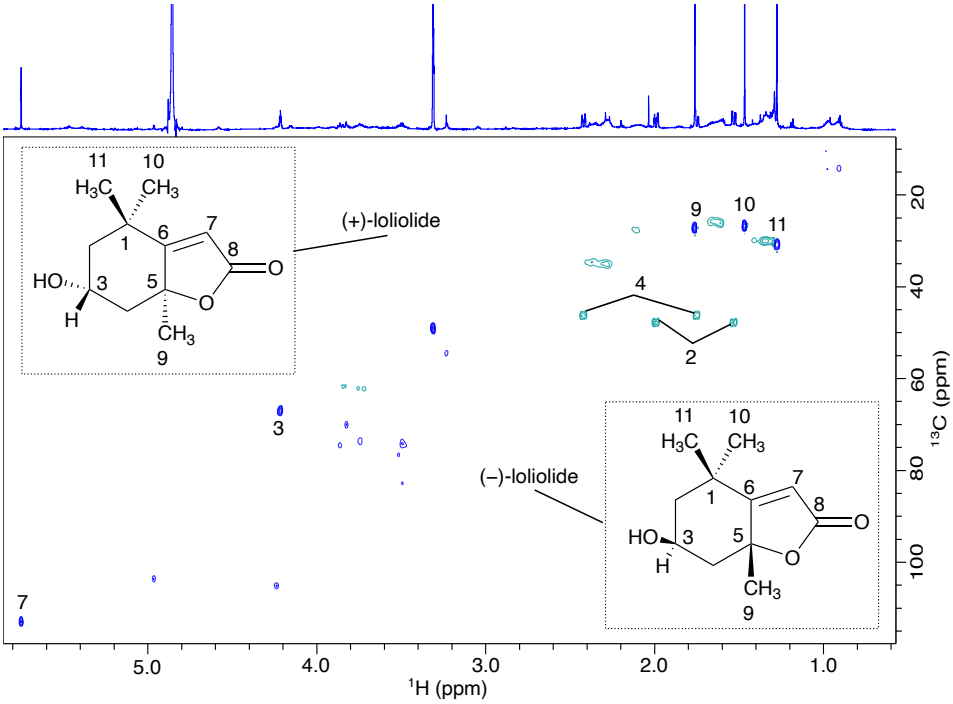


**Figure 4.6:** HSQC spectrum of compound 1: loliolide with $^1$H spectrum on top. CH or $CH_3$ groups were represented in blue, and $CH_2$ groups were in green. The structures shown in the dotted rectangle are (+)-loliolide (left upper corner) and (−)-loliolide (right bottom corner).

**Table 4.4:** NMR data for compound 1: loliolide (800 MHz).

| Position | $\delta_H$ Multiplicity ($J$ in Hz) | $\delta_C$ | COSY ($\delta_H$) | HMBC | NOE |
|---|---|---|---|---|---|
| 1 | - | 37.1 | - | - | - |
| 2 | 1.54 dd (14.4, 3.7) | 47.4 | H2 (2.00), H3 | C11, C1, C6, C10 | H3 |
| | 2.00 dt (14.5, 2.6) | | H2 (1.54), H11, H10 | | - |
| 3 | 4.22 qu (3.4) | 67.3 | H2 (1.54), H4 (2.43) | - | H2, H4 |
| 4 | 1.77 dd (13.4, 3.6) | 46.1 | H4 (2.43) | C5 | - |
| | 2.43 dt (13.4, 2.6) | | H4 (1.77), H3 | - | - |
| 5 | - | 88.5 | - | - | - |
| 6 | - | 185.4 | - | - | - |
| 7 | 5.76 s | 113.1 | - | C5, C8 | - |
| 8 | - | 173.8 | - | - | - |
| 9 | 1.78 s | 27.2 | - | C4, C6 | - |
| 10 | 1.48 s | 26.5 | H2 (2.00), H11 | C11, C1, C2, C6 | - |
| 11 | 1.28 s | 31.2 | H2 (2.00), H10 | C10, C1, C2, C6 | - |

From the HSQC spectrum (Figure 4.6), functional groups including three methyl groups (9, 10 and 11), two methylene groups (2 and 4), a secondary alcohol group (3) and a double bond signal (7) were identified.

COSY correlations from the two methylene hydrogens H2 and H4 to the primary alcohol hydrogen H3 indicated that H2 and H4 are neighboring hydrogens of H3. The connections were confirmed in the NOESY spectrum indicating that H2, H4 and H3 were in close spatial proximity (Figure 4.7 B). In addition, both methyl hydrogens H10 and H11 are in vicinal positions of H2. Partial fragment of a chain attached with one hydroxyl and two methyl groups was therefore obtained.

Up to 4-bond longer range correlations from the chain was identified through the HMBC experiment. H10 and H11 showed two-bond correlations to the quaternary carbon of C1, and three-bond correlations to C6 quaternary carbon and the methylene carbon C2. Protons of the methyl group H9s were more deshielded and were connected to the quarternary carbon at C5 based on HMBC correlations to C4, C5, and the quaternary carbon C6. Besides the three groups of methyl hydrogens, correlations to C6 were also observed from the two methylene hydrogens H2. From these correlations as well as the very deshielded effect on C6, the double bond was shown to be in a ring structure, where the other end of the double bond was confirmed by the 1H and 13C chemical shifts at the 7 position, neighboring the carbonyl carbon C8. The 3-bond correlation from H3 ($\delta_{\mathrm{H}}$ 1.77) to the quaternary carbon C5, and from H9 to C4 demonstrated the second ring of the lactone structure.

The m/z ratio of 197 ($[\mathrm{M}+\mathrm{H}]^{+}$) and the chemical shifts of the identified structure were consistent with the compound loliolide based on

previous literature (Mori and khlebnikov, 1993; Silva et al., 2021). In fact, the conformation of the loliolide could be either (+)-loliolide or (−)-loliolide, differing in the orientations of the hydroxyl group at 3 position and the methyl groups attached at C5 position. In addition, signals in the sugar and lipid region were observed in the HSQC spectrum, suggesting the impurity of fraction MF2.

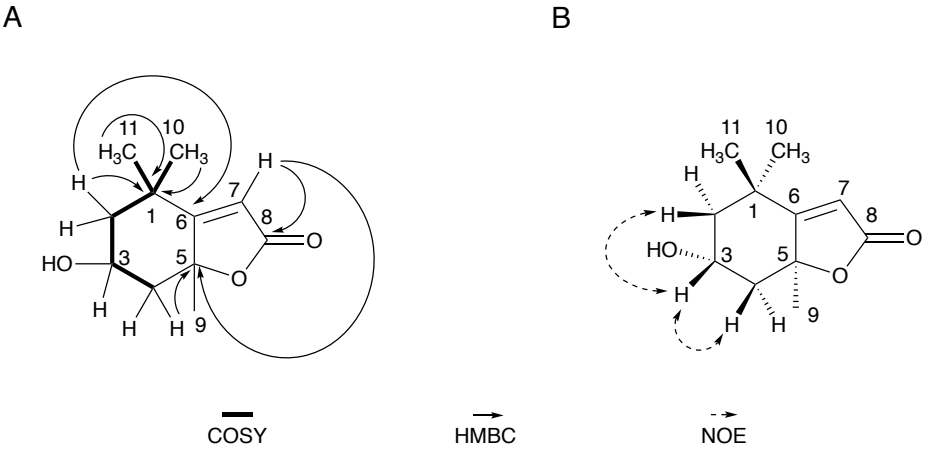


**Figure 4.7:** HMBC (A) and NOE (B) correlations of compound 1 loliolide. In this figure, (+)-loliolide is demonstrated. HMBC correlations from a hydrogen to a carbon are represented with single-sided arrows, whereas NOE correlations between hydrogens are represented with double-sided, dashed arrows.

## (+)-epiloliolide

Compound 2 isolated from MF1 with the same m/z ratio of 197, the same functional groups from HSQC spectrum and HMBC correlations (Table A.1) was indicated as an isomer of loliolide. $^{1}$H and $^{13}$C shifts as well as the corresponding multiplicity information were consistent with literature (da Silva Mota and Costa, 2021; Kimura and Maki, 2002; Mori and khlebnikov, 1993; Silva et al., 2021), confirming the identity of compound 2 as an isomer of loliolide with its hydroxyl group at the equatorial position and the methyl group 9 at the axial position

with a recognized name of (+)-epiloliolide (Figure 4.8).

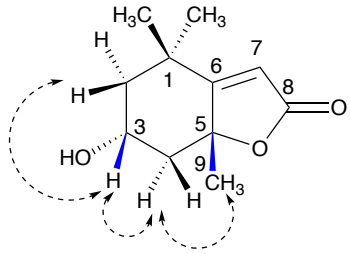


**Figure 4.8:** The structure of compound 2 (+)-epiloliolide. NOE correlations (Table A.1) between hydrogens were visualized by the double-sided, dashed arrows. H3 and H9 are highlighted with blue color, demonstrating their axial orientations.

Its configuration was solved based on $J$-coupling constants and the chemical shifts (Table A.1). The multiplicity of H3 in compound 2 appeared to be a triplet of triplets with the coupling constants $J$ = 11.6 and 4.2 Hz (Appendix 1D NMR figure), characterizing an axial position of H3. The fact that the methyl hydrogen H9 ($\delta_{\mathrm{H}}$ 1.60) in compound 2 was more shielded than that in compound 1 ($\delta_{\mathrm{H}}$ 1.78) was evident for the axial positions of this $CH_3$ group, because the effect of 1,3-diaxial interactions from the hydroxyl group would give more chemical shift of H9 as in compound 1 ($\delta_{\mathrm{H}}$ 1.78) (Kimura and Maki, 2002). An additional NOE spatial correlation between the equatorial hydrogen H5 and the axial hydrogen H3 was observed in (+)-epiloliolide compared to loliolide (Figure 4.8).

### 4.4.2 Characterization of glycerolipid and $\beta$-galactolipid moieties

Glycerolipid and $\beta$-galactolipid were characterized in MF6 fraction. Other sugar, glycerol, and lipid moieties that were observed with clear H2BC, HMBC and COSY correlation were presented as well (Figure

4.9 and Figure 4.10).

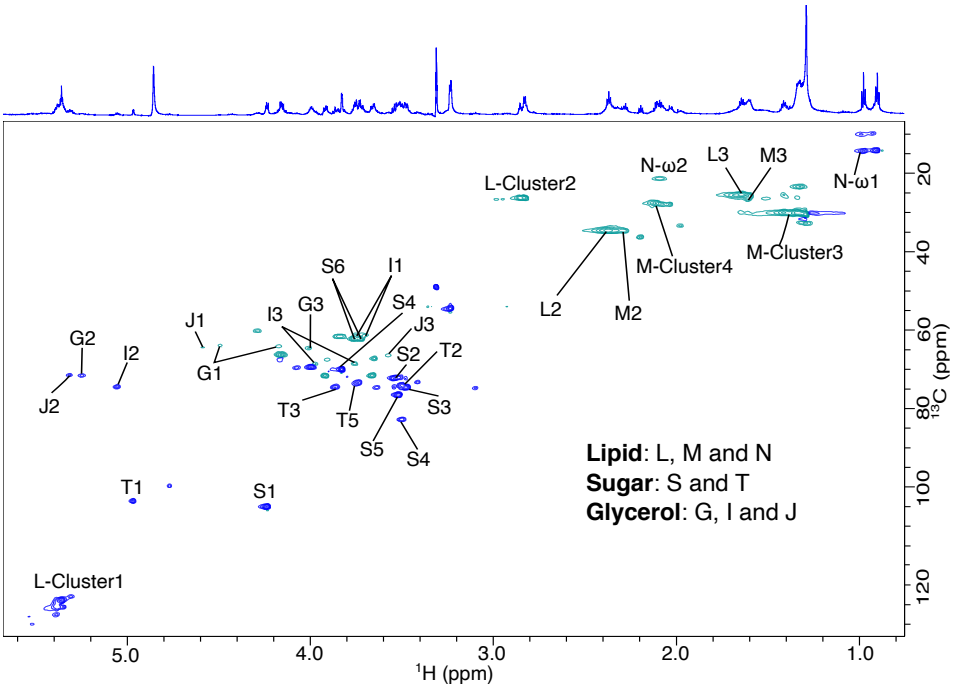


**Figure 4.9:** HSQC spectrum of the fraction MF6. Glycerol moieties G, I and J, sugar moieties S and T, and lipid moieties L, M and N were characterized. $^{1}H$ spectrum was displayed on top. CH or $CH_3$ groups are represented in blue, and $CH_2$ groups in green.

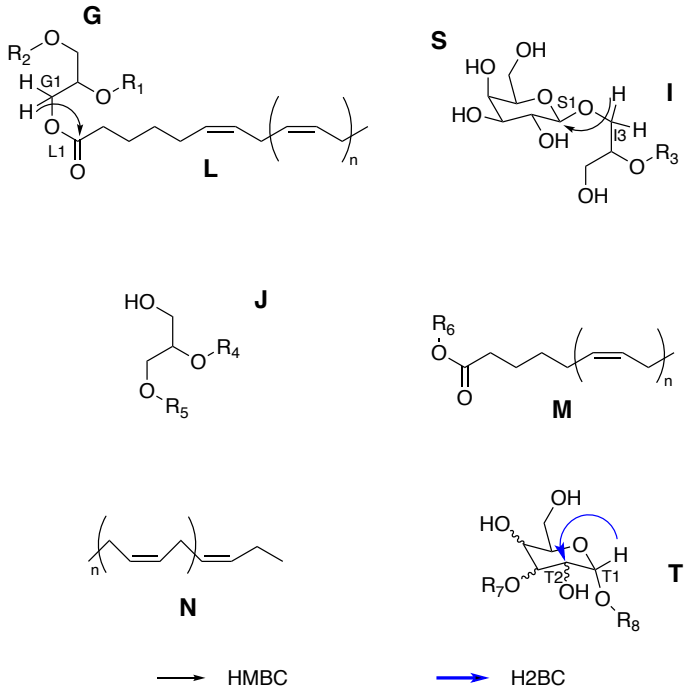


**Figure 4.10:** Characterized fragments in the fraction MF6. G, I and J are glycerol moieties, S and T are sugar moieties, and L, M and N are lipid moieties. Representative HMBC correlations connecting two moieties in the fragments and H2BC correlation from the anomeric T-H1 to T-C2 were demonstrated.

Three-bond correlations for the moieties were obtained from H2BC experiment (Table A.2). For the sugar moiety S, its anomeric proton S-H1 was correlated with S-C2, and S-H2 showed correlation to S-C3. Rest of the fragments within S was determined as well, and the structure was confirmed by observing COSY $^{1}$H-$^{1}$H vicinal correlations and up-to-four-bond correlations in the HMBC spectrum. The chemical shifts and the $J$ constant (7.7 Hz) of S-H1 revealed this sugar as a $\beta$-galactopyranose (Buedenbender et al., 2020). Two-bond correlations of sugar T, glycerol G, I, and J, and lipid L, M, and N moieties in MF6 fraction were achieved in the same manner.

While characterizing lipid moieties, the chemical shifts of the allylic,

bis-allylic and olefinic positions were difficult to differentiate that clusters instead of clear points were shown. As a result, lipid L, M and N were presented with their partial structures in the chains, among which N was characterized from the $\omega$ end, and it was observed with an $\omega$-3 chain. Furthermore, the chemical shifts of the double bond carbons were around $\delta_C$ 26, which were evident of the *cis*-configuration (Buedenbender et al., 2020) in the lipid chain (Figure 4.10).

HMBC correlation from the glycerol G-H1 to the lipid L-C1 demonstrated the connection of the two moieties, suggesting a glycerolipid fragment. Although no HMBC correlations were observed to the glycerol G-C2 and G-C3, the chemical shifts were indicative for more shielded effects likely from another esterified fatty acid chain and sugar(s), respectively, suggesting a MGDG compound of which the category has been commonly observed in brown seaweeds (Buedenbender et al., 2020; Lopes et al., 2021; Lu et al., 2019; Society, 2022). Although the complete chains of the esterified fatty acids were unable to be fully solved due to clustering of NMR peaks, the characterized partial structure was indicative for repeating double bonds in the chains, suggesting the presence of PUFA, likely a $\omega$-3 type, which is also ubiquitous in brown seaweeds (Lu et al., 2019).

Another glycerol I-H1 correlated to the $\beta$-galactopyranose S-C1 three bonds away that were indicative for a $\beta$-galactolipid. Similarly to the characterization of the proposed MGDG compound, a fatty acid chain was likely connected to the oxygen atom attached on the I2 position of the glycerol I, indicating a MGMG compound (Lopes et al., 2021; Society, 2022).

For sugar moiety T, its identification was not achieved due to the overlapping signals in $^1$H spectrum that the multiplicity and the $J$-constants were not clear (Appendix figure of 1H NMR). However, the

higher chemical shift of its anomeric carbon ($\delta_H$ 4.97) was likely due to a glycosidic bond to another sugar molecule. T3 ($\delta_H$ 3.86/$\delta_C$ 74.6) also implied a more shielded environment from a more electronegative atom attached to the T3 oxygen, possibly through glycosidic linkage to another sugar (Bubb, 2003; Duus et al., 2001).

### 4.4.3 Aromatic and other signals

Many HSQC signals from MF10 overlapped with that from MF6, only MF10 showed the peaks including those that were characterized as aromatic fragments. H2BC and HMBC experiments were utilized for two-bond and longer-range bond correlations (Figure 4.11).

In HSQC spectrum, signals at around $\delta_H$ 7.1 and $\delta_C$ 130 indicated the electron delocalization effect in the moiety. The aromaticity was resolved by the HMBC correlation from A-H2 (A-H6) to the quaternary carbon A-C1 ($\delta_C$ 143.9). Hydrogens that were three bonds away were assigned through H2BC experiment, connecting from A-H2 to A-C3 and A-H3 to A-C4, and the assignments were confirmed in the HMBC spectrum. Observing 3 aromatic signals and a single quaternary carbon signal, the symmetry in the structure was clear that there was only one substituent on the benzene ring. HMBC 3-bond correlation from A-H4 to A-C7, as well as H2BC 2-bond correlations from A-H7 to A-C8 then from A-H8 to A-C9 indicated a chain fragment as the substituent. The rest of the chain structure was not characterized due to clustering in the methylene regions in the HSQC spectrum.

Besides the aromatic peaks, distinct signals at around $\delta_H$ 4.2 and $\delta_C$ 88 ppm were present in MF10. The chemical shifts often represent C-H signals in a sugar residue (for example in position 3 or 4) that are in a glycosidic linkage (Bubb, 2003; Duus et al., 2001). However, no H2BC, COSY or HMBC correlations rigorously pointed to the sugar

structures. One definite HMBC signal was observed from a hydrogen of the U-cluster5 to U-C1, explaining the higher chemical shift of the U1 affected by the olefinic U-cluster5 than that of a simple hydroxyl group. Thus, moiety U could represent the structure of a hydroxylated lipid chain, which was found in seaweed before (Lu et al., 2019).

Similarly, unambiguous H2BC and HMBC correlations from V-H2 to V-C1 and V-C3 were observed, which could be a lipid fragment of hydroxynated hydrocarbon chain (Lu et al., 2019).

HMBC correlations from U-H1 to the double bond U-cluster5 carbons, and from V-H1 to methyl and methylene carbons V-C2 and V-C3 were observed. However, no more structural information could be extracted due to the clustering in the double bond, methyl and methlene group regions.

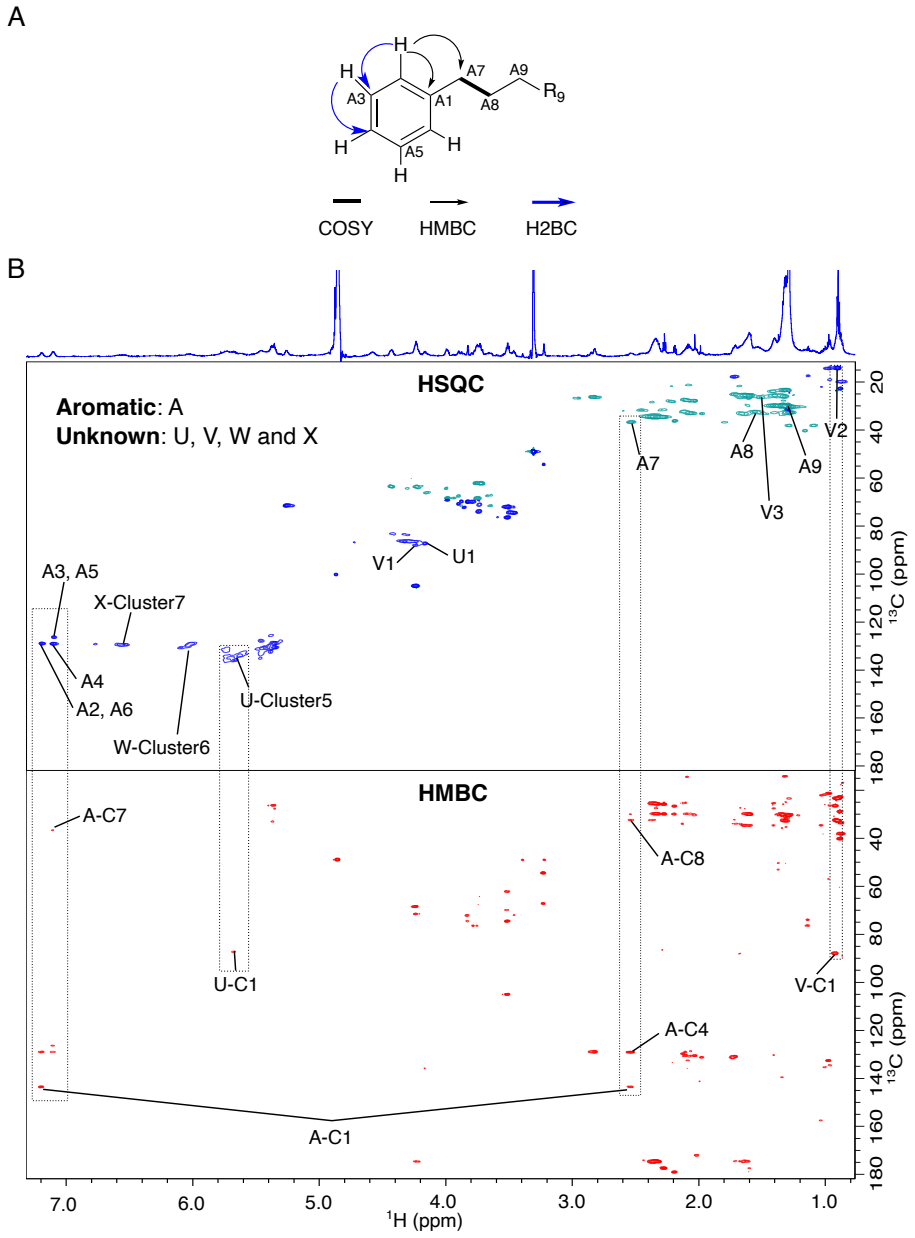


**Figure 4.11:** The structure of the aromatic moiety in MF10 and its COSY, HMBC and H2BC correlations (A). Functional groups/fragments A, U, V, W and X were demonstrated in the HSQC spectrum. HSQC and HMBC spectra were aligned vertically to show correlations within the aromatic fragments (dotted rectangles) (B).

## 4.5 Comparison of the mass-targeting fractions MF1–MF11

By overlaying the HSQC spectra, many signals overlapped in the mass-targeting fractions of MF1–MF11. Comparison was made based on the presence of the characterized moieties (Table 4.5).

Fraction MF3 shared the same moieties with MF6, however, their abilities in suppressing $\alpha$-amylase differed greatly, with MF3 showing highest inhibition while MF6 did not. MF3 was the early eluting fraction that exhibited more hydrophilic properties than MF6 did, which could be attributed to the additional sugar moieties observed in its HSQC spectrum (Figure A.2).

Fractions MF4 and MF5 had close elution times as MF6, and similar moieties excluding the glycerol I. That is, the galactoglycerol fragment including I and S was not present in MF4 or MF5, despite the presence of the sugar moiety S. MF7 with no inhibition did not have the galactoglycerol moiety, instead potential conjugated chains W and X were shown. The next eluted fraction MF8 did not show any signals in the sugar region in HSQC spectrum, and no inhibition effect was considered. Distinct from other fractions, MF9 and MF10 had moieties of U and V of which the structural details were unable to obtain. Aromatic moieties were present in both MF10 and MF11 fractions, however, MF10 exhibited relatively high inhibition whereas MF11 did not inhibit $\alpha$-amylase, with this fraction lacking U and V moieties.

Other signals in the sugar and lipid regions were observed in the HSQC spectrum of each fraction (Figure A.2–Figure A.8), however, the characterization was not achieved due to the heavy clustering in the HSQC, HMBC and H2BC spectra.

**Table 4.5:** Comparison of the mass-targeting fractions MF1–MF11 based on the characterized moieties. The fractions are listed in the order from high $\alpha$-amylase inhibition to low inhibition, among which the right columns starting from MF8 to MF6 had inhibition less than 10% and were considered inactive.

| Moiety type | Moiety ID | Fraction ID (% inhibition: high to low) | | | | | | | | | | |
|---|---|---|---|---|---|---|---|---|---|---|---|---|
| | | MF3 | MF10 | MF2 | MF9 | MF1 | MF8 | MF4 | MF11 | MF5 | MF7 | MF6 |
| Glycerol | G | ✓ | ✓ | | ✓ | | ✓ | ✓ | ✓ | ✓ | ✓ | ✓ |
| | I | ✓ | ✓ | | ✓ | | | | ✓ | | | ✓ |
| | J | ✓ | | | | | | ✓ | | ✓ | ✓ | ✓ |
| Lipid | L | ✓ | ✓ | ✓ | ✓ | | | ✓ | ✓ | ✓ | ✓ | ✓ |
| | M | ✓ | ✓ | ✓ | ✓ | ✓ | ✓ | ✓ | ✓ | ✓ | ✓ | ✓ |
| | N | ✓ | ✓ | | ✓ | | ✓ | ✓ | ✓ | ✓ | ✓ | ✓ |
| Sugar | S | ✓ | ✓ | ✓ | ✓ | | | ✓ | ✓ | ✓ | ✓ | ✓ |
| | T | ✓ | | ✓ | ✓ | ✓ | | ✓ | | ✓ | ✓ | ✓ |
| Aromatic | A | | ✓ | | | | | | ✓ | | | |
| Unknown | U | | ✓ | | ✓ | | | | | | | |
| | V | | ✓ | | ✓ | | | | | | | |
| | W | | ✓ | | ✓ | | | | ✓ | | ✓ | |
| | X | | ✓ | | ✓ | | | | ✓ | | ✓ | |

# 5 Discussion and Future Prospects

The brown seaweed species *A. esculenta* and *S. latissima* have been investigated by several studies for their nutritional values (Blikra et al., 2019; Kerrison et al., 2020; Lytou et al., 2021; Reid et al., 2013; Stévant et al., 2017), demonstrating one utilization of their biomass. There is also a growing interest in the bioactive natural products to measure the total phenolic contents (Castejón et al., 2021b; Mohammed et al., 2021b; Sapatinha et al., 2022), and evaluating the activities including the antioxidant and antifungal abilities (Andreea et al., 2010; Castejón et al., 2021b; Mohammed et al., 2021b; Ummat et al., 2020). Additionally, inhibition effect on the metabolic enzymes including $\alpha$-glucosidase, $\alpha$-amylase and collagenase have been reported (Castejón et al., 2021b; Nwosu et al., 2011; Sapatinha et al., 2022). However, not many studies have strictly characterized the compound classes responsible for the bioactivities. In this work, the TPhCs, enzyme (collagenase and $\alpha$-amylase) inhibition activities of the crude extracts from both *A. esculenta* and *S. latissima* were investigated. Through a systematic bioassay-guided fractionation scheme, the carotenoid metabolites, loliolide and its isomer were for the first time characterized from the species *A. esculenta* through QToF LC-MS and rigorous 1D and 2D NMR experiments. The compounds were believed to exhibit the bioactivity of $\alpha$-amylase inhibition, implying their antidiabetic potential. Another category of compounds present in the bioassay-positive fractions, the glycerolipids, were also partially characterized.

## 5.1 Comparison of the crude extracts from the two species and two solvents by small-scale extraction

When extracted with the same solvent, *S. latissima* had higher yield of dried crude extracts (8.0% and 14.0%) than *A. esculenta* did (3.3% and 8.9%). This difference could be attributed to the higher mineral content in *S. latissima* (Schiener et al., 2015; Stévant et al., 2017), as minerals are often present in the form of salt, which dissolves well in a polar solvent like methanol. Compared to absolute methanol, 70% (v/v) aqueous ethanol was more polar due to the water content and would result in a higher salt content in the extract, where greater amounts of the dried residues from ethanol extraction were obtained as anticipated. The variance in mineral contents could be one factor contributing to the bioactivity difference between the crude extracts: the higher proportion of the salts, the less amount of the active components while using the same mass of the dried crude extracts in the bioassays. Hence, a salt-removing step could be included before measuring the bioactivities.

The *A. esculenta* extracts showed a general trend of inhibition on both $\alpha$-amylase and collagenase as well as greater amounts of phlorotannin contents. *A. esculenta* was therefore selected for the subsequent fractionation procedures. However, *S. latissima*'s bioactive potentials should not be overlooked: the methanol and the aqueous ethanol extract of this species showed 38% and 23% inhibition on $\alpha$-amylase, which were slightly higher than the inhibitor control.

In terms of the extracting solvents, bioactivities of the methanol and ethanol extracts were not greatly different, with methanol extracts being slightly more effective in inhibiting $\alpha$-amylase and in extracting phlorotannins. The TPhC values determined by the DMBA as-

say have not been previously reported on either *A. esculenta* or *S. latissima*. However, by comparing to another brown seaweed species, *Fucus vesiculosus*, the TPhCs of the crude extracts in this study were lower than the reported $10.7 \pm 1.5$ (mg phloroglucinol equivalent/g dry residue) (Catarino et al., 2019). The variance may be due to the different brown seaweed species, and/or due to the choice of the extracting solvents as a critical factor affecting the phlorotannin amounts. Previous studies have reported that aqueous acetone is a more powerful solvent mixture in extracting phlorotannins than aqueous methanol or aqueous ethanol (Catarino et al., 2019).

Two-dimensional $^{1}$H-$^{13}$C HSQC experiments illustrating direct correlation between hydrogens and carbons were used to characterize the chemical moieties in the crude extracts. Based on the observed chemical shifts, sugars, glycerols, lipids and aromatic fragments were annotated (Figure 4.1). The presence of sugar signals in all four crude extracts could provide a source of $\alpha$-amylase inhibition, as the sugar structures may compete with the starch substrate, blocking the degradation of the substrate (Jayaraj et al., 2013). In addition, aromatic fragments could resemble polyphenolic compounds. Polyphenols rich in hydroxyl groups were proved to bind to the enzyme through hydrogen bonds to cause suppression (Jayaraj et al., 2013; Sales et al., 2012).

Generally low collagenase inhibition was considered to be related to the absence of protein or amino acids, which may have similar structures to the substrate collagen and compete with them for enzyme binding (Schönauer et al., 2017). The examples are tissue inhibitors of metalloproteinases (TIMP) and $\alpha$2-macroglobulin (Leite, 2009) and The weak suppression observed in *A. esculenta* species could be attributed to some small molecules with the ability to chelate the catalytic zinc and thus inhibiting the enzyme (Leite, 2009; Schönauer et al., 2017).

However, this hypothesis needs to be validated with further purification and characterization. Due to low collagenase inhibition activities, the assay was not used in the subsequent fractionation procedure.

Since the results from the DMBA assay suggested the presence of phlorotannins, the signals in the aromatic region of the HSQC spectrum were considered to represent their benzene ring structures. However, other chemical moieties, such as olefinic and conjugated olefinic fragments that also possess delocalized electrons, have similar $^{1}H$ and $^{13}C$ chemical shifts. In fact, some of these peaks were assigned as double bond signals using H2BC and HMBC correlations from spectral data that were analyzed later in this work.

## 5.2 Fractionation scheme

The absolute methanol crude extract of *A. esculenta* was purified through liquid-liquid partitioning, and the lipid-reduced aqueous phase was fractionated following a bioassay-guided scheme and a scheme of combining a mass-guided strategy and a bioassay-guided strategy. Through the DMBA assay on the liquid-liquid partitioning fractions, phlorotannins were approximately double amounts in the absolute methanol phase than in the n-hexane phase. Even though the methanol phase was selected for further purification, the n-hexane phase should not be overlooked. Although phlorotannins are generally polar due to the hydroxyl groups, variation in polymeric structures (Okeke et al., 2021a) could presumably result in distinct polarities that would make them dissolve in n-hexane. It is therefore worthwhile to analyze the components in the non-polar phase to investigate the presence of phlorotannins.

Both n-hexane and methanol phases exhibited higher TPhCs of 1.5 $\pm$ 0.05 and 3.1 $\pm$ 0.04 mg phloroglucinol/dry residue, respectively,

than the 0.63 ± 0.083 of the crude methanol extract (Table 4.1 and Table 4.2). An increase in TPhC after partitioning was also observed by Catarino et al. (2019) in the ethyl acetate fraction applying the same partitioning method, proving the effectiveness of this purification strategy to reduce inactive components from the aqueous phase of interest. Additionally the TPhCs can also be affected by degradation of phlorotannins. Phlorotannins belong to the category of polyphenols, and are prone to oxidative degradation. Okeke et al. (2021a) specified the influences of the external factors on the stability of phlorotannins with unpredicatable oxygen, light and temperature change. Every use of the crude extract and the fractions could be attributed to the degradation of phlorotannins.

Adsorptive macroporous resins were used to recover non-polar or less polar compounds from aqueous phases (Li and Chase, 2010), and in this work to generate two fractions differing in their polarities. The less polar 100% (v/v) methanol flowthrough showed a much higher TPhC of 0.97 ± 0.006 mg phloroglucinol equivalent/g dry residue than the 0.039 ± 0.007 of the 70% (v/v) methanol flowthrough, as well as a noticeably better $\alpha$-amylase inhibition of 58% over 13%. The TPhCs for both resin fractions, however, were not higher than that of the liquid-liquid partitioning phases (3.1 ± 0.04 and 1.5 ± 0.05 mg phloroglucinol equivalent/g dry residue), which may be that more hydrophilic phlorotannins were washed off in the 50% (v/v) methanol that was used to dissolve the dried residue after the purification, or the phlorotannins were not eluted from the resins into either the absolute or 70% (v/v) methanol. Whereas the $\alpha$-amylase % inhibition increased to 58% compared to the 46% of the crude extract, illustrating that the concentration of the active components have increased. Furthermore, the chromatograms of the two resin fractions (Figure 4.3) showed a similar pattern in terms of the identified m/z ratios. It implies that

the activity difference between the two fractions was likely due to the different proportion of each active component, and that a single eluting solvent of absolute methanol may be sufficient to concentrate the active compounds.

## 5.3 Evaluation of the mass-selection strategy

Fractionation was followed by the m/z ratios of interest in the $\alpha$-amylase inhibiting fractions. Masses were considered to represent the active compounds when they appeared in the active fractions until the last round of separation. The accuracy of the QToF LC-MS technique allowed the determination of m/z ratios up to two-demical place (Allen and McWhinney, 2019), therefore the same m/z ratios identified from the fractions were believed to represent the same compounds. At the same time, masses that were found in both active and inactive fractions were not considered interesting (Appendix).

However, this selection scheme was biased towards the active compounds present in higher concentrations, whereas the ones in low amounts were overlooked, causing a false negative result. Material loss was inevitable during the processes of two rounds of separation, which caused a low concentration of each fraction used in the $\alpha$-amylase inhibition test. The active fractions were subject to QToF LC-MS analysis, and thereby the concentration of the active compounds below the detection limit would be missed. This could explain the later observation that the mass-targeting fractions containing compounds with the identified m/z ratios of 313, 468 and 544 were inactive in the enzyme inhibition test (Table 4.3), suggesting that the signals of the actual active compounds were suppressed by the signals at these m/z ratios.

The retention time of the compounds from QToF LC-MS analyses can

be used to provided an early indication on the compound characteristics in terms of their hydrophilicity. Since the column of the QToF LC-MS was C18, more hydrophobic compounds that had higher affinity would be retained in the stationary phase and elute at a later time. For instance, loliolide and (+)-epiloliolide eluted early indicating they are more hydrophilic molecules compare to the compound with a m/z ratio of 593.28 that eluted after. This was in line with the characterized results that the fractions showing a m/z ratio of 593.28 were consisted of mainly glycerolipids with more hydrophobic properties than the fractions with loliolide and (+)-epiloliolide (Table 4.3).

## 5.4 Loliolide and its stereoisomer

### 5.4.1 Characterization of Loliolide and (+)-epiloliolide

The compounds with a m/z ratio of 197 were identified as loliolide and (+)-epiloliolide through NMR experiments (Figure 4.6 and Figure 4.8). However, the absolute configuration of loliolide was unable to be confirmed: both (+)-loliolide and (−)-loliolide exhibit similar $^{1}$H and $^{13}$C chemical shifts, multiplicity and coupling constants ($J$), as well as COSY and NOE correlations (Mori and khlebnikov, 1993). The difference between the two isomers is that the orientation of both the hydroxyl group at C3 and the methyl group attached on C5 are flipped, which is not expected to affect either the through-bond couplings or NOE in NMR. Previous works that successfully characterized loliolide from brown seaweeds often presented the compound with the structure of (+)-loliolide, yet failed to clarify its isomeric compound (−)-loliolide (Chi et al., 2021a; Kimura and Maki, 2002; Silva et al., 2021). In fact, (−)-loliolide was isolated as early as in 1938 and were reported as an ant-repellent compound and more recently as a signaling chemical in barnyardgrass–rice allelopathic interactions (Mori and khlebnikov, 1993), while (+)-loliolide were not found with these activities.

Compared to the loliolide, the conformation of (+)-epiloliolide was determined by the more shielded more deshield H9 ($\delta_{\mathrm{H}}$ 1.78), suggesting the 1-3 diaxial interactions between H3 and H9 (Kimura and Maki, 2002). Its conformational isomer (-)-epiloliolide has only been reported as a synthetic product and was never isolated from natural sources (Mori and khlebnikov, 1993). It was worth mentioning that the commonly recognized name nowadays for (−)-epiloliolide is isololioide (da Silva Mota and Costa, 2021), but it also used to represent the compound with the structure of (+)-epiloliolide (Kimura and Maki, 2002; Mori and khlebnikov, 1993).

Loliolide and (+)-epiloliolide have been isolated from the brown macroalgae species including *Sargassum crassifolium* (Kuniyoshi, 1985), *Ascophyllum nodosum* (Chi et al., 2021b), *C. spongiosus f. verticillatus* (El Hattab et al., 2008), and *Sargassum horneri* (Fernando et al., 2021). The common observation in brown seaweeds is not surprising, as their abundant carotenoid fucoxanthin can degrade into loliolide, epiloliolide, dihydroactinidiolide and others through fragmentation of the bicyclic furanoxide intermediates (Repeta, 1989). The two carotenoid metabolites have also been reported in green algae (Chung et al., 2021), plants (Colom et al., 2007; Kato-Noguchi et al., 2014; Neergaard et al., 2010) and animals (Pettit et al., 1980; Rocca et al., 1983). However, these studies did not specify the conformational isomers of loliolide, and the antioxidant, antiinflammatory and other bioactivities reported need to be carefully evaluated.

### 5.4.2 Comparison of the $\alpha$-amylase inhibiting abilities of MF1 and MF2 containing (+)-epiloliolide and loliolide, respectively

MF1 and MF2 containing (+)-epiloliolide and loliolide, respectively, both exhibited $\alpha$-amylase inhibition. These two isomers with a 6-

membered ring structure could mimic the sugar substrate of $\alpha$-amylase, and possibly compete for the active site to inhibit the enzyme (Jayaraj et al., 2013). It was proposed that the inhibition was due to hydrogen bonding, as the interactions with the residues in the active sites of $\alpha$-amylase were observed in some terpenes and terpenoids (Ghosh and Rangan, 2014; Kamble et al., 2022). The inhibition of loliolide was in line with literature where the loliolide from a plant species *Sesbania grandiflora* inhibited $\alpha$-amylase 1.2 times than the standard positive control acarbose (Thissera et al., 2020). Comparably, Pure (+)-epiloliolide was not tested with $\alpha$-amylase inhibition assay, but the similar structure to loliolide and generally to terpenoids may explain its activity.

The inhibiting ability of the MF2 fraction was higher than that of the MF1 fraction, which could be attributed to the better effect exhibited by loliolide than by (+)-epiloliolide. A study on a labdane diterpene and its derivative (Ghosh and Rangan, 2014) suggested the influence of non-bonding interactions with $\alpha$-amylase in its inhibition in addition to hydrogen-bond interactions. The conclusion provides insight into the different inhibition abilities in this work: the orientational difference of the methyl groups at position 9 between loliolide and (+)-epiloliolide may result in distinct non-bonding interactions with the enzyme, causing different inhibition effects. Furthermore, the conformation of the loliolide, whether it was (+)-loliolide or (−)-loliolide, was not specified, as discussed in Section 5.4. The orientation of the hydroxyl and methyl groups may also affect binding to the enzyme and result in distinct suppression effects. However, the presence of impurities could also contribute to the inhibition difference. Isolated or commercially available loliolide and (+)-epiloliolide were therefore necessary to exclude any interfering factors in the $\alpha$-amylase inhibition assays.

## 5.5 Glycerolipid, aromatic and other moieties in MF3–MF11

### 5.5.1 Characterization

Glycerolipid and $\beta$-galactolipid fragments, as well as other glycerol and lipid moieties from MF6 fraction were characterized through HSQC, H2BC, HMBC and COSY experiments (Figure 4.10), and MGMG and MGDG compounds were proposed.

While comparing the HSQC spectra of MF6 to that of other fractions which had similar peaks, aromatic signals were observed only in the last two fractions of MF10 and MF11. The later elutions implied more non-polar compounds in the fractions, which were likely attributed to the symmetric structure of the aromatic compounds: the benzene ring was monosubstituted with a hydrocarbon chain that were characterized until A9 (Figure 4.11). Two primary hypotheses on the identity of the aromatic compound were proposed: the compound may result from polyphenol degradation, or the phenyl structure was in the fatty acid chains.

It was discussed in Section 5.2 that phlorotannins and polyphenols are labile compounds and are sensitive to environmental oxygen, light and high temperature. In fact, the stability of polyphenols are greatly affected by their structures even without external factors. Due to the different degrees of polymerization as well as the great structural variability (Okeke et al., 2021a; Wang et al., 2014), the degraded polyphenol structures were not widely studied, with only detecting the decreased contents (Catarino et al., 2021; Okeke et al., 2021b). As a result, the formation of the monosubstituted phenyl fragments in this case would not be surprising due to dehydroxylation, ring opening and other possible degradation reactions (Cao et al., 2021; Sağdıçoğlu Celep et al., 2013). It was reported that the more hydroxyl groups on polyphenols,

the less stable they were (Wang et al., 2014). Furthermore, interactions with other components such as proteins, pigments and carbohydrates affect the stability: new compounds with unpredictable structures may form under different environmental conditions (Cao et al., 2021).

Considering the abundant lipid signals in MF10 and MF11's HSQC spectra, it was also hypothesized the aromatic fragment could belong to a fatty acid with a terminal benzene ring. Although not reported in seaweeds, $\omega$-phenyl fatty acids were found in the plants including the orders Acorales and Alismatales (Meija and Soukup, 2004; Ohlrogge et al., 2018). As many natural products were common in plants and brown seaweeds including carbohydrates and carotenoids, phenyl-terminated fatty acids discovered in plants could be present in brown seaweeds as well. However, further characterization of the compound is certainly necessary to validate the hypothesis.

From MF9 and MF10's HSQC spectra, W and X signals were in the allylic region, only more shielded. Although not in brown seaweeds, conjugated eicosapentaenoic acid and conjugated arachidonic acid were found in red seaweed (Narayan et al., 2004). As a result, it was hypothesized that W and X represented conjugated double bond in the lipid chains.

### 5.5.2 Comparison of the $\alpha$-amylase inhibiting abilities of MF3–MF11

HSQC, H2BC and HMBC cross peaks from the MF6 fraction were used as a reference for comparison to other fractions with similar signals. Fraction MF3 was observed with same characterized glycerol, lipid and sugar moieties A.2) as in MF6, but the two fractions exhibited distinct $\alpha$-amylase inhibition abilities. As a result, these two fractions

were discussed in detail. There are two hypotheses for the inhibition difference: the higher inhibition of MF3 could be attributed to the extra sugar signals observed or to the variance in the GL structures. As discussed in Section 5.1, the sugar could mimic the substrate structure of $\alpha$-amylase and cause inhibition (Jayaraj et al., 2013).

While looking at the analytical HPLC-MS data (Table 4.3), MF3 contained the compound with a m/z ratio of 567, where as MF6 contained that of 564. Considering the characterized glycerolipid and glycolipid structures in both fractions, the mass difference could be attributed to the lipid chain length. The longer lipid chain in the compound in MF3 could result in a stronger hydrophobic interactions with the enzyme (Vaezi et al., 2020) and exhibit a more effective inhibition.

However, these hypotheses need to be validated, as the compounds with different masses may not even be the glycerolipids but other compounds in the fractions; the masses were then not comparable dealing with different compounds; and the extra signals observed in the spectra may not represent sugars but other oxygenated compounds with similar chemical shifts. Hence, further purification, isolation and characterization are certainly needed to verify the identity and the enzyme-inhibiting ability of a pure compound.

Other fractions were also complex mixtures that no patterns specifically on the compound or fragment types could be concluded and attributed to the $\alpha$-amylase suppression bioactivity of each fraction. For instance, the aromatic signals (Moiety A), and the signals of the proposed variations in the lipid chains, either hydroxylated (Moieties U and V) or conjugated (Moieties W and X) were seen in both active and inactive fractions. However, sugars were generally present in the active fractions. Considering that the major bioassay used throughout this study was $\alpha$-amylase inhibition assay, it was not surprising that

the separated fractions contained sugars or sugar-like compounds (loliolide and (+)-epiloliolide), and presumably the sugar moieties contributed primarily on the binding and the inhibition of the enzyme (Jayaraj et al., 2013).

## 5.6 Evaluation on the bioassays of DMBA and enzyme inhibition

In this work, the extraction, purification and fractionation were principally guided by bioassays: DMBA assays for quantification of TPhCs, collagenase and $\alpha$-amylase inhibition assays for enzyme-suppressing bioactivities. The DMBA assay, compared to the Folin–Ciocalteu assay of measuring the total polyphenol contents, were more specific in quantifying 1,3- and 1,3,5-substituted polyphenols, or phlorotannins, with less interference from sugars, ions and so on (Ford et al., 2019; Stern et al., 1996). However, the variability of the phlorotannin structures as well as the measurement of the monomer phloroglucinol equivalents do not reflect the actual amounts (Stern et al., 1996). This finding possibly explained the lack of the common phlorotannin signals ($\delta_H$ 5.7-5.9/$\delta_C$ 95) (Buedenbender et al., 2020; Ford et al., 2019; Yotsu-Yamashita et al., 2013) in the crude extracts (Figure 4.1 and Figure **??**–Figure **??**) despite the positive results from the DMBA assays. The allylic signals were mistaken as the aromatic signals of phlorotannins, but only clarified with HMBC and H2BC experiments on the mass-targeting fractions. Therefore, the DMBA results for the crude extracts, fractions from the liquid-liquid partitioning, the macroporous resin separation and the column chromatographic fractionation may be misleading.

As a result of the single experiment for the enzyme assays, the % inhibition might not be representative of the actual inhibition ability

that false negative results may occur. In order to select the active fractions for further investigation, the extracts or fractions were considered inhibiting the enzymes with their % inhibition numbers higher than 10%. The reasonability could be argued, in particular when 9% and 1%, for instance, were of great difference although they both did not exceed 10%, whereas fractions with 11% inhibition may not inhibit better than that with 9% inhibition. As a result, the data could possibly be either false positive or false negative. In addition, the reference inhibitor did not exhibit an effective inhibition on the $\alpha$-amylase, making it difficult to validate the experimental setup. An known inhibitor acarbose could be used in the future research.

$\alpha$-amylase inhibition assay was used throughout the study to select the enzyme suppressing fractions and potential compounds with certain m/z ratios. Hence, being biologically *active* in this study actually represented the activity against this specific enzyme, where the characterized compounds and fragments were observed with common sugar or sugar-like structures that mimicked the starch substrate of the enzyme (Jayaraj et al., 2013). In other words, the results from this work were biased on obtaining certain types of compounds. Although other bioactives including phlorotannins and polyphenols in brown seaweeds were reported to inhibit $\alpha$-amylase (Mahmood, 2014), the extraction scheme as well as the degradation mentioned in Section 5.1 could affect the amount and the stability in the extracts.

## 5.7 Future prospects

While the fractions containing loliolide and (+)-epiloliolide showed $\alpha$-amylase inhibition, the impurities present in each fraction make it difficult to make a solid conclusion on the compounds' inhibiting effects. Isolation or commercially available pure loliolide and (+)-epiloliolide should be tested with the enzyme inhibition test to confirm the bioac-

tivity. In addition, the specific conformation of the loliolide should be determined, as the orientations of the hydroxyl group (at C3) and the methyl group (at C5) may result in different interactions $\alpha$-amylase. Circular dichroism (CD) spectroscopy can be used to measure the rotational strength between the isomers, and thus identify the conformation (da Silva Mota and Costa, 2021) and to determine the bioactivity of the specific isomer.

The GLs, the aromatic moieties, and the proposed hydroxylated and conjugated lipid chain moieties can be fully characterized with the assistance of tandem MS/MS technique. This spectroscopy uses two mass analyzers to deliberately separate fragments with very close m/z ratios, and achieve identification of rather large biomolecules like proteins (Gross, 2017d).

Due to the limited amount of the extract, enzyme assays were performed in single experiments. Triplicates should be done in the future studies. This requires more materials, or a better yield can be achieved by using novel extraction techniques such as microwave-assisted extraction, supercritical fluid extraction and subcritical water extraction, which not only produce more masses, but are non-toxic and solvent-efficient (Ummat et al., 2021).

Despite of the uncertainties discussed, there is no doubt about the great potential of loliolide, (+)-epiloliolide and glycoglycerolipids from the brown seaweed *A. esculenta* on inhibiting $\alpha$-amylase. As a metabolic enzyme involved in the development of type II diabetes, which was reported to be one of the most serious chronic disease in the world, $\alpha$-amylase inhibition is an important strategy to prevent the disease. In fact, extracts of multiple seaweed species were often observed with both $\alpha$-amylase and another carbohydrate-degrading enzyme, the $\alpha$-glucosidase inhibition abilities, strengthening the antidiabetic effect by

the brown seaweeds (Firdaus and Prihanto, 2014; Lordan et al., 2013; Sharifuddin et al., 2015; Thissera et al., 2020). In the future studies, $\alpha$-glucosidase inhibition assay could be applied, and the compounds' antidiabetic effects could be investigated further.

The DMBA assay was performed targeting the phlorotannins. Given their antidiabetic, antidiabetic and other bioactivities (Yotsu-Yamashita et al., 2013), the future studies can optimize the extraction process in the choice of the extracting solvent. 70% (v/v) acetone was reported to produce higher TPhCs (Catarino et al., 2019). Protection on these labile bioactive compounds should also be considered. Encapsulation by micro- or nanocapsules to isolate the phlorotannins from interacting with the external light and oxygen can be a protection strategy (Okeke et al., 2021a).

For the fractions exhibiting no considered $\alpha$-amylase inhibition effect, compounds with other bioactivities may be present nevertheless. Bioassays designed for screening antimicrobial, antiinflammatory and anticancer activities could be potentially tested to explore further on the great potentials of the biomass.

# 6 Concluding Remarks

This study has demonstrated the presence of bioactive natural products in the brown seaweed species *Alaria esculenta* and *Saccharina latissima* by using the bioassays of 2,4-dimethoxybenzaldehyde (DMBA) and enzyme inhibition assays including $\alpha$-amylase and collagenase. Through a systematic investigation from crude extracts to $\alpha$-amylase inhibiting fractions, loliolide and its isomer (+)-epiloliolide were for the first time identified from *A. esculenta*. Furthermore, glycerolipids (GLs) were partially characterized. These natural products were likely to inhibit $\alpha$-amylase. The conclusions were developed as follows:

While comparing the bioactivities of the absolute methanol and 70% (v/v) ethanol crude extracts of *A. esculenta* and *S. latissima*, all four extracts indicated the presence of phlorotannins and the ability of inhibiting $\alpha$-amylase. The extracts of *A. esculenta* indicated inhibition on collagenase, whereas *S. latissima* extracts were not considered to inhibit the enzyme. The methanol extract of *A. esculenta* had the greatest phlorotannin content, and showed the highest % inhibition on both $\alpha$-amylase and collagenase. *A. esculenta* was therefore selected for the large-scale methanol extraction followed by fractionation and characterization;

Fractions were obtained by tracking the $\alpha$-amylase inhibition, and the m/z ratios of 197.12, 313.28, 468.31, 544.34, 609.27 and 593.28 were successfully identified based on their presence in the enzyme-inhibiting fractions until the last round of fractionation step;

New fractions containing the compounds with the identified m/z ratios were characterized through 1D and 2D NMR experiments. Loliolide (either (+)- or (−)-loliolide) and (+)-epiloliolide were identified in MF2 and MF1 fractions, respectively. Structures of GLs were partially assigned in MF6, and MF3–MF11 were observed with similar

cross peaks in their $^{1}$H-$^{13}$C one-bond correlation HSQC spectra. Additionally, distinct signals were specified in MF10: an aromatic fragment was characterized and hypothesized as degraded phlorotannin or phenyl-terminated lipid chain, and the peaks with chemical shifts of approximate $\delta_{\mathrm{H}}$ 6.0 and 6.5 (both with $\delta_{\mathrm{C}}$ around 130) were hypothesized as hydroxylated and conjugated lipid chain, respectively.

Combining the information of the $\alpha$-amylase inhibition of each fraction, comparisons were made based on the annotated moieties and signals, and the distribution among the fractions. It is important to acknowledge that all fractions were mixtures, that the structures were partially assigned, and that it was difficult to make a correlation between a specific compound in the fractions and the $\alpha$-amylase inhibition ability. Nonetheless, loliolide and its isomers, as well as the GLs from *A. esculenta* are highly likely to inhibit $\alpha$-amylase, implying their antidiabetic potential.

# 7 References


Afonso, C., Matos, J., Guarda, I., Gomes-Bispo, A., Gomes, R., Cardoso, C., Gueifão, S., Delgado, I., Coelho, I., Castanheira, I., and Bandarra, N. (2021). Bioactive and nutritional potential of alaria esculenta and saccharina latissima. *Journal of Applied Phycology*, 33:1–13.

Akash, M. S. H. and Rehman, K. (2020). *Column Chromatography*, pages 167–174. Springer Singapore, Singapore.

Alexandri, E., Ahmed, R., Siddiqui, H., Choudhary, M. I., Tsiafoulis, C., and Gerothanassis, I. (2017). High resolution nmr spectroscopy as a structural and analytical tool for unsaturated lipids in solution. *Molecules*, 22:1663.

Allen, D. and McWhinney, B. (2019). Quadrupole time-of-flight mass spectrometry: A paradigm shift in toxicology screening applications. *The Clinical biochemist. Reviews*, 40:135–146.

Amorati, R. and Valgimigli, L. (2015). Advantages and limitations of common testing methods for antioxidants. *Free Radical Research*, 49(5):633–649. PMID: 25511471.

Andreea, C., Axine, O., and Iacomi, B. (2010). Antifungal activity of macroalgae extracts. *Scientific papers*, LIII:442–447.

Araújo, R., Vázquez Calderón, F., Sánchez López, J., Azevedo, I. C., Bruhn, A., Fluch, S., Garcia Tasende, M., Ghaderiardakani, F., Ilmjärv, T., Laurans, M., Mac Monagail, M., Mangini, S., Peteiro, C., Rebours, C., Stefansson, T., and Ullmann, J. (2021). Current status of the algae production industry in europe: An emerging sector of the blue bioeconomy. *Frontiers in Marine Science*, 7.

Batool, A. and Menaa, F. (2020). *Concentration and purification of seaweed components by chromatography methods*, pages 315–370.

Billakanti, J. M., Catchpole, O. J., Fenton, T. A., Mitchell, K. A., and MacKenzie, A. D. (2013). Enzyme-assisted extraction of fucoxanthin and lipids containing polyunsaturated fatty acids from undaria pinnatifida using dimethyl ether and ethanol. *Process Biochemistry*, 48(12):1999–2008.

Blikra, M. J., Løvdal, T., Vaka, M. R., Roiha, I. S., Lunestad, B. T., Lindseth, C., and Skipnes, D. (2019). Assessment of food quality and microbial safety of brown macroalgae (alaria esculenta and saccharina latissima). *Journal of the Science of Food and Agriculture*, 99(3):1198–1206.

Bubb, W. A. (2003). Nmr spectroscopy in the study of carbohydrates: Characterizing the structural complexity. *Concepts in Magnetic Resonance Part A*, 19A(1):1–19.

Buedenbender, L., Astone, F., and Tasdemir, D. (2020). Bioactive molecular networking for mapping the antimicrobial constituents of the baltic brown alga fucus vesiculosus. *Marine Drugs*, 18:311.

Cao, H., Saroglu, O., Karadag, A., Diaconeasa, Z., Zoccatelli, G., Conte-Junior, C. A., Gonzalez-Aguilar, G. A., Ou, J., Bai, W., Zamarioli, C. M., de Freitas, L. A. P., Shpigelman, A., Campelo, P. H., Capanoglu, E., Hii, C. L., Jafari, S. M., Qi, Y., Liao, P., Wang, M., Zou, L., Bourke, P., Simal-Gandara, J., and Xiao, J. (2021). Available technologies on improving the stability of polyphenols in food processing. *Food Frontiers*, 2(2):109–139.

Castejón, N., Thorarinsdottir, K. A., Einarsdóttir, R., Kristbergsson, K., and Marteinsdóttir, G. (2021a). Exploring the potential of ice-

landic seaweeds extracts produced by aqueous pulsed electric fields-assisted extraction for cosmetic applications. *Marine Drugs*, 19(12).

Castejón, N., Thorarinsdottir, K. A., Einarsdóttir, R., Kristbergsson, K., and Marteinsdóttir, G. (2021b). Exploring the potential of ice-landic seaweeds extracts produced by aqueous pulsed electric fields-assisted extraction for cosmetic applications. *Marine Drugs*, 19(12).

Catarino, M., Marçal, C., Bonifácio, T., Campos, D., Mateus, N., Silva, A., Pintado, M., and Cardoso, S. (2021). Impact of phlorotannin extracts from fucus vesiculosus on human gut microbiota. *Marine Drugs*, 19:375.

Catarino, M., Silva, A., Mateus, N., and Cardoso, S. (2019). Optimization of phlorotannins extraction from fucus vesiculosus and evaluation of their potential to prevent metabolic disorders. *Marine Drugs*, 17:162.

Cavaliere, C., Capriotti, A. L., La Barbera, G., Montone, C. M., Piovesana, S., and Laganà, A. (2018). Liquid chromatographic strategies for separation of bioactive compounds in food matrices. *Molecules*, 23(12).

Cazarin, C. B. B., Bicas, J. L., Pastore, G. M., and Marostica Junior, M. R. (2022). Chapter 1 - introduction. In Cazarin, C. B. B., Bicas, J. L., Pastore, G. M., and Marostica Junior, M. R., editors, *Bioactive Food Components Activity in Mechanistic Approach*, pages 1–3. Academic Press.

Chapman, R. L. (2013). Algae: the world's most important "plants"—an introduction. *Mitigation and Adaptation Strategies for Global Change*, 18:5–12.

Chi, H., Qi, X., Wang, X., Wang, Y., Han, X., Wang, J., and Wang, H. (2021a). Preparative separation and purification of loliolide and epi-

loliolide from ascophyllum nodosum using amine-based microporous organic polymer for solid phase extraction coupled with macroporous resin and prep-hplc. *Analytical Methods*, 13.

Chi, H., Qi, X., Wang, X., Wang, Y., Han, X., Wang, J., and Wang, H. (2021b). Preparative separation and purification of loliolide and epiloliolide from ascophyllum nodosum using amine-based microporous organic polymer for solid phase extraction coupled with macroporous resin and prep-hplc. *Anal. Methods*, 13:1939–1944.

Chung, Y., Jeong, S., Lee, I.-K., Yun, B.-S., Lee, J. S., Ro, S., and Park, J. K. (2021). Regulation of p53 activity by (+)-epiloliolide isolated from ulva lactuca. *Marine Drugs*, 19(8).

Colom, O. A., Popich, S., and Bardon, A. (2007). Bioactive constituents from rollinia emarginata (annonaceae). *Natural Product Research*, 21(3):254–259. PMID: 17365716.

da Costa, E., Domingues, P., Melo, T., Coelho, E., Pereira, R., Calado, R., Abreu, M. H., and Domingues, M. R. (2019). Lipidomic signatures reveal seasonal shifts on the relative abundance of high-valued lipids from the brown algae fucus vesiculosus. *Marine Drugs*, 17(6).

da Silva Mota, G. V. and Costa, F. L. P. (2021). A theoretical study to the loliolide molecule and its isomers: a study by circular dichroism, qtaim, and nmr theoretical methods. *Journal of Molecular Modeling*, 27.

Data, N. S. R. (2022). Aocs lipid library.

Deal, M. S., Hay, M. E., Wilson, D., and Fenical, W. (2003). Galactolipids rather than phlorotannins as herbivore deterrents in the brown seaweed fucus vesiculosus. *Oecologia*, 136(1):107–114.

Do, Q.-D., Angkawijaya, A., Tran-Nguyen, P. L., Huynh, L.-H., Edi-Soetaredjo, F., Ismadji, S., and Ju, Y.-H. (2013). Effect of extraction solvent on total phenol content, total flavonoid content, and antioxidant activity of limnophila aromatica. *Journal of Food and Drug Analysis*, 22.

Doucleff, M., Hatcher-Skeers, M., and Crane, N. J. (2011). *Atomic Bells and Frequency Finders*, pages 1–18. Springer Berlin Heidelberg, Berlin, Heidelberg.

Duus, J., Gotfredsen, C., and Bock, K. (2001). Carbohydrate structural determination by nmr spectroscopy: Modern methods and limitations †. *Chemical reviews*, 100:4589–614.

E. O' Keeffe, H. H. and McLoughlin, P. (2019). Methods of analysis for the in vitro and in vivo determination of the fungicidal activity of seaweeds: a mini review. *Journal of Applied Phycology*, 31:3759–3776.

Einarsdóttir, R., órarinsdóttir, K. A., Aalbjörnsson, B. V., Gumundsson, M., Marteinsdóttir, G., and Kristbergsson, K. (2022). Extraction of bioactive compounds from alaria esculenta with pulsed electric field. *Journal of Applied Phycology*, 34:597–608.

El Hattab, M., Culioli, G., Valls, R., Richou, M., and Piovetti, L. (2008). Apo-fucoxanthinoids and loliolide from the brown alga cladostephus spongiosus f. verticillatus (heterokonta, sphacelariales). *Biochemical Systematics and Ecology*, 36(5):447–451.

El-Shouny, W., Gaafar, R., Ismail, G., Elzanaty, M., and el Zanaty, M. (2017). Antibacterial activity of some seaweed extracts against multidrug resistant urinary tract bacteria and analysis of their virulence genes. *International Journal of Current Microbiology and Applied Sciences*, 6.

FAO (2022). Global aquaculture production.

Fernando, I. P. S., Heo, S.-J., Dias, M. K. H. M., Madusanka, D. M. D., Han, E.-J., Kim, M.-J., Sanjeewa, K. K. A., Lee, K., and Ahn, G. (2021). ()-loliolide isolated from sargassum horneri abate uvb-induced oxidative damage in human dermal fibroblasts and subside ecm degradation. *Marine Drugs*, 19(8).

Firdaus, M. and Prihanto, A. (2014). a-amylase and a-glucosidase inhibition by brown seaweed (sargassum sp) extracts. *Research Journal of life science*, 1:6–11.

Fiskeridirektoratet (2022). Harvesting of farmed algae.

Ford, L., Theodoridou, K., Sheldrake, G., and Walsh, P. (2019). A critical review of analytical methods used for the chemical characterisation and quantification of phlorotannin compounds in brown seaweeds. *Phytochemical Analysis*, 30:1–13.

Ghosh, S. and Rangan, L. (2014). Molecular docking and inhibition studies of a-amylase activity by labdane diterpenes from alpinia nigra seeds.

Gross, J. H. (2017a). *Electrospray Ionization*, pages 721–778. Springer International Publishing, Cham.

Gross, J. H. (2017b). *Fragmentation of Organic Ions and Interpretation of EI Mass Spectra*, pages 325–437. Springer International Publishing, Cham.

Gross, J. H. (2017c). *Hyphenated Methods*, pages 831–887. Springer International Publishing, Cham.

Gross, J. H. (2017d). *Instrumentation*, pages 151–292. Springer International Publishing, Cham.

Gross, J. H. (2017e). *Matrix-Assisted Laser Desorption/Ionization*, pages 651–720. Springer International Publishing, Cham.

Hamzam1olu, A. and Gökmen, V. (2016). Interaction between bioactive carbonyl compounds and asparagine and impact on acrylamide.

Hanson, J. R. (2003). The classes of natural product and their isolation. In Hanson, J. R., editor, *Natural Products: The Secondary Metabolites*, volume 17, pages 1–34. The Royal Society of Chemistry.

Hermund, D. B. (2018). 10 - antioxidant properties of seaweed-derived substances. In Qin, Y., editor, *Bioactive Seaweeds for Food Applications*, pages 201–221. Academic Press.

Holdt, S. and Kraan, S. (2011). Bioactive compounds in seaweed: Functional food applications and legislation. *Journal of Applied Phycology*, 23:543–597.

Isaza Martínez, J. H. and Torres Castañeda, H. G. (2013). Preparation and Chromatographic Analysis of Phlorotannins. *Journal of Chromatographic Science*, 51(8):825–838.

Jacobsen, S. S. (2021). Investigation into the presence of polyphenols and carotenoids in the two seaweed species alaria esculenta and saccharina latissima, with a focus on extracting, purifying, and characterizing the xanthophyll fucoxanthin.

Jayabarath, J. and Jeyaprakash, K. (2015). Screening of phytochemical compounds in brown seaweed (turbinaria conoides) using tlc, uv-vis and ftir analysis. *Journal of Chemical and Pharmaceutical Sciences*, 8:952–956.

Jayaraj, S., Suresh, S., and Kadeppagari, R. K. (2013). Amylase inhibitors and their biomedical applications. *Starch - Starke*, 65.

Joana Gil-Chávez, G., Villa, J. A., Fernando Ayala-Zavala, J.,

Basilio Heredia, J., Sepulveda, D., Yahia, E. M., and González-Aguilar, G. A. (2013). Technologies for extraction and production of bioactive compounds to be used as nutraceuticals and food ingredients: An overview. *Comprehensive Reviews in Food Science and Food Safety*, 12(1):5–23.

Kamble, R. P., Ghosh, P., and Kulkarni, A. A. (2022). Identification of -amylase inhibitory compounds from leaves of careya arborea roxb. and in silico docking studies. *South African Journal of Botany*.

Kato-Noguchi, H., Moriyasu, M., Ohno, O., and Suenaga, K. (2014). Growth limiting effects on various terrestrial plant species by an allelopathic substance, loliolide, from water hyacinth. *Aquatic Botany*, 117:56–61.

kawee ai, A., Kim, A., and Kim, S. M. (2019). Inhibitory activities of microalgal fucoxanthin against -amylase, -glucosidase, and glucose oxidase in 3t3-l1 cells linked to type 2 diabetes. *Journal of Oceanology and Limnology*, 37:928–937.

Kellogg, J. and Kang, S. (2020). Metabolomics, an essential tool in exploring and harnessing microbial chemical ecology. *Phytobiomes Journal*, 4.

Kenar, J. A., Moser, B. R., and List, G. R. (2017). Chapter 2 - naturally occurring fatty acids: Source, chemistry, and uses. In Ahmad, M. U., editor, *Fatty Acids*, pages 23–82. AOCS Press.

Kerrison, P., Innes, M., MacLeod, A., McCormick, E., Elbourne, P., Stanley, M., Hughes, A., and Kelly, M. (2020). Comparing the effectiveness of twine- and binder-seeding in the laminariales species alaria esculenta and saccharina latissima. *Journal of Applied Phycology*, 32.

Kim, J., Yoon, M., Yang, H., Jo, J., Han, D., Jeon, Y.-J., and

Cho, S. (2014). Enrichment and purification of marine polyphenol phlorotannins using macroporous adsorption resins. *Food chemistry*, 162:135–42.

Kimura, J. and Maki, N. (2002). New loliolide derivatives from the brown alga undaria pinnatifida. *Journal of natural products*, 65:57–8.

Kruve, A. and Kaupmees, K. (2017). Adduct formation in esi/ms by mobile phase additives. *Journal of The American Society for Mass Spectrometry*, 28:1–8.

Kuniyoshi, M. (1985). Germination inhibitors from the brown alga sargassum crassifolium (phaeophyta, sargassaceae). 28(11):501–504.

Leite, S. (2009). Inhibitors of human collagenase, mmp1. *Ecletica Quimica*, 34:87–102.

Leyton, A., Vergara-Salinas, J., Pérez-Correa, J., and Lienqueo, M. (2017). Purification of phlorotannins from macrocystis pyrifera using macroporous resins. *Food Chemistry*, 237:312–319.

Li, J. and Chase, H. (2010). Cheminform abstract: Development of adsorptive (non-ionic) macroporous resins and their uses in the purification of pharmacologically-active natural products from plant sources. *Natural product reports*, 27:1493–510.

Li, Y., Fu, X., Duan, D., Liu, X., Xu, J., and Gao, X. (2017). Extraction and identification of phlorotannins from the brown alga, sargassum fusiforme (harvey) setchell. *Marine Drugs*, 15:49.

Lopes, D., Rey, F., Leal, M., Lillebø, A., Calado, R., and Domingues, M. R. (2021). Bioactivities of lipid extracts and complex lipids from seaweeds: Current knowledge and future prospects. *Marine Drugs*, 19:686.

Lordan, S., Smyth, T. J., Soler-Vila, A., Stanton, C., and Ross, R. P. (2013). The -amylase and -glucosidase inhibitory effects of irish seaweed extracts. *Food Chemistry*, 141(3):2170–2176.

Lu, Y., Chen, Y., Wu, Y., Hao, H., Liang, W., Liu, J., and Huang, R. (2019). Marine unsaturated fatty acids: structures, bioactivities, biosynthesis and benefits. *RSC Adv.*, 9:35312–35327.

Lytou, A. E., Schoina, E., Liu, Y., Michalek, K., Stanley, M. S., Panagou, E. Z., and Nychas, G.-J. E. (2021). Quality and safety assessment of edible seaweeds alaria esculenta and saccharina latissima cultivated in scotland. *Foods*, 10(9).

Mahmood, N. (2014). Erratum to: A review of -amylase inhibitors on weight loss and glycemic control in pathological state such as obesity and diabetes. *Comparative Clinical Pathology*, 24.

Majik, M. S., Adel, H., Shirodkar, D., Tilvi, S., and Furtado, J. (2015). Isolation of stigmast-5,24-dien-3-ol from marine brown algae sargassum tenerrimum and its antipredatory activity. *RSC Adv.*, 5:51008–51011.

Marinho, G., Sørensen, A.-D., Safafar, H., Pedersen, A., and Holdt, S. (2019). Antioxidant content and activity of the seaweed saccharina latissima: a seasonal perspective. *Journal of Applied Phycology*, 31.

Meija, J. and Soukup, V. G. (2004). Phenyl-terminated fatty acids in seeds of various aroids. *Phytochemistry*, 65(15):2229–2237.

Mohammed, H. O., O'Grady, M. N., O'Sullivan, M. G., Hamill, R. M., Kilcawley, K. N., and Kerry, J. P. (2021a). An assessment of selected nutritional, bioactive, thermal and technological properties of brown and red irish seaweed species. *Foods*, 10(11).

Mohammed, H. O., O'Grady, M. N., O'Sullivan, M. G., Hamill, R. M.,

Kilcawley, K. N., and Kerry, J. P. (2021b). An assessment of selected nutritional, bioactive, thermal and technological properties of brown and red irish seaweed species. *Foods*, 10(11).

Mori, K. and khlebnikov, V. (1993). Synthesis of ( + )-dihydroactinidiolide, ( + )- and ( - )-actinidiolide, ( + )- and ( - )-loliolide as well as ( + )- and ( - )-epiloliolide. *Justus Liebigs Annalen der Chemie*, 1:77–82.

Mottaghipisheh, J. and Iriti, M. (2020). Sephadex® lh-20, isolation, and purification of flavonoids from plant species: A comprehensive review. *Molecules*, 25(18).

Narayan, B., Kinami, T., Miyashita, K., Park, S.-B., Endo, Y., and Fujimoto, K. (2004). Occurrence of conjugated polyenoic fatty acids in seaweeds from the indian ocean. *Zeitschrift für Naturforschung. C, Journal of biosciences*, 59:310–4.

Neergaard, J., Rasmussen, H., Stafford, G., Van Staden, J., and Jäger, A. (2010). Serotonin transporter affinity of ()-loliolide, a monoterpene lactone from mondia whitei. *South African Journal of Botany*, 76(3):593–596.

Nwosu, F., Morris, J., Lund, V. A., Stewart, D., Ross, H. A., and McDougall, G. J. (2011). Anti-proliferative and potential anti-diabetic effects of phenolic-rich extracts from edible marine algae. *Food Chemistry*, 126(3):1006–1012.

Ohlrogge, J., Thrower, N., Mhaske, V., Stymne, S., Baxter, M., Yang, W., Liu, J., Shaw, K., Shorrosh, B., Zhang, M., Wilkerson, C., and Matthäus, B. (2018). Plantfadb: A resource for exploring hundreds of plant fatty acid structures synthesized by thousands of plants and their phylogenetic relationships. *The Plant Journal*, 96.

Okeke, E. S., Nweze, E. J., Chibuogwu, C. C., Anaduaka,

E. G., Chukwudozie, K. I., and Ezeorba, T. P. C. (2021a). Aquatic phlorotannins and human health: Bioavailability, toxicity, and future prospects. *Natural Product Communications*, 16(12):1934578X211056144.

Okeke, E. S., Nweze, E. J., Chibuogwu, C. C., Anaduaka, E. G., Chukwudozie, K. I., and Ezeorba, T. P. C. (2021b). Aquatic phlorotannins and human health: Bioavailability, toxicity, and future prospects. *Natural Product Communications*, 16(12):1934578X211056144.

P. Stévant, C. R. and Chapman, A. (2017). Seaweed aquaculture in norway: recent industrial developments and future perspectives. *Aquaculture International*, 25:1373–1390.

Patel, K. N., Patel, J. K., Patel, M. P., Rajput, G. C., and Patel, H. A. (2010). Introduction to hyphenated techniques and their applications in pharmacy. *Pharmaceutical Methods*, 1(1):2–13.

Petersen, B. O., Vinogradov, E., Kay, W., Würtz, P., Nyberg, N. T., Duus, J. , and Sørensen, O. W. (2006). H2bc: a new technique for nmr analysis of complex carbohydrates. *Carbohydrate Research*, 341(4):550–556.

Pettit, G. R., Herald, C. L., Ode, R. H., Brown, P., Gust, D. J., and Michel, C. (1980). The isolation of loliolide from an indian ocean opisthobranch mollusc. *Journal of Natural Products*, 43(6):752–755. PMID: 20707399.

Purnomo (2017). Identification of fucoxanthin from brown algae ( sargassum filipendula ) from padike village , talango district , sumenep regency , madura islands , using nuclear magnetic resonance ( nmr ).

Ramsay, R. and Tipton, K. (2017). Assessment of enzyme inhibition:

A review with examples from the development of monoamine oxidase and cholinesterase inhibitory drugs. *Molecules*, 22:1192.

Reid, G., Chopin, T., Robinson, S., Azevedo, P., Quinton, M., and Belyea, E. (2013). Weight ratios of the kelps, alaria esculenta and saccharina latissima, required to sequester dissolved inorganic nutrients and supply oxygen for atlantic salmon, salmo salar, in integrated multi-trophic aquaculture systems. *Aquaculture*, 408-409:34–46.

Repeta, D. J. (1989). Carotenoid diagenesis in recent marine sediments: Ii. degradation of fucoxanthin to loliolide. *Geochimica et Cosmochimica Acta*, 53(3):699–707.

Rocca, J., Tumlinson, J., Glancey, B., and Lofgren, C. (1983). The queen recognition pheromone of solenopsis invicta, preparation of (e-6-(1-pentenyl)-2h-pyran-2-one. *Tetrahedron Letters*, 24(18):1889–1892.

Roleda, M. Y., Skjermo, J., Marfaing, H., Jónsdóttir, R., Rebours, C., Gietl, A., Stengel, D. B., and Nitschke, U. (2018). Iodine content in bulk biomass of wild-harvested and cultivated edible seaweeds: Inherent variations determine species-specific daily allowable consumption. *Food Chemistry*, 254:333–339.

Salehi, B., Sharifi-Rad, J., Seca, A., Pinto, D., Michalak, I., Trincone, A., Mishra, A., Nigam, M., Zam, W., and Cruz-Martins, N. (2019). Current trends on seaweeds: Looking at chemical composition, phytopharmacology, and cosmetic applications. *Molecules*, 24:4182.

Sales, P., Souza, P., Simeoni, L., and Silveira, D. (2012). -amylase inhibitors: A review of raw material and isolated compounds from plant source. *Journal of pharmacy pharmaceutical sciences : a publication of the Canadian Society for Pharmaceutical Sciences, Société canadienne des sciences pharmaceutiques*, 15:141–83.

Sapatinha, M., Oliveira, A., Costa, S., Pedro, S., Gonçalves, A., Mendes, R., Bandarra, N., and Pires, C. (2022). Red and brown seaweeds extracts: A source of biologically active compounds. *Food Chemistry*, 393:133453.

Sağdıçoğlu Celep, G., Rastmanesh, R., and Marotta, F. (2013). Microbial metabolism of polyphenols and health. *Polyphenols in Human Health and Disease*, 1:577–589.

Schiener, P., Black, K., Stanley, M., and Green, D. (2015). The seasonal variation in the chemical composition of the kelp species laminaria digitata, laminaria hyperborea, saccharina latissima and alaria esculenta. *Journal of Applied Phycology*, 27:363–373.

Schönauer, E., Kany, A., Haupenthal, J., Hüsecken, K., Hoppe, I., Voos, K., Yahiaoui, S., Elsässer, B., Ducho, C., Brandstetter, H., and Hartmann, R. (2017). Discovery of a potent inhibitor class with high selectivity toward clostridial collagenases. *Journal of the American Chemical Society*, 139.

Sellimi, S., Maalej, H., Rekik, D. M., Benslima, A., Ksouda, G., Hamdi, M., Sahnoun, Z., Li, S., Nasri, M., and Hajji, M. (2018). Antioxidant, antibacterial and in vivo wound healing properties of laminaran purified from cystoseira barbata seaweed. *International Journal of Biological Macromolecules*, 119:633–644.

Sharifuddin, Y., Chin, Y. X., Lim, P.-E., and Phang, S. (2015). Potential bioactive compounds from seaweed for diabetes management. *Marine Drugs*, 13:5447 – 5491.

Shepard, T. (2007). Nature publishing group, all natural. *Nat. Chem. Biol*, 3:351.

Silva, J., Alves, C., Martins, A., Susano, P., Simões, M., Guedes, M., Rehfeldt, S., Pinteus, S., Gaspar, H., Rodrigues, A., Goettert, M.,

Alfonso, A., and Pedrosa, R. (2021). Loliolide, a new therapeutic option for neurological diseases? in vitro neuroprotective and anti-inflammatory activities of a monoterpenoid lactone isolated from codium tomentosum. *International Journal of Molecular Sciences*, 22:1888.

Simpson, J. H. (2012a). Chapter 1 - introduction. In Simpson, J. H., editor, *Organic Structure Determination Using 2-D NMR Spectroscopy (Second Edition)*, pages 1–20. Academic Press, Boston, second edition edition.

Simpson, J. H. (2012b). Chapter 4 - 1h and 13c chemical shifts. In Simpson, J. H., editor, *Organic Structure Determination Using 2-D NMR Spectroscopy (Second Edition)*, pages 101–112. Academic Press, Boston, second edition edition.

Simpson, J. H. (2012c). Chapter 6 - through-bond effects: Spin-spin (j) coupling. In Simpson, J. H., editor, *Organic Structure Determination Using 2-D NMR Spectroscopy (Second Edition)*, pages 123–168. Academic Press, Boston, second edition edition.

Simpson, J. H. (2012d). Chapter 7 - through-space effects: The nuclear overhauser effect (noe). In Simpson, J. H., editor, *Organic Structure Determination Using 2-D NMR Spectroscopy (Second Edition)*, pages 169–184. Academic Press, Boston, second edition edition.

Skoog, D. A. and Holler, F. Jamesand Crouch, S. R. (2007). In *Principles of instrumental analysis*. Belmont, CA : Thomson Brooks/Cole, Belmont, CA, sixth edition edition.

Society, T. A. O. C. (2022). Aocs lipid library.

Springob, K. and Kutchan, T. M. (2009). *Introduction to the Different Classes of Natural Products*, pages 3–50. Springer US, New York, NY.

Stefaniak, M. M., Gudjónsdóttir, M., Marteinsdottir, G., Omarsdottir, S., Bravo, E., Sigurjónsson, O. E., and Kristbergsson, E. S. (2019). Determination of bioactive properties of food grade extracts from icelandic edible brown seaweed sugar kelp (saccharina latissima)with in vitro human cell cultures (thp-1). *Functional Foods in Health and Disease*, 9:1–15.

Stern, J., Hagerman, A., Steinberg, P., Winter, F., and Estes, J. (1996). A new assay for quantifying brown algal phlorotannins and comparisons to previous methods. *Journal of Chemical Ecology*, 22:1273–1293.

Stuart, K. A., Welsh, K., Walker, M. C., and Edrada-Ebel, R. (2020). Metabolomic tools used in marine natural product drug discovery. *Expert Opinion on Drug Discovery*, 15(4):499–522. PMID: 32026730.

Stévant, P., Marfaing, H., Duinker, A., Fleurence, J., Rustad, T., Sandbakken, I., and Chapman, A. (2018). Biomass soaking treatments to reduce potentially undesirable compounds in the edible seaweeds sugar kelp (saccharina latissima) and winged kelp (alaria esculenta) and health risk estimation for human consumption. *Journal of Applied Phycology*, 30.

Stévant, P., Marfaing, H., Rustad, T., Sandbakken, I., Fleurence, J., and Chapman, A. (2017). Nutritional value of the kelps alaria esculenta and saccharina latissima and effects of short-term storage on biomass quality. *Journal of Applied Phycology*, 29:1–10.

Tanna, B. and Mishra, A. (2018). Metabolites unravel nutraceutical potential of edible seaweeds: An emerging source of functional food. *Comprehensive Reviews in Food Science and Food Safety*, 17.

Tanniou, A., Serrano león, E., Laurent, V., Elena, I., Mendiola, J.,

Cérantola, S., Nelly, K., La Barre, S., Marchal, L., and Stiger, V. (2013). Green improved processes to extract bioactive phenolic compounds from brown macroalgae using sargassum muticum as model. *Talanta*, 104C:44–52.

Thissera, B., Visvanathan, R., Khanfar, M., Qader, M., Hassan, H., Hassan, H., Bawazeer, M., Behery, F., Yaseen, M., Liyanage, R., Abdelmohsen, U., and Rateb, M. (2020). Sesbania grandiflora l. poir leaves: A dietary supplement to alleviate type 2 diabetes through metabolic enzymes inhibition. *South African Journal of Botany*, 130.

Tiwari, B. K. and Troy, D. J. (2015). Chapter 1 - seaweed sustainability – food and nonfood applications. In Tiwari, B. K. and Troy, D. J., editors, *Seaweed Sustainability*, pages 1–6. Academic Press, San Diego.

Ummat, V., Sivagnanam, S. P., Rajauria, G., O'Donnell, C., and Tiwari, B. K. (2021). Advances in pre-treatment techniques and green extraction technologies for bioactives from seaweeds. *Trends in Food Science Technology*, 110:90–106.

Ummat, V., Tiwari, B. K., Jaiswal, A. K., Condon, K., Garcia-Vaquero, M., O'Doherty, J., O'Donnell, C., and Rajauria, G. (2020). Optimisation of ultrasound frequency, extraction time and solvent for the recovery of polyphenols, phlorotannins and associated antioxidant activity from brown seaweeds. *Marine Drugs*, 18(5).

Vaezi, M., Behbehani, G. R., Gheibi, N., and Farasat, A. (2020). Thermodynamic, kinetic and docking studies of some unsaturated fatty acids-quercetin derivatives as inhibitors of mushroom tyrosinase. *AIMS Biophysics*, 7(4):393–410.

Wang, S., Moustaid-Moussa, N., Chen, L., Mo, H., Shastri, A., Su,

R., Bapat, P., Kwun, I., and Shen, C.-L. (2014). Novel insights of dietary polyphenols and obesity. *The Journal of Nutritional Biochemistry*, 25(1):1–18.

Wang, T., Jónsdóttir, R., Liu, H., Gu, L., Kristinsson, H., Raghavan, S., and Ólafsdóttir, G. (2012). Antioxidant capacities of phlorotannins extracted from the brown algae fucus vesiculosus. *Journal of agricultural and food chemistry*, 60.

Ye, Y., Sun, J., Wang, L., Zhu, J., Cui, W., Hou, H., Zhang, J., Zhou, C., and Yan, X. (2021). Isolation and purification of fucoxanthin from brown seaweed sargassum horneri using open ods column chromatography and ethanol precipitation. *Molecules*, 26.

Yotsu-Yamashita, M., Kondo, S., Segawa, S., Lin, Y.-C., Toyohara, H., Ito, H., Konoki, K., Cho, Y., and Uchida, T. (2013). Isolation and structural determination of two novel phlorotannins from the brown alga ecklonia kurome okamura, and their radical scavenging activities. *Marine drugs*, 11:165–183.

Yusof, Z., Khong, N. M., Choo, W. S., and Foo, S. C. (2022). Opportunities for the marine carotenoid value chain from the perspective of fucoxanthin degradation. *Food Chemistry*, 383:132394.

Zaharudin, N., Salmeán, A., and Dragsted, L. (2017). Inhibitory effects of edible seaweeds, polyphenolics and alginates on the activities of porcine pancreatic -amylase. *Food Chemistry*, 245.

Zhang, H., Tang, Y., Zhang, Y., Zhang, S., Qu, J., Wang, X., Kong, R., Han, C., and Liu, Z. (2015). Fucoxanthin: A promising medicinal and nutritional ingredient. *Evidence-Based Complementary and Alternative Medicine*, 2015:1–10.

Zhou, X., Yi, M., Ding, L., and He, S. (2019). Isolation and purification of a neuroprotective phlorotannin from the marine algae

ecklonia maxima by size exclusion and high-speed counter-current chromatography. *Marine Drugs*, 17:212.

# A Appendix

## A.1 NMR data

**Table A.1:** NMR data of compound 2 (+)-epiloliolide (800 MHz).

| Position | $\delta$H Multiplicity (J in Hz) | $\delta$C | COSY (ppm) | HMBC | NOE |
|---|---|---|---|---|---|
| 1 | - | 36.0 | - | - | - |
| 2 | 1.30 dd (24.0, 6.0)<br>2.01 ddd ( 13.3, 4.4, 2.3) | 50.4 | H3, H2 (2.01)<br>H2 (1.30), H3 | C11, C1, C6, C10 | -<br>H3 |
| 3 | 4.10 tt (11.6, 4.2) | 64.9 | H4, H2, H10 | - | H2, H4 |
| 4 | 1.42 dd (22.9, 11.2)<br>2.47 ddd (11.7, 4.0, 2.2) | 48.6 | H4 (2.47), H3<br>H4 (1.42), H3 | C5 | H3, H9<br>H3 |
| 5 | - | 88.3 | - | - | - |
| 6 | - | 183.7 | - | - | - |
| 7 | 5.78 s | 113.4 | - | C5, C8 | - |
| 8 | - | 173.8 | - | - | - |
| 9 | 1.60 s | 25.5 | - | C4, C6 | - |
| 10 | 1.32 s | 30.0 | - | C11, C1, C2, C6 | - |
| 11 | 1.29 s | 25.0 | - | C10, C1, C2, C6 | - |

**Table A.2:** NMR data of the characterized moieties of glycerol, lipid, and sugar signals (800 MHz). * These signals were unclear due to overlapping and thus unrecognizable correlations.

| Moeity type | Moeity ID | Position | $\delta$H Multiplicity ($J$ in Hz) | $\delta$C | H2BC | COSY | HMBC |
|---|---|---|---|---|---|---|---|
| Glycerol | G | 1 | 4.20 4.43 | 63.6 | G2 | G2 | L1 |
| | | 2 | 5.25 | 71.6 | G1, G3 | G1, G3 | _ |
| | | 3 | 4.01 | 64.7 | G2 | G2 | _ |
| | I | 1 | 3.70 3.75 | 61.5 | I2 | _ | I2 |
| | | 2 | 5.06 | 74.5 | I3 | I3 | _ |
| | | 3 | 3.76 3.97 | 68.6 | I2 | I2 | S1 |
| | J | 1 | 4.50 | 64.1 | _ | _ | _ |
| | | 2 | 5.32 | 71.4 | J1, J3 | _ | _ |
| | | 3 | 3.58 | 66.8 | J2 | _ | _ |
| Lipid | L | 1 | _ | 175.1 | _ | _ | _ |
| | | 2 | 2.37 | 34.7 | L3, L1 | _ | L3, L4 |
| | | 3 | 1.64 | 25.5 | L2, L4 | _ | L2, L5, L4 |
| | | 4 | 1.41 | 30.0 | L3, L5 | _ | L2, L3, L6 |
| | | 5 | 2.11 | 27.7 | L4, L6 | _ | L3, L4, L5, L7 |
| | | 6 | 5.38 | 130.5 | L5, L7 | _ | L5 |
| | | 7 | 5.36 | 129.0 | L6 | _ | L8 |
| | | 8 | 2.84 | 26.4 | _ | _ | L7, Cluster1 |
| | | Cluster1 | 5.31–5.43 | 128.0–131.0 | _ | Cluster2 | L7, Cluster2 |
| | | Cluster2 | 2.83-2.85 | 26.3 | _ | Cluster1 | Cluster1 |
| | M | 1 | _ | 177.5 | _ | _ | _ |
| | | 2 | 2.28 | 34.7 | M3 | _ | M1 |
| | | 3 | 1.61 | 25.9 | Cluster3 | _ | _ |
| | | Cluster3 | 1.29–1.41 | 30.0–30.5 | M3 | _ | Cluster4 |
| | | Cluster4 | 2.04–2.11 | 27.7 - 28.0 | _ | _ | Cluster3 |
| | | Cluster1 | 5.31–5.43 | 128.0–131.0 | _ | _ | Cluster4 |
| | | Cluster2 | 2.83–2.85 | 26.3 | _ | _ | Cluster1 |
| | N | Cluster1 | 5.31–5.43 | 128.0-131.0 | _ | Cluster2 | Cluster2 |
| | | Cluster2 | 2.83–2.85 | 26.3 | _ | $\omega$3, Cluster1 | Cluster1 |
| | | $\omega$3 | 5.31 | 128.0 | _ | $\omega$2, Cluster2 | $\omega$2, Cluster2 |
| | | $\omega$2 | 2.09 | 21.4 | $\omega$1, $\omega$3 | $\omega$1 | $\omega$1, $\omega$3 |
| | | $\omega$1 | 0.98 | 14.4 | $\omega$2 | $\omega$2 | $\omega$2 |
| Sugar | S | 1 | 4.24 d (7.7) | 105.1 | S2 | S1, S3 | S3, S2, S3 |
| | | 2 | 3.54 | 72.3 | S3, S1 | S1 | S3, S4 |
| | | 3 | 3.48 dd (9.8, 3.4) | 74.6 | S2 S4 | S4, S1 | S2 |
| | | 4 | 3.83 | 70.1 | S3 | S6, S4 | S2, S3, S5 |
| | | 5 | 3.52 | 76.6 | _ | S4 | S4, S6 |
| | | 6 | 3.76 3.73 | 62.2 | _ | _ | S5, S4 |
| | T | 1 | 4.97 d (3.4) | 103.6 | _ | T2 | T2, T3 |
| | | 2 | 3.50 | 74.1 | T1, T3 | T1 | T3 |
| | | 3 | 3.86 | 74.6 | T2, T4 | T4 | T2, T4 |
| | | 4 | 3.50 | 82.8 | T3, T5 | T3, T5 | T1, T3 |
| | | 5 | 3.74 | 73.6 | T4 | T5 | T4 |
| | | 6 | 3.76 3.73 * | 62.2 * | _ | _ | _ |

**Table A.3:** NMR data of the aromatic and unknown signals (800 MHz).

| Moeity type | Moeity ID | Position | $\delta$H Multiplicity ($J$ in Hz) | $\delta$C | H2BC | COSY | HMBC |
|---|---|---|---|---|---|---|---|
| Aromatic | A | 1 | – | 143.6 | | | |
| | | 2,6 | 7.19 | 129.0 | A3, A5, A4 | – | A1 |
| | | 3,5 | 7.10 | 126.4 | A2, A6 | – | A2, A6, A4 |
| | | 4 | 7.10 | 129.1 | A7, A3, A5 | – | A7, A2, A6 |
| | | 7 | 2.54 | 36.7 | A8, A4 | A8 | A8, A9, A1 |
| | | 8 | 1.56 | 32.4 | A7 | A7 | A9 |
| | | 9 | 1.29–1.41 | 30.0 | – | – | – |
| | U | 1 | 4.17 | 87.2 | – | – | – |
| | | Cluster 5 | 5.67 | 134.1–135.8 | U1 | – | – |
| Unknown | V | 1 | 4.24 | 88.0 | – | – | – |
| | | 2 | 0.92 | 9.8 | V1, V3 | – | V3 |
| | | 3 | 1.51 | 26.4 | V2 | – | V2 |
| | W | Cluster 6 | 6.00–6.10 | 129.0–130.7 | – | – | – |
| | X | Cluster 7 | 6.54–6.59 | 129.5 | – | – | – |

## A.2 HSQC spectra of the mass-targeting fractions of MF2–MF11

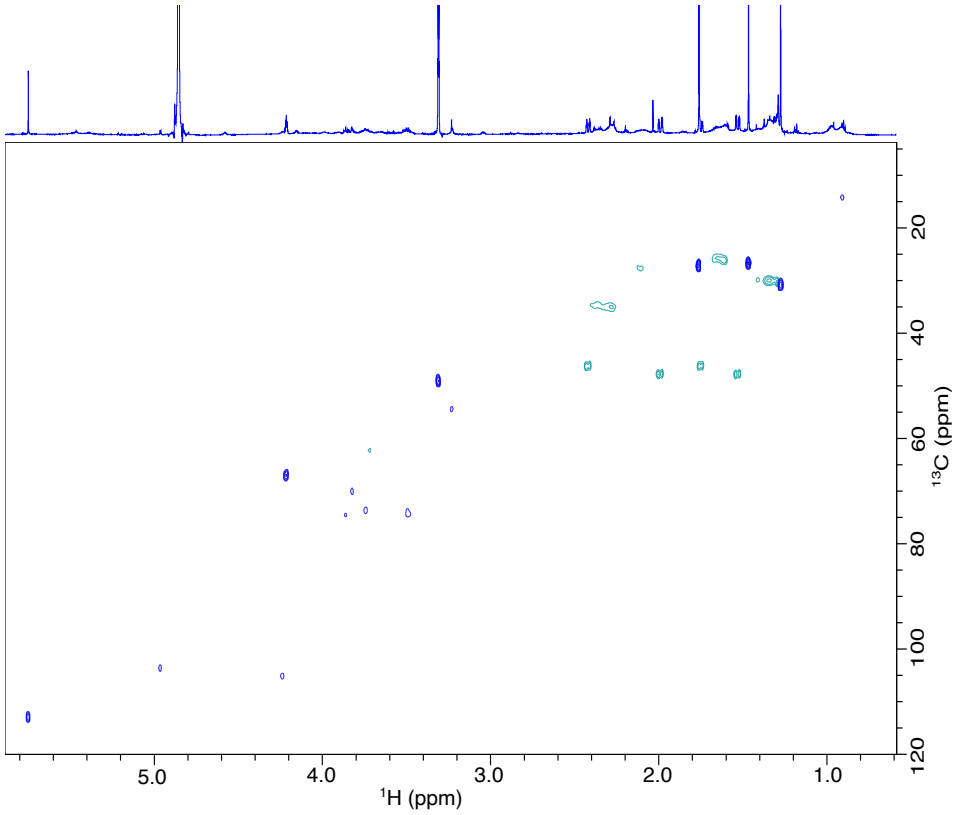


**Figure A.1:** $^{1}H/^{13}C$ HSQC spectra of MF2.

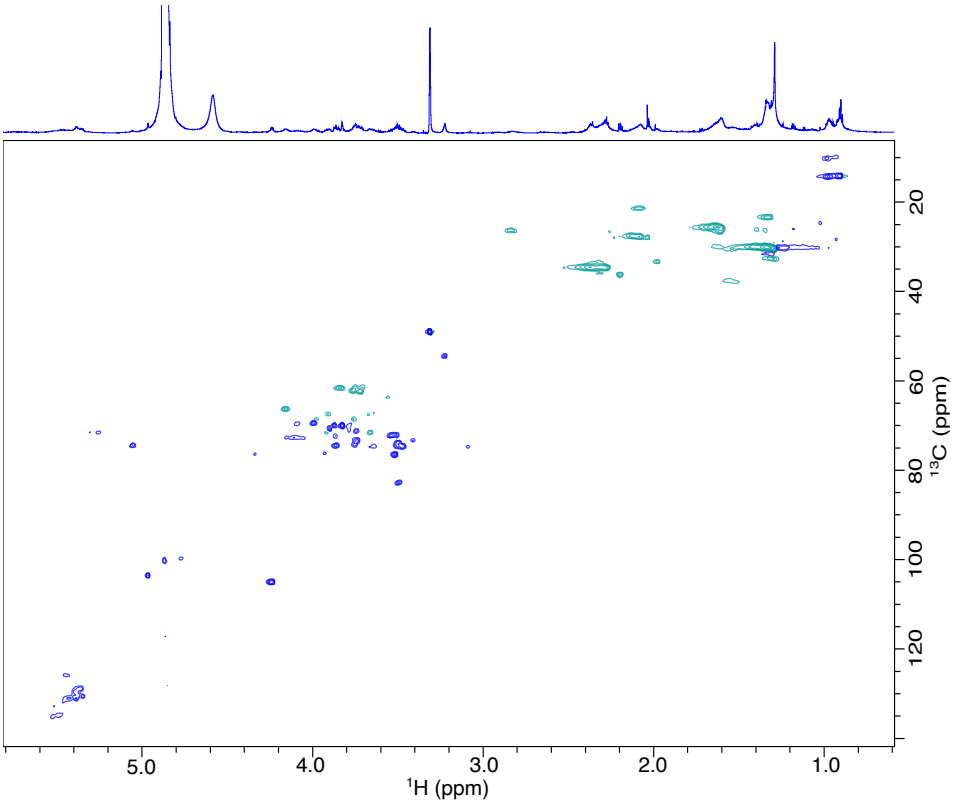


**Figure A.2:** $^{1}H/^{13}C$ HSQC spectra of MF3.

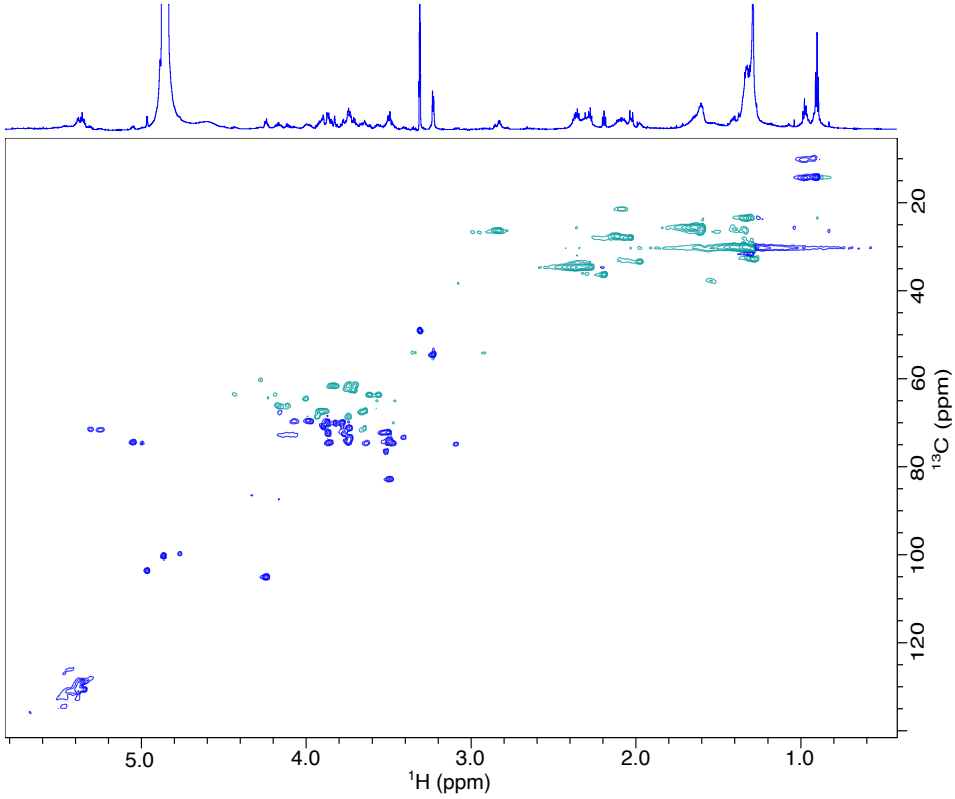


**Figure A.3:** $^{1}$H/$^{13}$C HSQC spectra of MF4.

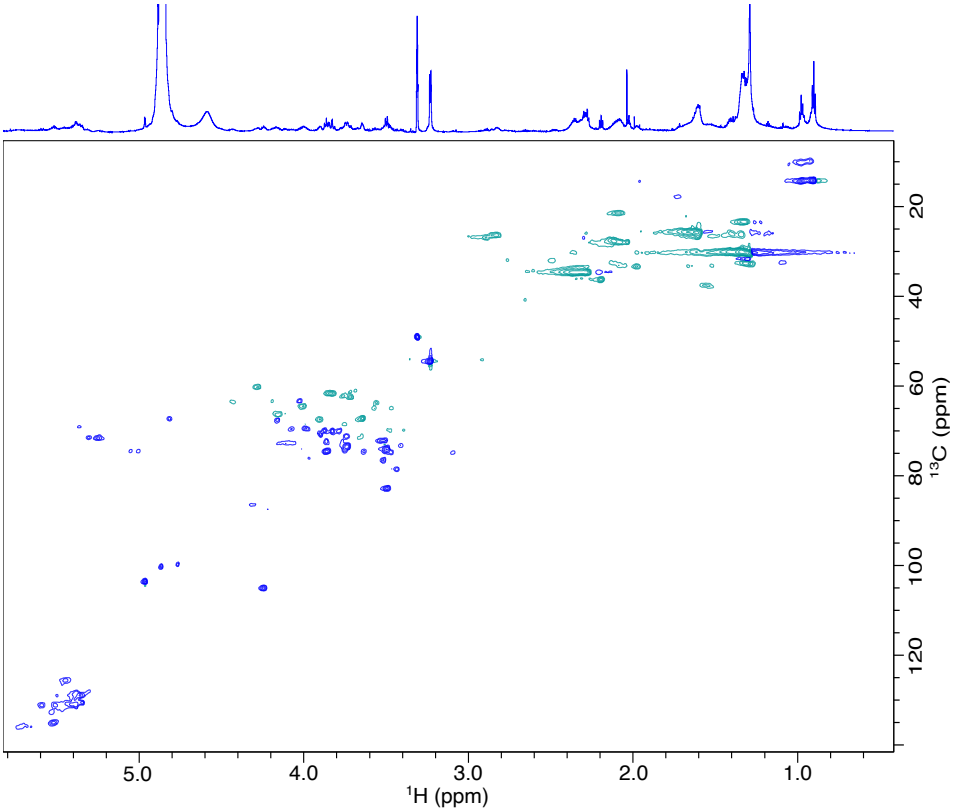


**Figure A.4:** $^{1}$H/$^{13}$C HSQC spectra of MF5.

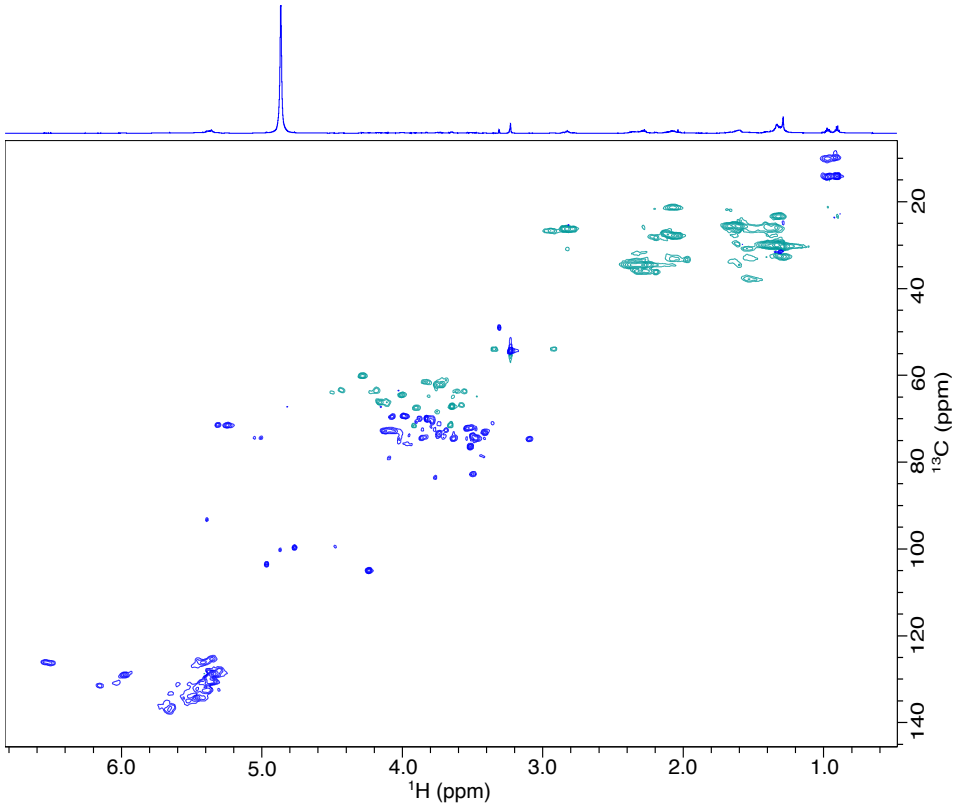


**Figure A.5:** $^{1}$H/$^{13}$C HSQC spectra of MF7.

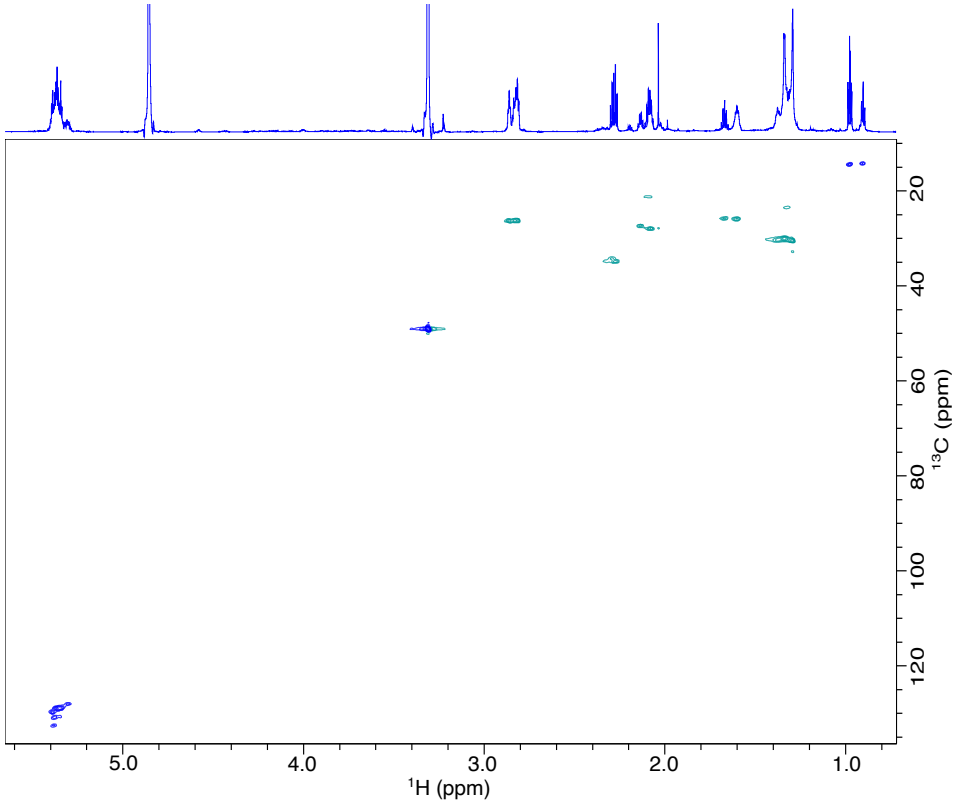


**Figure A.6:** $^{1}$H/$^{13}$C HSQC spectra of MF8.

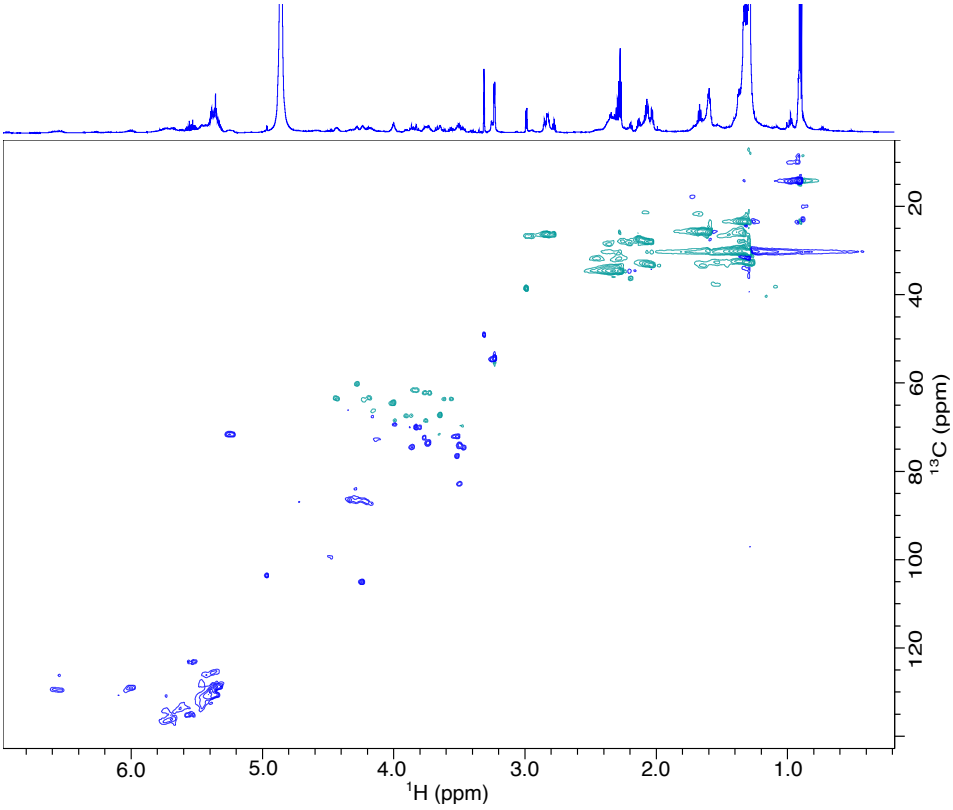


**Figure A.7:** $^{1}$H/$^{13}$C HSQC spectra of MF9.

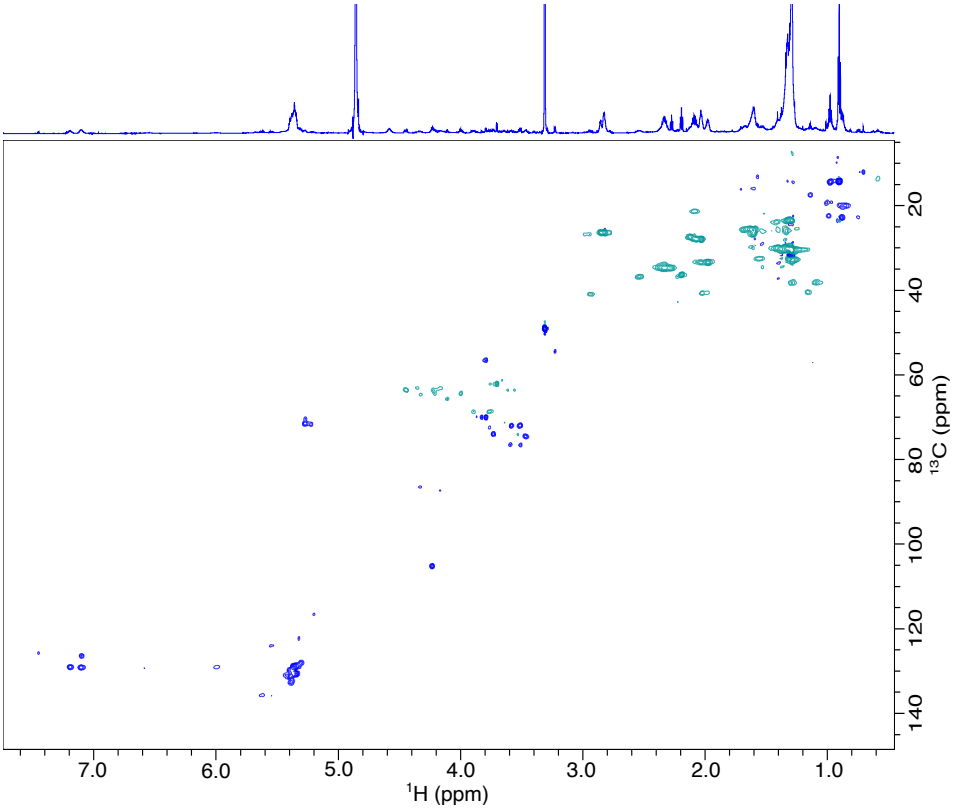


**Figure A.8:** $^{1}$H/$^{13}$C HSQC spectra of MF11.

## A.3 HMBC spectrum of the mass-targeting fraction of MF6

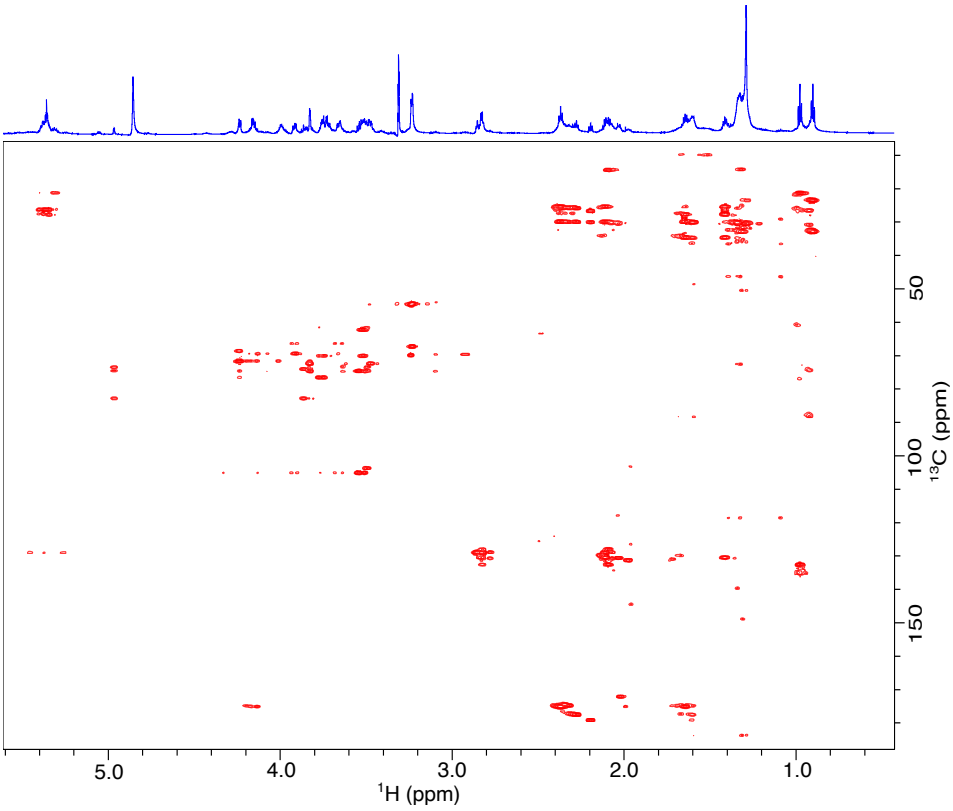


**Figure A.9:** $^{1}$H/$^{13}$C HMBC spectrum of MF6.